Universidad de Valladolid

Escuela de Doctorado Universidad de Valladolid

PROGRAMA DE DOCTORADO EN QUÍMICA: QUÍMICA DE SÍNTESIS, CATÁLISIS Y MATERIALES AVANZADOS

TESIS DOCTORAL:

Bioinspired functional polymers for regenerative medicine: contribution of biomimetic approaches to tissue engineering challenges

Presentada por María Puertas Bartolomé para optar al grado de Doctora por la Universidad de Valladolid

Dirigida por:
Prof. Julio San Román del Barrio
Dr. Blanca Vázquez Lasa

DEFENCE AUTHORIZATION BY THE DOCTORAL THESIS SUPERVISOR

(As required by Section 7.2. of the Regulation concerning doctoral thesis defence at UVa)

TO THE CHAIRMAN OF THE DOCTORAL COMMISSION OF THE UNIVERSITY OF VALLADOLID

Julio San Román del Barrio, with ID 3772952D, Research Professor in the Institute of Polymer Science and Technology of the Spanish National Research Council (ICTP-CSIC), and María Blanca Vázquez Lasa, with ID 15950394D, Scientific Researcher in the same center,

We **hereby authorize the defense** of the doctoral thesis entitled "Bioinspired functional polymers for regenerative medicine: contribution of biomimetic approaches to tissue engineering challenges" written by María Puertas Bartolomé, under our supervision, within the doctoral program: doctorate in chemistry: synthesis chemistry, catalysis and advanced materials, after taking into account that the PhD student has developed an original experimental work, has completed the different stages of training, and has achieved the proposed objectives.

Adress for notification purposes: Juan de la Cierva 3, 28006, Madrid (Spain)
e-mails: jsroman@ictp.csic.es, bvazquez@ictp.csic.es

The Supervisors Julio San Román del Barrio and María Blanca Vázquez Lasa:

Declare that they fulfil the requirements to be able to direct doctoral thesis as established in the Royal Decree RD 99/2011 (modified by the Royal Decree RD 195/2016) and the Agreement of the Directors' Committee of the Doctoral School of the University of Valladolid of February 17th, 2014, that is, that they possess at least a recognized period of research activity in accordance with the provisions set out in the Royal Decree RD 1086/1989 of August 28th".

Place and date: Madrid, 19th May 2020

Signature:

This work is presented for consideration as Doctoral Thesis by compendium of publications following the regulations established by the University of Valladolid (BOCYL no 114, page 26299, Article 4). In accordance with the established regulations, this Thesis includes five articles, three of which were already published at the time of its presentation to the Doctoral Committee. Articles, presented in **Chapters 2, 3, 4, 5 and 6**, are exposed below:

- **Biocompatible and bioadhesive low molecular weight polymers containing long-arm catechol-functionalized methacrylate.**
  Authors: Puertas-Bartolomé M, Fernández-Gutiérrez M, García-Fernández L*, Vázquez-Lasa B*, San Román J
  Published: European Polymer Journal 98 (2018) 47–55
  Journal information (WOS): Q1 in Polymer Science; 3.621 Impact Factor
  DOI:10.1016/j.eurpolymj.2017.11.011

- **Bioactive and Bioadhesive Catechol Conjugated Polymers for Tissue Regeneration.**
  Authors: Puertas-Bartolomé M, Vázquez-Lasa B*, San Román J
  Published: Polymers 10 (2018) 768
  Journal information (WOS): Q1 in Polymer Science; 3.164 Impact Factor
  DOI: 10.3390/polym10070768

- **Bioadhesive functional hydrogels: Controlled release of catechol species with antioxidant and antiinflammatory behavior.**
  Authors: Puertas-Bartolomé M, Benito-Garzón L, Fung S, Kohn J, Vázquez-Lasa B*, San Román J
  Published: Materials Science and Engineering: C 105 (2019) 110040
  Journal information (WOS): Q1 in Materials Science, Biomaterials; 4.959 Impact Factor
  DOI: 10.1016/j.msec.2019.110040

- **3D printing of a reactive hydrogel bioink using a static mixing tool.**
  Authors: Puertas-Bartolomé M, Wlodarczyk-Biegun M K, del Campo A, Vázquez-Lasa B*, San Román J
  Published: Under consideration for publication

- **3D printed construct with catechol functionalized nanoparticles for wound healing applications.**
  Authors: Puertas-Bartolomé M, Wlodarczyk-Biegun M K, del Campo A, Vázquez-Lasa B*, San Román J
  Published: Under consideration for publication

Finally, two articles published during the doctoral work period, although not included in the contributions chosen for consideration of the Thesis by compendium of publications, are presented in **Annexes I and II** and exposed below.

- **Contribution of bioactive hyaluronic acid and gelatin to regenerative medicine.**
  Authors: Mora-Boza A*, Puertas-Bartolomé M*, Vázquez-Lasa B, San Román J, Pérez-Caballer A, Olmeda-Lozano M

Published: European Polymer Journal 95 (2017) 11-26
Journal information (WOS): Q1 in Polymer Science; 3.621 Impact Factor
DOI: 10.1016/j.eurpolymj.2017.07.039

- ***In Situ* Cross-Linkable Polymer Systems and Composites for Osteochondral Regeneration.**

  Authors: Puertas-Bartolomé M*, Benito-Garzón L, Olmeda-Lozano M
  Published: Advances in Experimental Medicine and Biology 1058 (2018) 327-355
  Journal information: Chapter XXV in "Osteochondral Tissue Engineering", Oliveira J, Pina S, Reis R, San Roman J
  DOI: 10.1007/978-3-319-76711-6_15

References of the articles presented in this Thesis have been included in the corresponding Chapters and Annexes in order to facilitate the reading.

Contents

Resumen

1. INTRODUCCIÓN

La Ingeniería de Tejidos (IT) y la Medicina Regenerativa (MR) son áreas de gran interés y desarrollo en la medicina que han surgido para superar las limitaciones que presentan las metodologías actualmente utilizadas en la reparación de tejidos . Así, los campos de la IT y la MR están relacionados con la regeneración o reparación de tejidos u órganos dañados para restablecer su función biológica regular, centrándose en la estimulación de los mecanismos de reparación propios del cuerpo. La IT es un campo multidisciplinar que reúne conocimientos de los campos de la ciencia y tecnología de los materiales, la biología celular y la ingeniería biomédica para desarrollar dispositivos biomédicos que puedan implantarse en pacientes para inducir la regeneración de tejidos. Los dispositivos biomédicos generalmente combinan un andamio como material de soporte, células vivas y moléculas bioactivas. El andamio actúa esencialmente como plantilla o soporte para proporcionar un entorno celular apropiado que promueva la capacidad nativa de las células para adherirse, migrar, proliferar y diferenciarse dando lugar al crecimiento de nuevo tejido denominado tejido incipiente o equivalente tisular o constructo (del inglés *construct*). Hoy en día, el desarrollo de nuevas estrategias en IT y MR constituye uno de los principales retos científicos que se espera que tengan un impacto importante en el futuro en la práctica clínica, mejorando la calidad de vida del paciente.

Un andamio ideal para ingeniería de tejidos debe reunir una buena biocompatibilidad, biodegradación, así como las propiedades mecánicas y la arquitectura estructural adecuadas a los requisitos específicos de cada aplicación médica individual. Por lo tanto, un punto clave en la ingeniería de tejidos, es la elección del biomaterial para fabricar el andamio más adecuado. Actualmente se están dedicando grandes esfuerzos para desarrollar nuevos biomateriales que imitan la matriz extracelular (MEC) con una amplia gama de propiedades y respuestas biológicas controladas y que puedan usarse para la regeneración de diferentes tejidos. Paralelamente a la necesidad de nuevos biomateriales está el desarrollo de técnicas para producir andamios con propiedades adecuadas. Numerosas tecnologías de fabricación están disponibles para transformar biomateriales sintéticos y naturales en andamios de una amplia gama de formas y tamaños. La técnica de fabricación y la morfología del andamio elegidas deben adaptarse a la aplicación concreta. Sin embargo, el logro de la fabricación de estructuras de tejidos/órganos humanos personalizada sigue siendo un problema complejo en la comunidad científica, y, en este sentido la selección de los biomateriales y la tecnología adecuados, así como vencer los obstáculos para la traslación clínica deben ser abordados en mayor profundidad.

Las recientes investigaciones en los campos de la IT y la MR demuestran el creciente interés en el desarrollo de materiales biomiméticos y bioinspirados avanzados. La tecnología biomimética y bioinspirada considera a la naturaleza como una gran fuente de inspiración y utiliza características clave de materiales naturales y / o estructuras biológicas como base para el diseño de nuevos biomateriales. Concretamente, la forma natural de adhesión de los mejillones a las rocas ha sido una fuente de inspiración para desarrollar polímeros bioadhesivos que se adhieran a las interfaces biológicas, principalmente en condiciones húmedas. La capacidad de los mejillones de anclarse fuertemente a las rocas en condiciones marinas severas se atribuye a la secreción de un biso de proteínas adhesivas (Mfps) del pie del mejillón, cuyo principal componente es un aminoácido que contiene el grupo catecol llamado L-3,4-dihidroxifenilalanina (DOPA). En los últimos años, el diseño de polímeros sintéticos funcionalizados con grupos catecol ha aumentado considerablemente en el campo de los biomateriales abarcando diferentes aplicaciones en IT. En este sentido, la versatilidad de la química del catecol permite la preparación y el desarrollo de numerosas plataformas bioactivas y bioadhesivas para una amplia gama de aplicaciones biomédicas con una perspectiva muy prometedora.

Un objetivo específico importante en IT y MR es el desarrollo de apósitos o constructos eficientes para ayudar y mejorar el proceso de curación en heridas crónicas. La curación de heridas se refiere al proceso de reemplazo o restauración del tejido dañado por tejido nuevo para restablecer su función. Es un proceso gradual que comprende cuatro etapas integradas: (1) hemostasia e inflamación, caracterizadas por infiltración de macrófagos o leucocitos y secreción de citoquinas; (2) proliferación, que implica la eliminación del tejido dañado, el desarrollo del tejido de granulación, la angiogénesis y la reepitelización; (3) maduración, cuando la MEC producida se vuelve bien definida; y finalmente (4) la remodelación o la formación de tejido cicatricial y el logro del tejido funcional de la piel. Estas etapas complejas implican la interacción de diferentes tipos de células, moléculas bioactivas, y la MEC, que actúa como plataforma de soporte. Sin embargo, las heridas cutáneas traumáticas grandes debido a quemaduras o accidentes, así como aquellas derivadas de enfermedades como la diabetes pueden provocar el mal funcionamiento del proceso y la formación de heridas crónicas, que representan un importante problema de salud a nivel global. En las heridas crónicas, el proceso de cicatrización se obstruye generalmente en la fase inicial y difiere del patrón de cicatrización regular del tejido de la piel, por lo que es particularmente difícil de curar.

Las estrategias de curación de heridas en IT se basan en proporcionar un andamio artificial que ejerce la función de actuar como una matriz provisional para que las células proliferen y generen nuevo tejido. El diseño de un andamio adecuado implica la selección del biomaterial, tipo de célula y estructura apropiados. Los andamios diseñados deben ser no inmunogénicos,

biocompatibles, bioreabsorbibles y porosos. Además, la matriz debe mostrar una buena integración con la herida, una resistencia mecánica adecuada (similar a la piel) para proporcionar soporte físico, propiedades de barrera para proteger la herida y capacidad para promover la cicatrización del tejido. La terapia celular se ha convertido en una modalidad prometedora para mejorar el proceso de cicatrización de heridas. También, se han explorado enfoques basados en la funcionalización de andamios con moléculas bioactivas como factores de crecimiento o fármacos. De esta manera, los andamios pueden servir como un nicho para que las células proliferen, pero también para proporcionarles señales que puedan desencadenar el proceso de regeneración del tejido dañado. Otro punto crítico de la ingeniería del tejido epitelial radica en la ingeniería estructural de los andamios. En los últimos años, diferentes injertos de piel o apósitos para heridas disponibles comercialmente han demostrado resultados prometedores para el tratamiento de distintos tipos de heridas. Sin embargo, si bien se han reportado numerosos materiales y apósitos para heridas en las dos o tres últimas décadas, solo una minoría se ha sometido a ensayos clínicos. Por lo tanto, es necesario realizar más investigaciones y análisis clínicos para poder trasladar los nuevos sistemas desarrollados y tecnologías avanzadas implementadas a la clínica. La tendencia futura de las estrategias de IT en la curación de heridas abre la puerta a nuevas terapias que puedan acelerar el proceso de curación, disminuir el dolor y mejorar la calidad de vida del paciente.

2. OBJETIVOS

El objetivo global de esta Tesis es explorar el desarrollo de nuevos polímeros bioinspirados para su aplicación como materiales avanzados en el campo de la medicina regenerativa, como la regeneración osteocondral o de tejido epitelial. La bioactividad y la versatilidad sobresaliente de los grupos catecol que presentan propiedades adhesivas, antioxidantes y antiinflamatorias, permiten la preparación y fabricación de diferentes materiales avanzados utilizando técnicas que den lugar a sistemas con estructuras desde 2D a andamios 3D, así como explorar terapias celulares. Esta Tesis cubre por tanto los aspectos de diseño molecular, preparación de materiales, fabricación de soportes, análisis de propiedades y estudio del comportamiento biológico de los sistemas desarrollados. Para lograr este objetivo global, a lo largo de los capítulos se recopilan 5 trabajos científicos de acuerdo con los objetivos específicos que se describen a continuación.

-El primer objetivo específico de esta Tesis es la preparación y el estudio de polímeros inteligentes (aquellos que muestran cambios conformacionales en respuesta a estímulos ambientales) con propiedades bioadhesivas y termosensibles inspirados en el mecanismo de adhesión de los mejillones para su potencial aplicación como sistemas de liberación de fármacos o para regeneración osteocondral. Específicamente, en el **Capítulo 2** el objetivo se centra en la

síntesis de un monómero acrílico de cadena lateral larga portador de grupos catecol, la preparación de sus copolímeros con *N*-vinilcaprolactama y el estudio de la influencia de la composición de los copolímeros en las propiedades finales de los mismos.

-El segundo objetivo específico pretende diseñar una familia de polímeros de alto peso molecular conjugados con grupos catecol y portadores de propiedades bioactivas así como la evaluación de sus propiedades para su potencial aplicación como apósitos en curación de heridas. En el **Capítulo 3** se preparan dichos polímeros así como la formación de películas en 2D y se investiga la relación entre su estructura y propiedades finales, incluyendo su comportamiento biológico en cultivos celulares específicos.

-El siguiente objetivo individual de esta Tesis consiste en abordar el desarrollo de andamios en base a redes interpenetradas para el tratamiento efectivo de heridas crónicas. El **Capítulo 4** describe la preparación de un sistema híbrido que combina las propiedades beneficiosas de hidrogeles basados en quitosano (Ch) y ácido hialurónico oxidado (HAox) con polímeros sintéticos conjugados con grupos catecol y se investiga su aplicabilidad como áposito bioactivo para heridas.

-El último objetivo específico se centra en la fabricación de andamios de hidrogel impresos en 3D para estrategias de ingeniería de tejidos de terapias celulares. De esta manera, en el **Capítulo 5** se pone a punto una nueva estrategia de impresión 3D con el fin de mejorar las propiedades mecánicas de los hidrogeles. Esta nueva metodología se basa en el entrecruzamiento *in situ* de una biotinta basada en un hidrogel reactivo de dos componentes (Ch y HAox) en presencia de células vivas. Por otro lado, en el **Capítulo 6**, la nueva metodología se aplica para fabricar andamios impresos en 3D del hidrogel descrito cargado con nuevas nanopartículas funcionalizadas con catecol para su aplicación en el tratamiento del cuidado de heridas. En este sistema 3D se combinan las propiedades beneficiosas de los hidrogeles biomiméticos con las propiedades bioactivas de las nanopartículas.

3. METODOLOGÍA

La metodología llevada a cabo para la síntesis de polímeros, fabricación de materiales, caracterización fisicoquímica, estudio *in vitro* y comportamiento biológico de los sistemas desarrollados se resume brevemente a continuación:

La síntesis de polímeros funcionalizados con grupos catecol se ha llevado a cabo a través de dos estrategias: 1) funcionalización de un monómero acrílico de cadena lateral larga con grupos catecol y su posterior copolimerización radical con el monómero termosensible *N*-

vinilcaprolactama; y 2) copolimerización de *N*-vinilcaprolactama y metacrilato de 2-hidroxietilo y la posterior conjugación de los copolímeros a través del cloruro de ácido hidrocafeico para obtener terpolímeros conjugados con gran disponibilidad de los grupos catecol.

Seguidamente se han desarrollado materiales de diversas características utilizando los polímeros portadores de grupos catecol, polímeros naturales y sistemas híbridos que combinan ambos tipos de polímeros. La técnica de fabricación y la morfología del andamio elegida en base a estructuras 2D o 3D se adaptó a la aplicación de cada material. Así, se han desarrollado películas 2D de los polímeros conjugados con catecol mediante la técnica de "solvent-casting". Por otra parte, se ha llevado a cabo la preparación de soportes a base de sistemas interpenetrados formados por una red covalente de polímeros naturales (Ch y HAox) y una red iónica del terpolímero portador del grupo catecol. Finalmente, se han fabricado andamios celulares por impresión 3D aplicando una nueva estrategia de bioimpresión optimizada previamente en esta Tesis. Estos andamios 3D consisten en un hidrogel de quitosano y ácido hialurónico cargado con nanopartículas funcionalizadas con catecol. Previamente a la preparación de la biotinta se procedió a la fabricación de las nanopartículas autoensambladas de dos polímeros anfifílicos que contienen catecol en diferentes composiciones. Posteriormente, se desarrollaron los andamios 3D cargados con dichas nanoparticulas y fibroblastos.

En esta Tesis se ha aplicado un gran número de técnicas de caracterización para estudiar la composición fisicoquímica, la morfología, y las propiedades térmicas y reológicas de los sistemas desarrollados: RMN, FTIR, MS, UV, SEC, DSC, TGA e Instron principalmente. Además, debido al potencial de aplicación de estos sistemas en el ámbito biomédico, se ha estudiado su comportamiento *in vitro* en cuanto a hinchamiento, degradación y liberación de especies de catecol en condiciones fisiológicas así como su citotoxicidad, proliferación celular sobre los soportes desarrollados, y sus propiedades bioactivas en cultivos celulares *in vitro* usando fibroblastos humanos, macrófagos, células endoteliales o células madre, y siguiendo protocolos estandarizados. Finalmente, se ha evaluado la biocompatibilidad *in vivo* de determinados sistemas utilizando un modelo de rata.

4. RESULTADOS

En el **Capítulo 2**, la síntesis de un monómero acrílico de catecol de cadena lateral larga y flexible (CEMA) se ha llevado a cabo para la preparación de copolímeros con *N*-vinilcaprolactama. La reacción de copolimerización radical está claramente controlada por la naturaleza del grupo catecol del monómero CEMA, proporcionando sistemas poliméricos de bajo peso molecular con muy bajo índice de polidispersidad y alta homogeneidad. Los materiales han sido obtenidos con

éxito con contenidos de CEMA entre 0,9 y 13,5% en moles. Los resultados muestran que el gel de copolímero preparado con un contenido de catecol relativamente alto (13,5% en moles) y gelatina posee excelentes propiedades bioadhesivas a superficies óseas. Además, los copolímeros con un contenido de catecol relativamente bajo (0,9-3,6% en moles) proporcionan sistemas termosensibles y con excelentes propiedades antioxidantes y anti-inflamatorias que varían en función de la composición de catecol en el copolímero.

-La síntesis de copolímeros estadísticos de *N*-vinilcaprolactama y metacrilato de 2-hidroxietilo, y la posterior reacción de conjugación con cloruro de ácido hidrocafeico, portador de grupos catecol, se han llevado a cabo con éxito como se describe en el **Capítulo 3**. Esta vía de conjugación permite obtener polímeros de alto peso molecular, con un rendimiento relativamente alto y con alta disponibilidad de los grupos catecol laterales. Películas 2D preparadas con los terpolímeros funcionalizados han demostrado buenas propiedades bioadhesivas a piel porcina en condiciones húmedas; prevención del daño cutáneo inducido por los rayos UV; propiedades antioxidantes que controlan las especies reactivas de oxígeno generadas por células madre; y atenuación de la respuesta inflamatoria en cultivos de macrófagos. Además, se ha comprobado que estas propiedades están directamente relacionadas con la composición de catecol en los terpolímeros.

-En el **Capítulo 4**, se han desarrollado hidrogeles basados en redes de polímeros interpenetrados. Estos sistemas consisten en una red entrecruzada covalentemente obtenida por reacción de Ch y HAox en presencia de un terpolímero de catecol sintético, que posteriormente se coordinó con Fe^{3+} para dar una red entrecruzada iónicamente. Los estudios *in vitro* demuestran que estos hidrogeles funcionalizados con catecol proporcionan un entorno adecuado para soportar el crecimiento, la migración y la proliferación celular; protegen las células contra el daño por estrés oxidativo inducido por especies reactivas de oxígeno; y promueven la disminución de la citoquina proinflamatoria IL-1ß. Las membranas de hidrogel han demostrado también una alta fuerza de adhesión tisular en condiciones húmedas a piel porcina. Además, el diseño del sistema interpenetrado permite la liberación controlada y sostenida de especies de catecol *in situ*. Finalmente, los experimentos *in vivo* revelan su biocompatibilidad y estabilidad, y los estudios histológicos indican respuestas inflamatorias normales y una vascularización más rápida atribuida a la presencia de los grupos catecol.

-El estudio presentado en el **Capítulo 5** describe el desarrollo de una biotinta reactiva de hidrogel con una metodología de impresión por extrusión basada en un sistema de doble jeringa con una herramienta de mezcla estática. Este método ha sido desarrollado con éxito y presenta múltiples ventajas dentro de la bioimpresión por extrusión 3D que ayudan a contrarrestar las débiles propiedades mecánicas intrínsecas de los hidrogeles: 1) la gelificación durante el proceso de extrusión proporciona suficiente viscosidad para imprimir con alta fidelidad de forma al usar

soluciones precursoras de baja viscosidad, lo que permite una alta viabilidad celular de las células impresas; 2) el entrecruzamiento durante la extrusión evita la necesidad de un tratamiento adicional para mantener la forma impresa; 3) la estabilidad del andamio, si se requiere para el cultivo a largo plazo, se puede aumentar en un simple paso de incubación. Además, esta técnica permite la impresión con células vivas, al contrario de los materiales preparados en los capítulos anteriores donde la siembra de las células tiene lugar después de la fabricación del soporte. Los andamios bioimpresos obtenidos mostraron buena biocompatibilidad de las células encapsuladas, hinchamiento moderado y estabilidad estructural durante 14 días de cultivo.

-En el **Capítulo 6**, se han desarrollado soportes de hidrogel por impresión 3D que contienen nuevas nanopartículas funcionalizadas con catecol (NP) aplicando la nueva metodología de bioimpresión por extrusión descrita en el Capítulo 5. En este caso, se han obtenido con éxito soportes por impresión de 2 capas con buena resolución y fidelidad de forma y con las NP distribuidas de forma uniforme. Los estudios *in vitro* realizados han demostrado la capacidad de la biotinta para promover la proliferación celular, así como la capacidad de las NP para promover la cicatrización de heridas: regulación de la producción de especies reactivas de oxígeno, respuesta antiinflamatoria y aumento de la expresión del factor de crecimiento endotelial vascular.

5. CONCLUSIONES

En esta Tesis se han desarrollado y aplicado nuevos polímeros inspirados en mejillones para la preparación de materiales avanzados con propiedades bioactivas para aplicación en medicina regenerativa, como la regeneración de tejidos de la piel.

-La síntesis de dos familias diferentes de polímeros de catecol de brazo largo se ha llevado a cabo con éxito siguiendo dos vías de reacción diferentes: 1) funcionalización de un monómero con grupos catecol y su posterior polimerización radical para obtener copolímeros estadísticos portadores de grupos catecol **(copolímeros VCL_CEMA)**, y 2) funcionalización directa de un copolímero con moléculas de catecol para obtener terpolímeros conjugados con grupos catecol **(polímeros conjugados con catecol)**. Por un lado, se obtuvieron copolímeros VCL_CEMA con contenidos de CEMA entre 0,9 y 13,5% en moles mediante copolimerización por radicales libres que estuvo claramente controlada por la naturaleza del monómero portador de catecol, CEMA, proporcionando sistemas poliméricos de bajo peso molecular con muy bajo índice de polidispersidad y alta homogeneidad. Por otro lado, los polímeros conjugados con catecol

proporcionaron polímeros de alto peso molecular con mayor disponibilidad de los grupos laterales de catecol.

-Los copolímeros VCL_CEMA se han utilizado para la fabricación de **polímeros "inteligentes"**. El contenido de la unidad monómerica con grupos catecol ha demostrado influir directamente en las propiedades biodhesivas, termosensibles, antioxidantes y anti-inflamatorias de los copolímeros resultantes. Por lo tanto, la composición de copolímero puede ser utilizada como una herramienta para la preparación de sistemas biomédicos con propiedades modulables y un gran potencial para el desarrollo de sistemas de administración de fármacos y geles bioactivos que pueden aplicarse en procesos de regeneración de tejidos.

-Se han fabricado **películas 2D** utilizando los terpolímeros conjugados con diferentes composiciones de catecol (2 y 22% en moles). Se ha demostrado que la presencia de catecol en los terpolímeros proporciona fuertes propiedades bioadhesivas, la prevención del daño cutáneo inducido por rayos UV, propiedades antioxidantes y atenuación del daño inflamatorio. Las propiedades bioactivas encontradas son características clave en el proceso de cicatrización de heridas y, por lo tanto, podemos decir que estos materiales bioinspirados pueden ser excelentes candidatos para la aplicación como apósitos bioadhesivos y bioactivos.

-Se han fabricado con éxito **andamios de hidrogel basados en redes poliméricas interpenetradas (IPN)** que contienen quitosano, ácido hialurónico y un terpolímero conjugado con catecol. La red obtenida ha demostrado que proporciona una buena proliferación celular, eficacia protegiendo las células contra el daño por estrés oxidativo, supresión de la respuesta inflamatoria y una alta bioadhesión a la piel porcina. Además, el diseño IPN proporciona una liberación controlada y sostenida de especies de catecol. Los estudios histológicos tras experimentación *in vivo* revelan buena biocompatibilidad y una vascularización más rápida en comparación a los sistemas que no contienen catecol. Por lo tanto, el terpolímero funcionalizado con catecol dota al hidrogel de una bioactividad que, junto con la liberación controlada de catecol, hace que este sistema posea un gran potencial de aplicación como áposito en heridas crónicas y mejorar el proceso de regeneración de la lesión.

-Se han fabricado de manera efectiva **andamios de hidrogel impresos en 3D** basados en carboximetilquitosano y ácido hialurónico oxidado utilizando una novedosa estrategia de impresión 3D que permite la impresión con células vivas. La optimización de una biotinta de hidrogel reactivo de forma que la cinética de entrecruzamiento coincida con el proceso de impresión, ha hecho que los andamios bioimpresos resultantes presenten una buena fidelidad de forma, estabilidad estructural, y buena biocompatibilidad durante 14 días de cultivo. Dado que las concentraciones de los precursores y las condiciones de impresión pueden ser variadas

fácilmente, esta metodología de impresión ofrece una gran versatilidad y se prevé que pueda adaptarse a una amplia gama de sistemas reactivos, previo ajuste de su cinética de reticulación, para ser utilizada en el futuro para diversas aplicaciones en medicina regenerativa e ingeniería de tejidos.

-La técnica de nanoprecipitación ha permitido fabricar nanopartículas (NP) autoensambladas de los terpolímeros conjugados de catecol con dos composiciones de catecol (2 y 29% en moles). Las nanopartículas resultantes presentaron morfología esférica y tamaños de partícula con baja polidispersidad. Además, demostraron alta estabilidad y capacidad para servir como nano-vehículos para transportar fármacos hidrófobos como la cumarina-6. Los estudios celulares *in vitro* demostraron que estas NP funcionalizadas con catecol protegen a las células contra el daño por estrés oxidativo inducido por las especies radicales de oxígeno, regulan la respuesta inflamatoria y promueven la regulación positiva del factor de crecimiento endotelial vascular (VEGF). Por lo tanto, las NP desarrolladas presentan propiedades para promover la cicatrización de heridas y potencial para aplicación en la IT y liberación controlada de fármacos.

-Aprovechando la estrategia de bioimpresión 3D desarrollada anteriormente, se han fabricado **andamios 3D de hidrogel impresos que contienen las nanopartículas funcionalizadas con catecol**. Los andamios cuadrados de 2 capas presentaron NP uniformemente distribuidas, una buena resolución y fidelidad de forma. Un ajuste adicional del cabezal de impresión de mezcla permitiría construir estructuras más grandes en estudios posteriores. Estos sistemas resultaron adecuados para soportar el crecimiento y proliferación de fibroblastos y presentaron propiedades bioactivas provenientes de las nanopartículas. La biotinta cargada con NP desarrollada en este trabajo tiene una aplicación prometedora en terapias de curación de heridas con varias ventajas: 1) la liberación controlada de las NP en el sitio de la herida proporciona una función bioactiva localizada; 2) las NP funcionalizadas pueden actuar como nano-vehículos para múltiples fármacos hidrófobos; 3) el enfoque de impresión utilizado permite adaptar la geometría, los materiales y las dosis de formulación según los requisitos del paciente para tratamientos específicos de heridas.

CHAPTER

01

GENERAL INTRODUCTION: STATE OF THE ART, OBJECTIVES AND METHODOLOGY

State of the art

1. INTRODUCTION TO TISSUE ENGINEERING AND REGENERATIVE MEDICINE

Thousands of treatments and surgical procedures are performed every day to repair or replace damaged tissues in the human body, caused by disease, injury or trauma. Currently, two different treatments are used, e.g. autografts and allografts. Autografts consist of the transplanting of tissue from one site to another in the same patient. This approach has some disadvantages since harvesting autografts is painful, expensive, limited and it can be related to donor-site morbidity. On the other hand, allograft is the transplanting of a tissue or organ from one individual to another. However, it can be associated to immunological compatibility complications in the patient's body, and it is a potential risk of disease transmission from the donor to the patient.[1,2] Moreover, over the past decades, the gap between the increasing demand for organ transplants and the organs supply continues to increase.[3-5] Alternatively, tissue engineering (TE) and regenerative medicine (RM) are new rapidly growing areas in medical science of great interest to overcome current treatments.[6-9]

The fields of TE and RM are concerned with the regeneration or repair of damaged tissues or organs to restore their regular biological function, focusing on the stimulation of the body's own repair mechanisms. TE strategies are multidisciplinary approaches that gathers knowledge from the fields of materials science and technology, cellular biology and biomedical engineering to develop biomedical devices that can be implanted in patients to induce tissue regeneration.[5,10,11] Biomedical devices usually combine a scaffold as supporting material, living cells and bioactive molecules. Scaffolds must provide temporal mechanical support for the period the newly tissue is formed. They can be classified into decellularized tissues or molecularly defined biomaterials, which improve quality and safety issues that inherently accompany decellularization strategies.[12] The biomaterial scaffolds essentially act as templates that provide an appropriate environment to promote the native capacity of cells to adhere, migrate, proliferate and differentiate towards the growth of new tissue. TE approaches are based on stimulating the body's natural self-healing capacity typically using cell-seeded biomaterial scaffolds, which can be either cultured *in vitro* using bioreactors to form "TE constructs" which are implanted into the damaged site (represented in Figure 1), or directly implanted into the damaged site, where regeneration of the tissue is performed *in vivo*.[1,13,14] Many scaffolds contain also bioactive compounds, which can be slowly delivered to the damaged site. In this sense, the use of scaffolds as drug delivery system (DDS) for growth factors, peptides,

cytokines or drugs is having noticeably attention in TE and DDS fields, two disciplines that are intimately related.[1,5,15]

Nowadays, TE and RM strategies constitute one of the biggest scientific challenges which are expected to have an important impact on the future of the practical medicine, enhancing quality of the patient's life.[14-16] This section aims to provide an overview of the current state-of-the-art of the scaffolds requirements, composition, and fabrication techniques for successful TE and RM strategies in which this Thesis is framed.

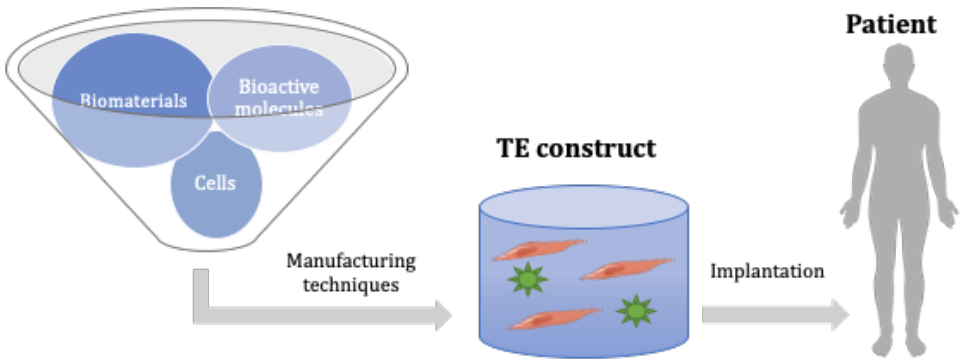

Figure 1. Overview of a tissue engineering strategy using cell-seeded biomaterial scaffolds cultured *in vitro* and implanted into a damaged site.

1.1. SCAFFOLD REQUIREMENTS

An adequate scaffold to support the regeneration process is a very important aspect in tissue engineering strategies, and to achieve this goal several structural and physical specifications must be considered. The ideal tissue engineering scaffold must provide appropriate biocompatibility, biodegradability, mechanical properties and scaffold architecture to match the specific requirements of each individual medical application.

A clearly important criterion is that the scaffold must be biocompatible. But biocompatibility is not an inherent property of the material, it depends on the biological environment.[17] The scaffold must allow the tissue-specific cells to attach, migrate, proliferate and differentiate onto or within the scaffold, to synthesize their own extracellular matrix (ECM). In addition, bioactive molecules added to the scaffold will enhance the regeneration process. In this way, diffusion of nutrients and metabolites is very important, and the scaffold surface area, porosity, and pore interconnectivity

have a significant role.[11,13,18-20] Previous studies have reported that highly porous scaffolds can better support nutrients transport, cell proliferation, and vascularization (which remains as one of the most daunting challenges[14]).[5,21,22]. Ideally, the scaffold must degrade at an adequate rate to match the healing or tissue regeneration process. The material would be resorbed at the same time that it is replaced with cells and newly deposited ECM. Importantly, the material and the degradation by-products must be biologically inert and should not evoke inflammatory response. Characteristics such as suitable structural strength and dimensional shape for the indicated application as well as manufacturing feasibility, are also essentials for the correct function of the scaffold.[11,13,17,23] Moreover, most tissue engineering strategies utilize cells. There are different sources of cells that could be used such as cells derived from the patient or autologous cells (it is often a limited supply), cells from a human donor or allogenic cells, or stem or progenitor cells. The last studies indicate that the use of stem cells is very attractive due to their high proliferative capacity and pluripotency or aptitude to differentiate into cells of multiple lineages.[13,24] Finally, economic issues regarding to materials and manufacturing requirements need to be taken into account together for a successful clinical translation.[25-27]

Therefore, a crucial point to fabricate suitable scaffolds in tissue engineering, and from which most of the aspects named above are dependent upon, is the choice of the biomaterial that gathers the optimal properties for the specific medical application.

1.2. BIOMATERIALS

According to the European Society of Biomaterials, the current definition for biomaterial is "a material intended to interface with biological systems to evaluate, treat, augment or replace any tissue, organ or function of the body".[1] One of the recent challenges of tissue engineering strategies is the design of appropriate biomaterials that mimic the native ECM.[11,20,28-30] The ECM is the network surrounding the cells (produced by the cells themselves) that provides the structural and mechanical support in the tissues, and mediate the most important biological processes for tissue functionality.[31] Every tissue has a specific biological ECM microenvironment that regulates the cellular response and function, so it is important to consider this critical aspect for the design of successful tissue engineering approaches. Implanted ECM mimicking materials with or without cells into the damage site act as a template that allow cells to function as they would do in the native tissue, so they can adhere, proliferate and differentiate stimulating the formation of new functional tissues. Therefore, many efforts are currently dedicated to develop new ECM mimicking biomaterials with a wide range of properties and controlled biological responses that can be used for regeneration of different tissues.

Traditionally, ceramic biomaterials such as hydroxyapatite or tri-calcium phosphate have been used for hard tissue regeneration applications.[1,10,32] Their mechanical, chemical and structural properties, similar to the mineral phase of native bone, makes them suitable for bone and dental regeneration. Last trends in bone regeneration therapies, are focused on the preparation of functionalized bioactive ceramics and composite scaffolds combining ceramic and polymeric materials to better reproduce the ECM of the bone.[10,33-35]

Otherwise, polymeric biomaterials have been the subject of intense research in tissue engineering since the mid-twentieth century, and have a significant impact in today's health care technology.[2,17,18] The inherent properties of polymers such as their material chemistry, molecular weight, solubility, structural shape or degradability can be controlled and tuned to get the ideal scaffold for each specific application. One of the most prominent and versatile polymeric biomaterials for preparing scaffolds are hydrogels.[3,20,36] Hydrogels are 3D networks of crosslinked hydrophilic polymers with high water absorption capacity and a highly interconnected porous structure. The crosslinking design of the hydrogel network dictates the swelling ratio, porosity and mechanical properties of the gel, and it is critical to obtain favorable properties for diffusion of nutrients, cell infiltration and proliferation. Hydrogel crosslinking can be classified into chemical or physical, obtained through covalent or non-covalent bonds respectively, resulting in very different gel properties.[20,37] In addition, more elaborated strategies are based on semi- or interpenetrated polymer networks (semi-IPN or IPN respectively). They incorporate a second polymeric chain that can be trapped into a first crosslinked network (semi-IPN) or can be crosslinked forming a second network entangled into the first one (IPN). These network designs have a great interest to provide structural reinforcing to hydrogels, and also for the development of biomimetic hydrogels since their structure can better mimic the native ECM.[37,38]

According to the source of its components, hydrogels can be formed by natural or synthetic polymers. Natural hydrogels are extracted from biological systems such as plants, micro-organisms, algae, or animals, and they are widely used in drug delivery systems, cosmetics or wound healing applications. They offer the advantage of resembling the ECM of native tissues, so they are usually biocompatible, improve cellular behavior, avoid immunological reactions and have reduced toxicity, and polymers derived from mammalian ECM contain natural ligands that enhance the cellular attachment. In addition, natural polymers offer degradability through natural enzymatic or chemical processes.[18,28,29,39] The natural-based hydrogels used in TE include peptide- and protein-based materials (like collagen, elastin, silk, elastin-like polypeptides or fibrin) and polysaccharide-based materials (like alginate, chitosan, hyaluronic acid or chondroitin sulfate). Disadvantages, however, include batch to batch variation or their poor mechanical strength, which difficult the

manipulation processes. Moreover, they often require chemical modifications that can lead to toxicity, and the possible cytotoxicity of the crosslinking agents used in their preparation must be also taken into account. Improved approaches regarding manufacturing, purification, used of crosslinking agents, or control of degradation and mechanical properties, are extensively investigated to minimize their disadvantages. This kind of biomaterials have many applications for regeneration of different tissues like cartilage, bone, nerve, muscle, skin, liver and pancreas.[20,29,40]

Alternatively, many synthetic polymers, particularly those capable of forming hydrogels, have been developed for tissue engineering applications. Several have been investigated such as poly(vinyl alcohol) (PVA), poly(*N*-isopropylacrylamide) (PNIPAM), poly(ethylene glycol) (PEG), or biodegradable polymers including poly(glycolic acid) (PGA), poly(lactic acid) (PLA) or poly(caprolactone) (PCL) among others.[15,20,41,42] Synthetic-based hydrogel scaffolds can be fabricated with adjustable features including structural and mechanical properties, degradation rates and porosity. But these materials do not promote cell adhesion due to the absence of bioactive sites, which has limited their application in inducing tissue-specific regeneration.[5,15,18,23] Therefore, they can be combined with biological or chemical compounds to obtain suitable cellular responses. Current approaches in TE are focused on the combination of natural and synthetic polymers in hybrid systems in an attempt to unite the biological activities of natural hydrogels as well as the mechanical strength of the synthetic material.[18]

Additionally, there is a growing interest in the development of advanced bioinspired materials. The biomimetic and bioinspired strategy consists of the design of new biomaterials based on key characteristics of natural materials or biological structures.[43-48] This topic will be described in more detail in section 2. Polymers have particularly attracted much attention in bioinspired approaches to develop materials such as protein-, peptide-, or polysaccharide-based hydrogels resembling the natural ECM, recombinant protein-based polymers as vector-building blocks, dendrimers as promising carriers for drug delivery or synthetic polymers.[43,49-53]

Finally, a new range of biomaterials named as “smart polymers” is also being explored which does not just provide an architectural support but actively participates in the formation of functional tissue.[15,18,19] These smart materials include those that show conformational changes in response to environmental stimuli (such as temperature, ionic strength, pH, or light) or those DDS incorporating exogenous stimuli such as soluble growth and differentiation factors or bioactive molecules that can be released after implantation. In addition, the development of new biomaterials obtained through recombinant DNA technology has offered a significant improvement in the

polymer functionality.[54] These new kind of polymers may offer promise in diverse areas of TE including bioseparation, drug delivery, biosensors, microfluidics or gene therapy.

Specifically, this Doctoral Thesis is focused on the development of novel bioinspired synthetic polymers for the preparation of “smart" polymers and hybrid hydrogel systems combining natural polymers with bioinspired synthetic polymers, for TE applications.

1.3. SCAFFOLD FABRICATION STRATEGIES

Running parallel to the need of new biomaterials is the development of techniques to produce scaffolds with suitable properties using molecularly defined materials. Numerous fabrication technologies are available to transform both synthetic and natural biomaterials into scaffolds of a wide array of shapes and sizes. The fabrication technique and scaffold morphology chosen should be adapted to the application in question.[55] Here, we will discuss the main conventional and emerging advances technologies used to develop engineered scaffolds.

1.3.1. Conventional techniques

Traditional technologies to create porous scaffolds have been widely used. Inducing interconnected pore-like structures should facilitate cell infiltration and diffusion of nutrients and oxygen. Shape and size of pores as well as interconnectivity are important to mimic the target tissue. The commonly used conventional scaffold fabrication processes are solvent casting, particulate leaching, phase separation, gas foaming, melt molding, and freeze-drying. An advantage of these techniques is that they are usually compatible with different materials and they can be easily adapted for straightforward scaling-up. However, these conventional methodologies often do not provide sufficient physical and mechanical properties, and most of the techniques require high or extremely low processing temperatures.[2,3,27,56-62]

Some TE applications may require 2D scaffolds such as films or coatings. Films and coatings are usually thin non-porous scaffolds or with low porosity. Films have been frequently used in TE of the cornea, nerve regeneration, or wound healing, and coatings can be used to add specific properties to other materials, so scaffolds properties like transparency, strength or elasticity must be studied depending on the application.[63-69] Melting/dissolving and subsequent solidification is a frequently used technique, especially for synthetic materials due to the high processing temperatures. Natural-based polymers are usually compatible with less aggressive techniques such as dip coating, spray coating, spin coating, or solvent casting and subsequent drying.[70-72]

Meshes design for biomaterials has several advantages with respect to defined fiber alignment, adjustability, reproducibility and versatility. Meshes can be fabricated using electrospinning or fabric-based techniques like weaving, knitting or winding.[73] Electrospinning technique has received most of the attention. It is based on applying a difference in potential to a charged polymer solution that is deposited as fibers in the oppositely charged collector surface. This technique allows the control over the fiber direction or alignment in 2D meshes and 3D tubular constructs. Meshes fabrication techniques are highly compatible with synthetic polymer-based biomaterials. In the case of electrospinning, several natural polymers such as collagen, gelatin, chitosan or cellulose have been also used.[74-77]

1.3.2. Emergent techniques

Rapid prototyping has emerged as an advancing in the field of scaffold fabrication used for quick processing by computer aided design (CAD) and automatic manufacturing of the scaffold according to the computer design. Thus, scaffolds can be customized to match patient's individual needs. Main rapid prototyping methodologies include fused deposition modeling, stereolithography, selective laser sintering, liquid frozen deposition manufacturing, multi-jet modeling and 3D printing. The utilization of this method provides better control of the macro-shape and the microstructure of the scaffold respect to the conventional techniques. Rapid prototyping techniques are compatible with synthetic polymers since normally require high temperatures and solvents.[38,78-85]

3D bioprinting has emerged in the last few years as a powerful and very promising additive manufacturing approach for TE applications. This technique is based on the utilization of the 3D printing technique to combine cells and bioactive molecules with the biomaterials (bioinks) to fabricate more complex scaffolds. The process consists of the layer-by layer deposition of the bioink to build 3D cell laden scaffolds following a customized computer design with high precision and control over scaffold geometry, and with efficient and homogeneous cells distribution.[3,38,79,86-90] Bioprinting technique has attracted much attention because of its exceptional capacity to mimic specific properties of the native ECM.[25,26,87,91-93] It allows the fabrication of scaffolds with interconnected macro and micro-porosity for nutrients supply and cellular ingrowth.[94-96] Moreover, contrary to the conventional technologies where the seeding of the cells takes place after the scaffold fabrication (except when using electrospinning in some works), bioprinting is characterized by enabling the presence of cells during the manufacturing process.[27,97] To date, there are four main bioprinting strategies: inkjet, extrusion-based, drop-based and laser-assisted bioprinting. Each of them present different ranges of resolution, manufacturing times and limitations.[98-100] However, the main challenge of bioprinting technique is the development of

bioinks with suitable rheological, mechanical and biological properties to be printed with high resolution and shape fidelity after the deposition process as well as supporting cell viability.[27,37,101-103] Hydrogels provide a biocompatible and biodegradable environment which make them suitable for cell encapsulation, but their weak mechanical properties make them challenging to print.[86,104-110] Some strategies have been performed to overcome this limitation, such as increasing polymer concentration, rapid crosslinking, ultraviolet (UV) curing, or pre-crosslinking procedures, but cell viability can be decreased.[37,101,111,112] Consequently, a biofabrication window can be defined by varying conditions such as polymer concentration and crosslinking density, and assessing the influence on the hydrogel printability and supporting for cell culture (represented in Figure 2).[37,113] Bioprinting strategies have made a huge impact on TE field and have demonstrated their potential to generate a variety of tissues, including skin, cartilage and bone. However, current bioprinting approaches still have technical challenges in terms of high-resolution cell deposition, vascularization and innervation.[114]

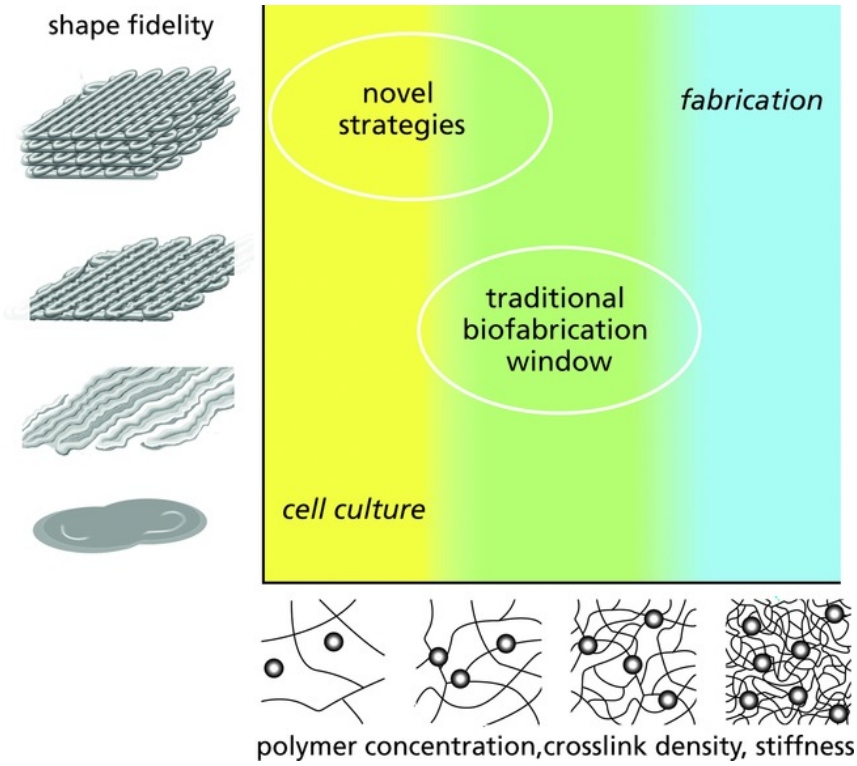

Figure 2. The image represents that a biofabrication window exists for crosslinked hydrogels compromising on both biological and fabrication properties. Reprinted with permission from Advanced materials. 2013;25(36):5011-5028, Malda

J, Visser J, Melchels FP, et al, 25th anniversary article: engineering hydrogels for biofabrication, Copyright (2013), with permission from Wiley.

Microfluidic technology also offers an attractive strategy to be used for TE applications such as single cell analysis, functional tissues for drug screening or engineering tissue-like structures. In particular, it has attracted much attention for the fabrication of 3D micro-engineered hydrogels (microgels and microfibers) with customizable chemistries and morphologies. Several microfluidics systems have been used: emulsion-based systems, flow lithograph microfluidic and fiber spinning. This technology has the advantage that enables the incorporation of cells during the manufacturing process.[38,115-118]

In conclusion, great and rapid advancements have been developed to produce structures with complex geometries for a wide variety of TE applications. However, some critical aspects need to be taken into account before clinical translation including the capacity for large scale fabrication, sterilization processes needed, rigorous quality controls for human trials and the medical costs. The achievement of on-demand fabrication of human tissues/organ structures is still a challenging issue in the scientific community together with the biomaterial and technology selection, as well as the hurdles for clinical translation, all of them issues that must be addressed in depth.[119-121]

In this Thesis, membranes and IPN hydrogel systems of developed bioinspired materials have been fabricated using conventional techniques such as solvent-casting and in the last stage, 3D scaffolds using emerging manufacturing techniques such as 3D bioprinting, were fabricated applying an innovative methodology.

2. MUSSEL INSPIRED POLYMERS FOR THE DESIGN OF INNOVATIVE MATERIALS

Recent research activities in TE and RM fields support the growing interest in the development of advanced biomimetic and bioinspired materials. The biomimetic and bioinspired concept looks at nature as a great source of inspiration for the development of biomaterials and strategies to improve TE developments. Nature provides systems with exceptional properties such as the super hydrophobicity of the lotus leaf due to its micro/nanostructure, or the highly adhesive properties of gecko's fingers, which has served as inspiration in the search of new advanced biomaterials. Scientists have observed the phenomena of nature and incorporate some of its principles to the materials science to develop materials that mimic the biological systems. Thus, biomimetic and bioinspired technology uses key features of natural materials and/or biological structures as the

basis for the design of new materials.[43-48] The process of mimicking biological systems is a very versatile concept that can proceed either at the chemical, physical or morphological level. The similarity of biological components at the chemical level can provide chemical specificity, functionality, enhanced biocompatibility, or modify biodegradability. In addition, by reproducing architected morphologies or structures of biological systems, bioinspired materials can offer aspects such as sophistication, miniaturization, hierarchical organizations, resistance, and adaptability. Bioinspired polymers have particularly raised a lot of attention in the last few years for bioinspired approaches based on DDS, self-healing materials, wound healing bandages, antibacterial surfaces or stimuli-responsive materials among others.[43,49-53] The development of advanced biomaterials intended to actively participate in functional TE processes is an important aspect of the research pursuits in the TE and RM fields.

Marine mussels have the ability to strongly anchor to rocks under harsh marine conditions through the secretion of a byssus of adhesive mussel foot proteins (Mfps). In 1981 this adherence was attributed by Waite and Tanzer to the presence of an amino acid called L-3,4-dihydroxyphenylalanine (DOPA), one of the main constituents in Mfps containing catechol groups (Figure 3).[122-126] Since then, this remarkable natural form of adhesion has been a source of inspiration to develop bioadhesive polymers that adhere to biological interfaces.

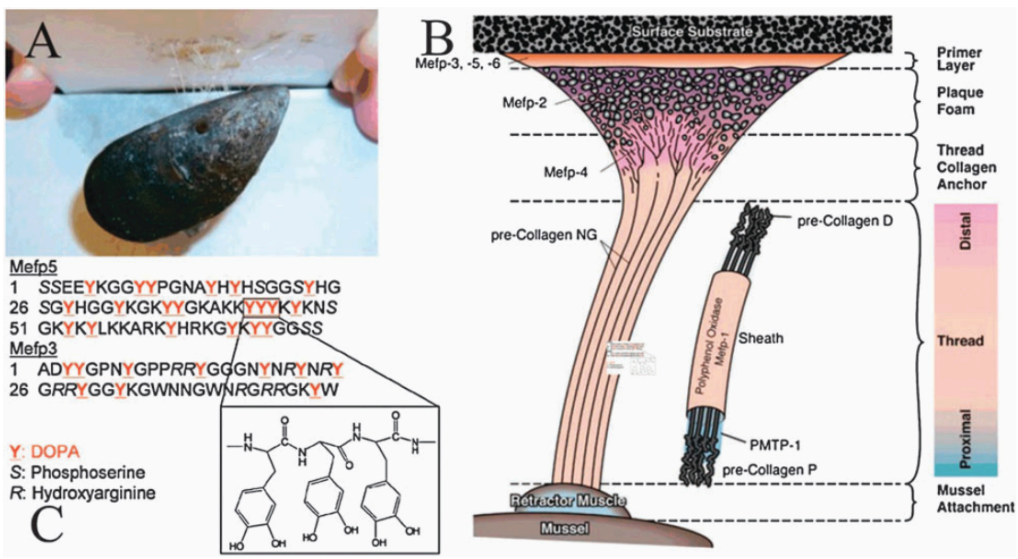

Figure 3. (A) Photograph of blue mussel binding to Teflon. (B) Location of adhesive-related proteins identified in the byssus of *Mytilus edulis*. (C) The amino acid sequences of Mefp-3 and Mefp-5. Reprinted from Chem Soc Rev. Jul 2011;40(7):4244-

Catechol groups are aromatic derivatives with two neighboring ortho-hydroxyl groups present ubiquitously in nature. These polyphenols take part in a remarkable variety of processes in living organisms such as mussels, squids and sandcastle worms, or food processes such as tea preparation.[127-131] In recent years, the design of synthetic catechol-functionalized polymers in materials science has increased to pursue a wide variety of TE applications.[132,133] The interest in developing catechol-functionalized polymers in TE, mainly lies in their bioadhesive properties in wet conditions but also in their recognized biological properties, due to its potent antioxidant activity and anti-inflammatory action. Natural phenolic compounds possess important antioxidant activity, higher even than vitamins.[134-137] Catechol has been demonstrated to have a great ability to scavenge free radicals such as reactive oxygen species (ROS) or reactive nitrogen species (RNS) mainly due to their redox properties.[138-144] Furthermore, catechol has shown great potential to mitigate inflammatory damage, as documented in the literature.[145-148] These activities can be beneficial for numerous biomedical applications. Likewise, catechol possesses a great functional versatility that can be explained by its chemistry.[133] In this context, this Thesis has explored the use of catechol containing polymers for the development of bioinspired materials and bioactive supports for TE and RM applications. The following subsections will describe the overall study of the crosslinking chemistry of catechol, the different routes of catechol containing polymers preparation and their most important biomedical applications, showing the potential of this chemical functionality to afford promising biomaterials for relevant TE and RM applications.

2.1. CHEMISTRY OF CATECHOL

Catechol groups can bind to different organic (e.g., amino acids, polymers) and inorganic (e.g., metal ions, metal oxides, silica, ceramics) compounds through the formation of covalent or reversible non-covalent interactions, although the adhesion mechanisms are still under debate.[126,133] Covalent crosslinking pathways rely on the catechol "auto-oxidation" to the *o*-semiquinone radical (one-electron oxidation) and finally to *o*-quinone (two-electron oxidation). Oxidation can be produced either by oxygen, enzymes present in natural systems (e.g. tyrosinase, horseradish peroxidase/H_2O_2) or chemical oxidants (e.g. sodium periodate).[149,150] The resulting oxidized form becomes highly reactive and it is susceptible to participate in intermolecular covalent reactions with nucleophilic groups such as amine groups, thiol groups or aryloxy radical couplings via Michael addition or Schiff base reaction.[151,152] Additionally, the *o*-quinone can react with other catechol groups leading to dimers formation and the subsequent polymerization.[153]

Catecholamines can also undergo oxidative self-polymerization via intramolecular cyclization, which was firstly demonstrated by Messersmith *et al.* for the widely used molecule dopamine.[153] These oxidation processes are highly influenced by multiple important factors such as pH, ring substituents, nucleophilic strength, the oxidant used etc. For example, the crosslinking degree increases at higher pH, because of a higher conversion of catechol to quinone. Variation of these factors allows tuning the kinetics of the oxidative reactions.

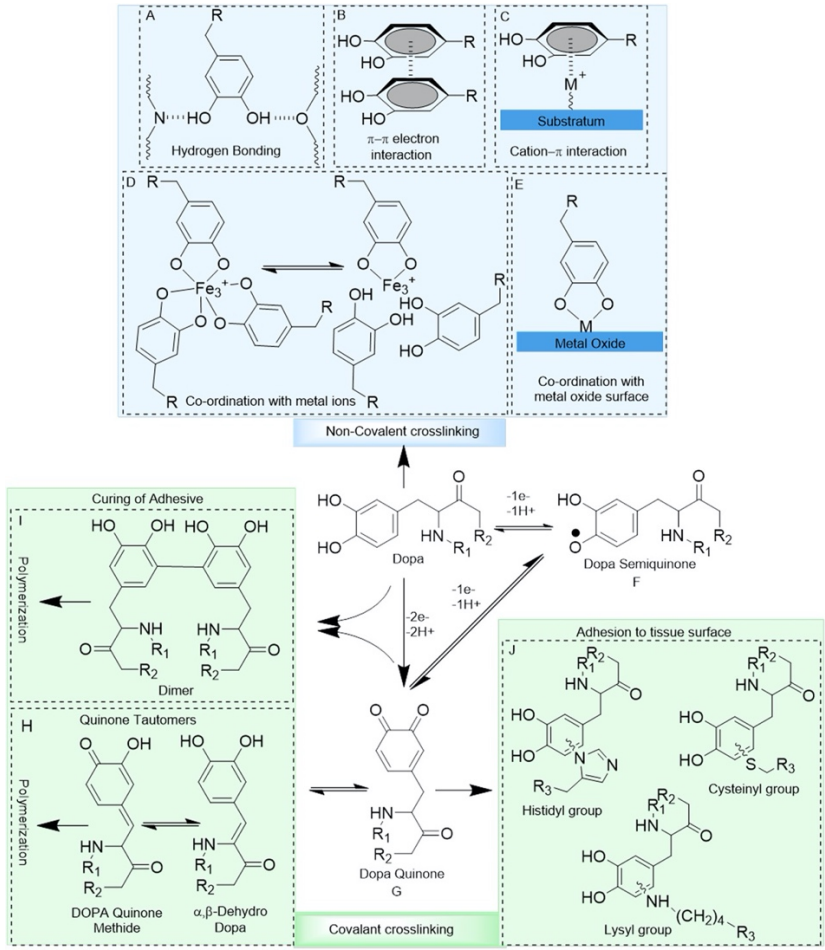

Figure 4. Possible interactions and reaction products of the catechol side chain of DOPA. Catechol forms hydrogen bonds through its -OH groups (A), pi–pi electron interaction with another benzene ring (B) and, cation–pi interaction with positively charged ions (C). Catechol chelates metal ions to form self-healing crosslinking (D) and, forms co-ordination bonds with metal oxide surfaces (E). DOPA oxidizes to its semiquinone and quinone forms which are highly reactive (F, G). Quinone

tautomerizes to form quinone- methide and a,b-dehydrodopa, leading to the subsequent polymerization of the catechol group (H). Quinone also forms dimers with another catechol moiety, resulting in dimer formation (I). Quinone reacts with nucleophiles (i.e., $-NH_2$, –SH) found on tissue surface, resulting interfacial covalent crosslinking (J). (Waiting for reprinting permission). Reprinted from Journal of Polymer Science Part A: Polymer Chemistry. 2017;55(1):9-33, Kord Forooshani P, Lee BP, Recent approaches in designing bioadhesive materials inspired by mussel adhesive protein, Copyright (2016), with permission from Wiley.

Furthermore, catechol groups can also form non-covalent interactions. Thanks to the phenyl groups, catechol can form hydrogen bonds, which have been associated to a better absorption to mucosal tissues and hydroxyapatite surfaces.[122,154] Catechol aromatic ring is able to form Π-Π electron interactions with other aromatic rings, or cation-Π interactions, which enables to improve the cohesive properties and the surface attachment to materials rich in aromatic or cationic functional groups.[150,155-158] In addition, catechol groups can form strong and reversible coordination bonds to different metal ions including Cu^{2+}, Zn^{2+}, Mn^{2+}, Fe^{3+}, V^{3+}, Ti^{3+} and Ti^{4+}.[133,159-161] Iron and other metals have been found in mussels adhesives in unusually high concentrations and they can play a key role in the mussel adhesive process.[133] The complex stoichiometry is influenced by the valency of the ion, the catechol:ion molar ratio, the ionic strength and the pH.[161,162] It has also been proposed that metal ions can oxidize catechol groups to form *o*-quinones and mediate covalent bonds.[133]

In brief, the chemistry of catechol is very versatile. Some reaction pathways have been identified but the detailed mechanisms of some crosslinking reactions is still matter of debate. An understanding of the catechol chemistry is important for the development of advanced catechol-based materials. Figure 4 presents a brief scheme of the crosslinking chemistry of catechol groups.

2.2. STRATEGIES FOR PREPARING CATECHOL-FUNCTIONALIZED POLYMERS

The design and preparation of synthetic catechol-functionalized polymers has increased in order to develop functional polymers for TE applications, especially water-resistant bioadhesives. These synthetic catechol-functionalized polymers have been prepared through different strategies.

The first strategy consists of the functionalization of a monomer with catechol groups, and the subsequent polymerization to obtain catechol containing polymers.[163-165] For example, the catechol-modified monomer dopamine methacrylamide (DMA) has been copolymerized with different acrylate and vinyl comonomers, and dopamine pendant polymers with a broad variety of properties have been obtained.[166,167] By varying the comonomers compositions, copolymers with

different properties can be prepared using, for example, bifunctional crosslinkers to provide 3D polymer networks, or polymer end-functionalized with an initiator to prepare block copolymers.[168-170] Since catechol groups are susceptible to oxidation, protection of the phenyl groups during the polymerization can be a useful tool for its preservation and to avoid undesirable chemical reactions.[126]

Another strategy is the direct functionalization of polymers with catechol molecules. Catechol containing molecules such as dopamine or eugenol can be directly conjugated to polymers with different functional groups through the formation of amide, urethane, or ester linkages. This strategy has been used to conjugate natural-based polymers such as hyaluronic acid, chitosan, gelatin or alginate in order to obtain biomaterials with bioadhesive properties. [126,171] Also, this strategy can be adopted to conjugate polymers with different architectures (branched or block copolymers) like PEG.[172-174]

A different strategy consists of using catechol-functionalized initiator for the polymer synthesis. Polymers end-functionalized with catechol molecules can be obtained through reversible addition-fragmentation chain transfer (RAFT), atom transfer radical polymerization (ATRP) or ring-opening metathesis polymerization (ROMP).[175-178]

Considering the biological properties of the catechol groups, catechol-containing polymers obtained through the three strategies explained before could be encompassed within the concept of "polymer therapeutics" firstly introduced by Ringsdorf in 1975.[179] The family of covalent polymer is a special type of polymer therapeutics drug-conjugates based on the covalent link between a drug or a bioactive molecule and the macromolecular backbone through a physiologically labile bond.[180] They can be prepared by initial reaction to link the bioactive molecule to a monomer and a subsequent polymerization, or by conjugation reaction of the bioactive molecule to the polymer (as pendant groups or at the end groups of the polymer chain). Ringsdorf's model provides different chemical possibilities to design covalent polymer-drug conjugates based on three different areas (solubilizing groups, drug or bioactive molecules and transport system), which can be a useful tool for specific applications such as drug delivery systems.[181,182]

Additionally, catechol-containing peptides have been prepared through solid-phase peptide synthesis or recombinant genetic engineering methodologies. Solid-phase peptide synthesis has been used to obtain peptoids end-modified with DOPA containing peptide, and recombinant technology allows replicating peptide sequences found in Mfps.[183,184]

2.3. CATECHOL IN BIOMEDICAL APPLICATIONS

As mentioned above, the incredible water-resistant adhesive property of Mfps has inspired biomaterials scientists to develop a wide array of advanced catechol functionalized materials. In addition, these catechol groups will provide the material with potent biological properties such as antioxidant and anti-inflammatory activities. The versatile chemistry of catechol has been a useful tool to design catechol-functionalized polymers for a wide range of biomedical applications including adhesive for biological tissues, coatings for biological and clinical devices, drug delivery systems, and bioactive scaffolds for TE applications.[185-187] The most important medical applications are explained in this section.

Tissue adhesives can be a useful tool to replace suture and staples and simplify the surgical processes. However, commercially available adhesives usually have some limitations such as toxicity concerns or low adhesive strength. Inspired by the mussel adhesion mechanism, natural and synthetic polymers have been functionalized with catechol groups to prepare biocompatible adhesives that can adhere to biological tissues in moist environments,[163,188-194] which remains as a big challenge in clinical applications.[195,196] Controlling some important factors such as oxidation of the catechol groups, swelling ability, degradation rate, biocompatibility and hemostasis is critical for the success of the bioadhesive polymers. Important progress is being made toward the achievement of bioadhesive mussel-mimetic polymers using synthetic and/or natural polymers able to repair both soft and hard tissues.[171,197-201]

The strong adhesion of DOPA to different surfaces offers many opportunities for the development of bioinspired polymers for coatings. Messersmith and co-workers pioneered the use of polydopamine coatings trough a straightforward coating method based on the auto-oxidation of dopamine and the *in situ* deposition on a wide range of substrates.[185,202] In addition, the authors opened up the possibility to use polydopamine films to react with nucleophilic groups trough Michael or Schiff base reactions to allow immobilization of organic species on top. In this regard, catechol groups can be useful to immobilize a polymer coating onto a surface, or to enhance the adhesive strength of the surface, which may be important for anchoring biomolecules and improve the cell proliferation during the clinical process.[164,203-205] An important amount of research has been carried out for tethering different coatings including: anti-fouling coatings with excellent protein-, bacterial and cell-resistant properties; orthopedic implant coatings for bone regeneration; or heparin-mimetic coatings for enhancing the blood compatibility of biomedical devices. Catechol coatings have a wide application prospect in the field of medicine.[206-209]

Catechol-functionalized polymers have also found important applications in TE and RM fields due to its wet adhesive properties, biocompatibility, and biological abilities, which can be used to enhance the bioactivity of the system. Particularly, catechol-derived injectable and membrane hydrogels (natural and/or synthetic based) have been explored.[188-194] For example, Huber *et al.* developed a bioactive chitosan based hydrogel with anti-oxidant and anti-inflammatory properties coming from catechol derivatives which are used as crosslinkers;[139] or Han *et al.* developed an adhesive and tough polydopamine-clay-polyacrylamide hydrogel with enhanced cell attachment and proliferation.[189] Several self-healing hydrogels have been prepared using the ability of catechol to form strong reversible bonds with various metal ions, such as polyacrylates and polymethacrylates with tunable stiffness.[210] Catechol-functionalized hydrogels have been also studied for the development of DDS, such as the work of Ren *et al*., where a dopamine-based injectable polysaccharide hydrogel was developed with great potential for localized drug delivery in Parkinson's disease treatment.[211] Results seemed to be encouraging, although drug release still must be studied.[211,212] In addition, catechol-functionalized polymers have been used for the preparation of nanoparticles for drug encapsulation, ROS inhibition, and inflammation regulation among others, or to be anchored to the surface of nanoparticles.[213-217] Finally, some emerging research has been conducted in the use of catechol hydrogels as bioinks for 3D printing technology: Lee *et al.* developed a writable chitosan-catechol bioink,[218] and Guo *et al.* reported the development of a catechol-containing naturally derived double-network as a potential bioink.[219] This research possesses a great upcoming potential for promising candidates for TE, although some challenges must be still addressed.

In summary, the versatile chemistry of catechol allows the preparation and development of numerous bioadhesive platforms with enhanced bioactivity for a wide range of biomedical applications, with a very promising outlook. In this sense, this Thesis intends to provide new insights on the design and application of catechol functionalized polymers as bioactive systems that can actively participate in tissue regeneration processes.

3. TISSUE ENGINEERING FOR WOUND HEALING AND SKIN REGENERATION

Wound healing refers to the process of replacement or restoration of the damaged tissue by living tissue to reestablish its function. It is a stepwise process that comprised three integrated stages: (1) hemostasis and inflammation, characterized by macrophage or leucocytes infiltration and cytokine secretion; (2) proliferation, that involves the damaged tissue removal, granulation tissue

development, angiogenesis and re-epithelialization; (3) maturation, when ECM produced becomes well-defined; and finally remodeling or the scar tissue formation and the achievement of functional skin tissue. These complex stages involve the interaction of different types of cells, bioactive molecules and the ECM as supporting platform.[220,221] The wound healing process is relatively similar in all kinds of tissues and organs, including skin. Large trauma skin wounds due to burns or accidents and several disease conditions such as diabetes can lead to the malfunction of the process and the formation of chronic wounds, which represent a major healthcare problem[222-225]. In chronic wounds the healing process gets obstructed usually at the initial phase and differs from the regular healing pattern of skin, becoming particularly difficult to heal. Tissue engineering wound healing strategies are based on providing an artificial scaffold (wound dressing or skin graft) as a provisional matrix for cells to proliferate and regenerate the damaged tissue (an overview schematic representation can be found in Figure 5). Thus, the development of efficient wound dressings or constructs to assist and enhance the healing process in chronic wounds constitutes a significant target in regenerative medicine.[222,226-228] Bioinspired approaches described in this Doctoral Thesis aim to provide *in situ* bioactive activities to the biomaterial that can help to promote the tissue regeneration and the healing of chronic wounds.

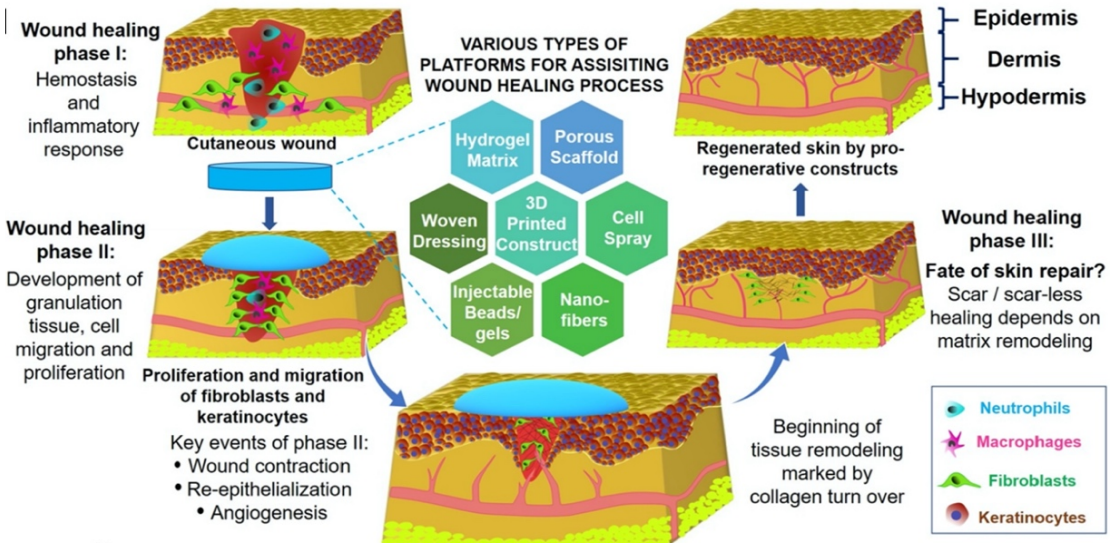

Figure 5. Schematic representation depicting concept of wound healing process assisted by a dressing material or skin graft. Wound healing process comprises of three major phases and their key events as described in the diagram. (Waiting for reprinting permission). Reprinted from Biomaterials, Vol 216 Sep 2019;216:119267, Chouhan D, Dey N, Bhardwaj N, Mandal

BB, Emerging and innovative approaches for wound healing and skin regeneration: Current status and advances, Copyright (2019), with permission from Elsevier.

3.1. RECENT TE APPROACHES FOR WOUND HEALING

Tissue engineered scaffolds for wound healing purposes should be non-immunogenic, biocompatible, bioresorbable and porous. Also, the matrix should show good integration to the wound, appropriate mechanical strength (similar to the skin) to provide physical support, barrier properties to protect the wound, and capability to enhance the tissue healing.[224,229] The desing of a suitable scaffold for skin tissue engineering involves the selection of an appropriate biomaterial, cell type and architectural structure of the platform.

During the last 30 years numerous natural polymers like collagen, chitosan, fibrin, gelatin, cellulose, silk and hyaluronic acid among others, have been investigated for this purpose.[230-233] Several commercial wound dressing products have been developed based on matrix proteins. Likewise, some synthetic polymers like PVA, PGA, PLA or PCL, have been widely explored with the advantage that they can be customized.[234] Also, hybrid scaffolds of natural/synthetic polymers have attracted much attention for skin regeneration. During the last five years, the development of bioactive natural or synthetic scaffolds with cell instructive cues has been an important focus of investigation in wound regeneration strategies. In this manner, scaffolds can serve as a niche for cells to proliferate but also to provide them cues that can trigger the regeneration process to restore the damaged tissue.[235,236] In this context and moreover with the aim of incorporating additional properties to the system, new approaches have been explored based on the functionalization of scaffolds with bioactive molecules like growth factors, drugs, antimicrobial molecules, other bioactive agents and nanoparticles or cell binding peptides. Two different strategies have been attempted: bioactive molecules are permanently linked to the scaffold to stimulate cells; or they are linked to the scaffold and afterwards slowly delivered to the wound site.[237-241]

Cell therapy has emerged as a promising modality to enhance the wound healing process.[242,243] Cell seeded scaffolds provide a 3D microenvironment or biomimetic niche that help to preserve the integrity of tissue architecture during the healing process, and recapitulate fetal wound regeneration.[244] Stem cells therapies are particularly attractive as they play a key function in the tissue regeneration process.[245-247] Moreover, different advanced cellular therapies such as effect of immunomodulation for enhanced angiogenesis or micro RNA (miRNA) and small interfering RNA (siRNA) based skin therapeutics are being explored.[220]

Another critical point in skin regeneration lies in the structural engineering of the scaffolds.[234,248] Different kind of matrices with different properties have been used depending on the particular type of wound: woven/non-woven mat, nanofibrous matrices, porous scaffolds, bilayer or trilayer constructs, hydrogels, injectable systems, micro-spheres and 3D bioprinted grafts.[249-254]

Electrospun nanofibrous mats are easy to functionalize and they have demonstrated to serve as successful delivery systems for bioactive molecules. Their nano-range architecture helps in the cells recruitment, binding and migration to the wound site, however cell infiltration is an important limitation.[249,255-257] Microporous scaffolds have been explored as tissue engineered skin grafts since interconnected pores provide a suitable 3D microenvironment that allows cell migration and cellular ingrowth promoting angiogenesis.[250-252] Commercially available examples of microporous scaffolds have been used as dermal grafts such as Integra® or Matriderm®. Hydrogel matrices have shown great potential as microporous constructs for skin regeneration since they closely mimic the native ECM structure. In this sense, bioadhesive and *in situ* forming injectable hydrogels have been developed during the last five years. The principal advantage of these materials is that they are easy to apply and can fit the exact shape of the wound without needing sutures or glue. They hold great promise in wound healing as stimuli responsive hydrogels, drug delivery systems and hemostatic materials.[253,254,258] Microfluidic technology has also shown great potential in this area in the developing of injectable microspheres or microgels.[259,260]

In the last years, 3D bioprinting technology has revolutionized this field with important advances in the fabrication of skin tissue constructs or skin grafts.[79,261-264] This advanced additive manufacturing technology has shown great potential to manufacture complex structures with extraordinary control over geometry. Advantages of this technology are : 1) fabrication of wound dressings with well-defined dimensional properties such as thickness or pore size to match the defects; 2) fabrication can be achieved in a reproducible manner, since scaffolds can be designed by computer software and the process is automatized; 3) geometry, materials and formulation doses can be tailored based on patient requirements; 4) cell-laden 3D scaffolds with homogeneous dispersion of encapsulated cells can be obtained;[265-267] 5) the possibility to define "hierarchy" or stratified structure similar to the skin structure, which is not easy to replicate by any other fabrication method. The development of a suitable bioink and the appropriate mechanical stiffness of the matrix need to be taken into account.

Furthermore, other innovative approaches have been proposed for skin therapies using smart technologies such as portable 3D printers, spray based technology or portable electrospinning.[220]

3.2. WOUND CARE IN THE CLINICAL SETTING

Efficacy of wound dressings and skin grafts has been evaluated through regulated clinical trials. Application of allografts is still a common and cost effective practice considered as a good option for the treatment of burn and trauma wounds. The use of decellularized human amniotic membrane and umbilical cord (AM/UC) has received especial attention since they have been proven not to provoke immunological rejection.[268] Epifix® (dehydrated human amnion/chorion membrane), Grafix® (placental allograft) and Neox® (cryopreserved human AM/UC tissue dressing) are some efficient grafts made using these decellularized tissues.[269-271] Acellular bioengineered skin grafts have been also explored in clinical trials, both as dermal and epidermal or skin grafts. For example, Integra® is a porous scaffold of collagen and glycosaminoglycan (GAG) covered with silicone layer used as dermal graft found to be successful in the management of complex and devastating wounds.[272] Matriderm® or Hyalomatrix® are other acellular dermal grafts based on bovine collagen or hyaluronic acid matrix respectively, indicated for burn, acute and chronic wounds.[273,274] In addition, cellular commercially available skin substitutes are found. Dermagraft®, composed of a polyglactin mesh seeded with fibroblasts, has been found to be very effective in treating diabetic foot and venous leg ulcers.[275] Clinical trials on others living cellular grafts like Apligraf®, CEA® and Orcel® have demonstrated their safety and efficiency.[221,276,277]

Over the past several years, different commercially available skin grafts or wound dressings focused on different types of wounds have shown clinical promise. However, while many advanced constructs and wound dressings have been reported in the 2-3 decades just a minority of materials have undergone clinical trials. Therefore, more clinical analysis needs to be done to translate the novel advanced materials and technologies to the clinic. Furthermore, more research must be performed following the recent TE strategies (explained in section 3.1) specially focused on functionalized scaffolds with cell instructive cues for promoting the wound healing process, and in the use of emerging technologies such as 3D printing to develop more advanced materials. As mentioned above, in this Thesis, novel mussel-inspired systems have been used to develop different supports such as porous membranes, or 3D bioprinted scaffolds for cell therapies. Thus, the application of these materials for wound healing purposes has been explored since the great bioactivity provided by the catechol groups can favorably act to enhance the tissue regeneration process and to promote the skin healing. The future trend of bioactive TE strategies for wound healing open gates for novel therapies that can accelerate the healing process, diminish the pain and improve the quality of life of the patient.

Objectives

The general objective of this Thesis is to explore the use of novel mussel-inspired polymers in the development of advanced materials for regenerative medicine applications, such as osteochondral and skin regeneration. The bioactivity and outstanding versatility of the catechol functionality allow fabricating numerous advanced materials and scaffolds from 2D structures to 3D scaffolds using different techniques, and exploring cell therapies. Thus, this Thesis covers all aspects of molecular design, catechol containing polymers preparation, fabrication of scaffolds and nanoparticles, properties analysis, and study of the biological behavior of the developed systems. In order to achieve this global objective, 5 scientific works are collected along the chapters in accordance with the more specific objectives described below.

-The first specific objective of this Thesis is the preparation and study of "smart" polymers with bioadhesive and thermosensitive properties for potential applications in drug delivery systems or ostechondral regeneration processes. Specifically, in **Chapter 2** we aim to investigate the influence of low molecular weight copolymers composition on the final properties of a family of designed mussel-inspired systems. For this, a flexible long-arm catechol acrylic monomer will be synthesized and subsequently reacted with the thermosensitive monomer *N*-vinylcaprolactam by free radical copolymerization varying feed monomers ratios. The family of copolymers obtained will be structurally characterized by different techniques in terms of thermal properties, thermosensitivity, antioxidant activity and bioadhesion performance versus bone tissue. Biological cytotoxicity and anti-inflammatory activity using fibroblasts and macrophages will be also analyzed.

-Second specific objective is aimed to design a family of catechol-conjugated polymers and investigate its bioactive properties for its potential application as wound dressings. In **Chapter 3**, we aim to synthetize and design 2D films of catechol conjugated polymers, and to investigate the influence of the catechol composition on the structural and biological properties of the films. To reach that goal, statistical copolymers of *N*-vinylcaprolactam and 2-hydroxyethyl methacrylate will be synthesized and a catechol bearing molecule will be subsequently conjugated. The pathway via postpolymerization conjugation reaction will provide flexible long-arm catechol conjugated terpolymers with high molecular weights and enhanced availability of the catechol side groups. 2D films of the synthesized catechol conjugated polymers will be fabricated and their wound promoting activities will be evaluated, such as bioadhesive properties versus porcine skin, biological cytotoxicity, antioxidant and anti- inflammatory properties using stem cells and macrophages respectively, and their ultraviolet screen ability.

-The third individual objective of this Thesis is to address the development of IPN hydrogels for the effective treatment of chronic wounds. **Chapter 4** describes the preparation of a hybrid system combining the beneficial properties of natural polymers and a catechol conjugated terpolymer and investigates its applicability as a bioactive wound dressing. The IPN hydrogel scaffold proposed is developed in a two-step process: firstly, a hydrogel backbone is obtained through a self-covalent crosslinking between chitosan and oxidized hyaluronic acid in the presence of the catechol conjugated terpolymer. Secondly, catechol groups of the terpolymer are ionically crosslinked with Fe^{3+}. The structural analysis, *in vitro* behavior and catechol release profile, bioadhesion against porcine tissue, *in vitro* biological behavior using stem cells and *in vivo* biocompatibility of the IPN scaffolds in a rat model will be studied for potential wound healing applications.

-The last specific objective of this Thesis lies in the fabrication of 3D printed hydrogel scaffolds for cell therapies tissue engineering strategies and it is addressed in two stages.

The first stage addressed in **Chapter 5** deals with the development of a novel 3D printing approach to overcome the poor printability and low stability of the currently obtained hydrogel structures due to their weak mechanical properties. This novel bioprinting methodology is based on a dual-syringe system provided with a static mixing tool that allows *in situ* crosslinking of a two-component hydrogel-based ink in the presence of living cells. The reactive hydrogel system consists of carboxymethyl chitosan and partially oxidized hyaluronic acid that will undergo fast self-covalent crosslinking via Schiff base formation. A bioink optimization study will be performed to match crosslinking kinetics with the printing process, as well a structural and biological characterization of the cell laden printed structures.

The second stage described in **Chapter 6** addresses the 3D bioprinting approach developed in the first stage to fabricate 3D bioprinted hydrogel constructs loaded with novel catechol functionalized nanoparticles for their application in wound care management. The system combines the beneficial properties of the biomimetic hydrogels based on carboxymethyl chitosan and hyaluronic acid with those of the bioactive nanoparticles. Previously, preparation of self-assembled nanoparticles of two amphiphilic catechol-containing terpolymers will be carried out, as well as the study of their drug encapsulation ability and their characterization at both structural and biological levels. Subsequently, 3D cell-laden scaffolds will be developed and their *in vitro* and rheological behavior, nanoparticle release profile, and *in vitro* biological performance using fibroblasts, macrophages and endothelial cells will be investigated to assess its applicability for promoting wound healing.

Methodology

Methodology of the synthesis of monomers, polymers, catechol polymer conjugates, materials fabrication, and their physico-chemical, i*n* vitro behavior and biological characterization performed in this Thesis, are exposed below. Nomenclature used in the following sections corresponds to the one used in the respective papers.

1. SYNTHESIS OF CATECHOL FUNCTIONAL POLYMERS

Catechol containing polymers have been synthesized following two different strategies: 1) functionalization of a monomer with catechol groups and the subsequent free-radical polymerization to obtain catechol statistical copolymers, and 2) direct functionalization of a copolymer with catechol molecules to obtain catechol conjugated terpolymers. In addition, different natural polymers have been used for hydrogels materials preparation as it is shown along the different articles recompiled in the chapters, some of them were used as received while others were modified prior to use.

1.1. SYNTHESIS OF A CATECHOL-CONTAINING MONOMER AND COPOLYMERS

The catechol-functionalized [2-(3-(3,4-dihydroxyphenyl) propanamido) ethyl methacrylate] monomer (named as **CEMA**) was prepared using the catechol functionality of hydrocaffeic acid (HCA). Preparation consisted of the reaction between the carboxylic group of HCA and the amine group of 2-aminoethylmethacrylate hydrochloride (AEMA), using *N-(*3-Dimetilaminopropil)-*N*′-etilcarbodiimida/*N*-hidroxisuccinimida (EDC/NHS) as coupling agent, while phenol groups of catechol were protected with $Na_2B_4O_7$. Subsequently, random copolymers were obtained by free radical copolymerization reactions of CEMA with *N*-vinylcaprolactam using 4,4'-azobis(4-cyanovaleric acid) (ACVA) as initiator and CEMA contents in the feed of 0.1, 2.5, 3.5 and 10 mole %, giving rise to low molecular weight copolymers (**VCL_CEMA**) with CEMA contents of 0.9, 2.3, 3.6 and 13.5 mole % respectively. Further details of the polymers preparation are explained in **Chapter 2**. A scheme of the monomer and copolymer synthesis is represented in Scheme 1.

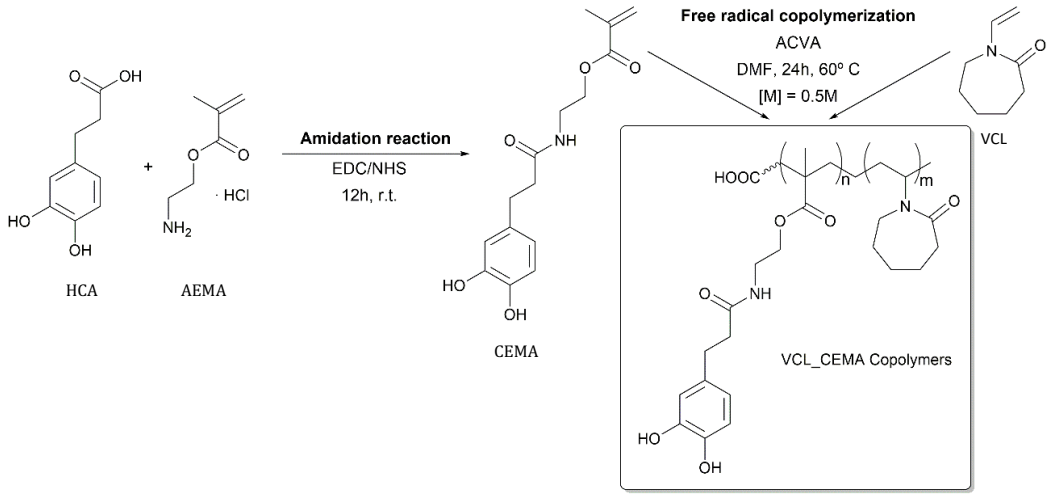

Scheme 1. Synthesis of CEMA monomer and VCL_CEMA copolymers.

1.2. SYNTHESIS OF CATECHOL CONJUGATED POLYMERS

First, *N*-vinylcaprolactam (V)-co-2-hydroxyethyl methacrylate (H) statistical copolymers (VH) were obtained by free radical copolymerization initiated by azobisisobutironitrile (AIBN). Two different V:H molar % feed compositions of the monomers were used: 80:20 and 60:40, giving copolymers with H contents of 16 and 36 mol % respectively (copolymers were designated as **VH16** and **VH36**). Secondly, catechol conjugated polymers were obtained by a conjugation reaction between a fraction of the hydroxylic groups of the H units in the VH16 and VH36 copolymers and one equivalent of the chloride acid derivative of the hydrocaffeic acid previously synthesized (HCCl) giving catechol conjugated terpolymers with catechol fractions of 2 and 22 mol % respectively. Terpolymers (VHC) were designated by the catechol composition values as **VHC2 and VHC22**. Further details of the polymers preparation are explained in **Chapter 3**. Terpolymer VHC22 was used in **Chapter 4** and designated as **T**. In **Chapter 6** VCH terpolymers with 2 and 29 molar % catechol contents were used, designated as **T2** and **T29** respectively, of which T29 was synthetized applying the methodology previously described in this section The synthesis schemes of the acid chloride derivative HCCl, VH copolymers, and the VHC catechol conjugated terpolymers are illustrated in Scheme 2.

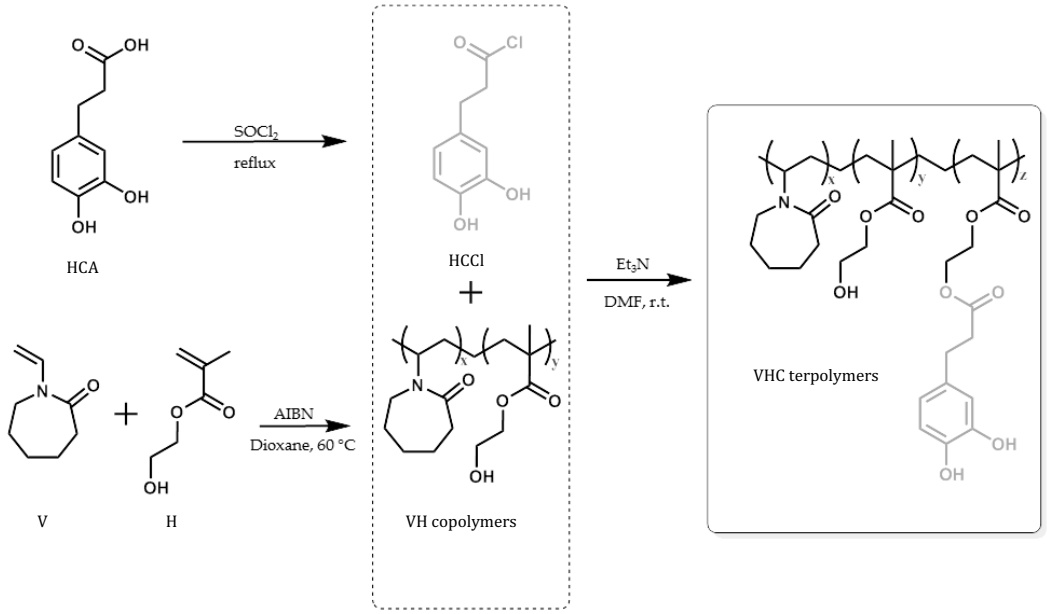

Scheme 2. Scheme of the synthesis of the acid chloride derivative HCCl, VH copolymers and the VHC catechol conjugated terpolymers.

2. NATURAL POLYMERS

Gelatin (pharmaceutical grade, pork skin origin, type A) was used in **Chapter 2** in order to test the bioadhesive properties of VCL_CEMA polymers. Following a bioinspired strategy, gelatin was used to simulate the mussel adhesion proteins in a gelatin-copolymer mixture.

Chitosan (**Ch**, degree of deacetylation 90%, M_w = 14 kDa, Altakitin) was used in **Chapter 4** to prepare interpenetrated hydrogel networks. The water soluble derivative carboxymethylchitosan (**CMCh**, degree of deacetylation 85 – 90 %, viscosity = 5-300 mPas, Chitoscience from Heppe Medical) was used in **Chapters 5 and 6** to prepare 3D printed cell-laden scaffolds.

In **Chapter 4**, sodium hyaluronan (**HA**) of high molecular weight (M_w ~ 814 kDa, Bioiberica,), was oxidized (**HA-ox**) according to an adaptation of an already reported method,[278] obtaining a highly oxidized hyaluronic acid (86.5 ± 5 %. oxidation degree). In **Chapters 5 and 6**, sodium hyaluronan of low molecular weight (M_w ~ 200 kDa, Bioiberica) was oxidized prior to use as reported elsewhere,[279] with a final oxidation degree of 48 ± 3%.[280,281] Further details of the polymers modification are explained in the corresponding chapters. Likewise, sodium hyaluronan (M_w ~1.5-1.8 x 10^6 Da, Sigma Aldrich) was used as a supplement in the ink formulations used in both chapters.

3. MATERIALS FABRICATION

Numerous materials have been fabricated in this Thesis using both synthesized and natural materials, and different fabrication techniques. The fabrication technique and scaffold morphology chosen from 2D to 3D structures was adapted to the application of each material. Further details can be found along the corresponding chapters.

3.1. 2D FILMS PREPARATION

2D films were prepared using the catechol conjugated polymers VHC2 and VHC22 synthesized in **Chapter 3**. Thin films were obtained by a casting/solvent evaporation technique with final average thickness of 12 ± 3 μm. Materials are designated as **VHC2 and VHC22 films**.

3.2. IPN HYDROGEL MEMBRANES PREPARATION

Hybrid IPN hydrogel membranes were prepared in **Chapter 4** using Ch, HAox and the catechol conjugated terpolymer containing 22 mol % of catechol fraction, T. The hydrogel backbone was obtained through a self-covalent crosslinking reaction between Ch and HAox in the presence of T which was subsequently coordinated to Fe^{3+} to obtain the interpenetrated polymer network. The resulting IPN sample was called as **Ch/HAox/T/Fe membrane**. In parallel, crosslinked Ch/HAox and semi-IPN Ch/HAox/T samples were obtained following similar procedures for comparison purposes.

3.3. 3D PRINTING OF SCAFFOLDS

3D printed hydrogel scaffolds were prepared in **Chapters 5 and 6**. In **Chapter 5**, a novel printing methodology is described in which the 3D Discovery printer (RegenHu, Switzerland) was modified to adapt a static mixing tool. Briefly, two similar syringes were loaded with the hydrogel precursors solutions (A and B). The solutions were simultaneously extruded by mechanical printer motor into the static mixing tool in a 1:1 ratio, where they were mixed and immediately began to crosslink. Finally, the crosslinked hydrogel was extruded through the needle. 3D scaffolds were fabricated using a 2 layer grid square design. A cytocompatible post-printing stabilization step was carried out by immersion of the scaffold in a $FeCl_3$ solution. 3D printed scaffolds were fabricated using this novel printing methodology. In **Chapter 5**, the composition of the two separate precursors solutions was: A) CMCh solution loaded with L929 fibroblasts, and B) HAox or HAox with

supplemented HA solution. Scaffolds developed in this chapter were designated as **CMChn/HAoxn-HAn**, where *n* corresponds to the weight percentage of the precursor solution. In **Chapter 6**, bioink was formulated similarly in two different hydrogel precursors solutions, but a catechol functionalized nanoparticle suspension (NP29) was added into the CMCh solution (NP29 fabrication is described in the subsection 3.4.). Scaffolds developed in this chapter were designated as **CMChNP29/HAox-HA**, and blank formulation without NP (CMCh/HAox-HA) was used as control.

3.4. SELF-ASSEMBLED NANOPARTICLES FORMATION

Self-assembled nanoparticles (NP) of the two amphiphilic terpolymers T2 and T29 were prepared in **Chapter 6** through the nanoprecipitation method. Briefly, the corresponding terpolymer was dissolved in ethanol/acetone 1:1 and added dropwise into a NaCl aqueous solution under continuous magnetic stirring, without any surfactant. Herein, these NP were designated by the catechol composition as **NP2 and NP29** (from T2 and T29 respectively). NP of both compositions were also loaded with the model drug coumarin-6 (C6), and were designated as **C6NP2 and C6NP29** (from T2 and T29, respectively).

4. MATERIALS CHARACTERIZATION

An extensive number of characterization techniques were applied in this Thesis to study the physico-chemical composition, morphology and rheological performance of the polymers, ink formulations and materials developed. In addition, *in vitro* behavior in terms of swelling, degradation and catechol release profiles along with *in vitro* biological evaluation and *in vivo* biocompatibility was also assessed on different cell lines as explained below. Further information can be found along the corresponding chapters.

4.1. PHYSICO-CHEMICAL CHARACTERIZATION

Proton nuclear magnetic resonance spectra (^{1}H-NMR), recorded on a Bruker Avance III HD-400 equipment, and combined attenuated total internal reflectance/Fourier transform infrared (ATR-FTIR) technique, recorded on a Perkin-Elmer (Spectrum One) spectrometer equipped with an ATR accessory, were used to confirm the chemical structure of the synthetized monomer, polymers and hydrogel networks prepared.

UV spectra were recorded using a NanoDrop one (Thermo Fisher Scientific, Waltham, MA, USA) to determine the catechol concentration in the polymers at 290 nm. A Cary 3 BIO-Varian UV–visible spectrophotometer equipped with a Peltier temperature control device was used to determine the lower critical solution temperature (LCST) of VCL_CEMA copolymers.

Molecular weights of the VCL_CEMA copolymers were determined by high resolution mass spectrometry (HR-MS) using an Agilent 1200 Series LC system (equipped with a binary pump, an auto sampler and a column oven) coupled to a 6520 quadrupole-time of flight (QTOF) mass spectrometer. For catechol conjugated polymers, gel permeation chromatography (GPC) equipped with a Perkin Elmer Isocratic LC pump 250 and a refraction index detector (Series 200) was used to determine the number and weight average molecular weights and polydispersity (M_n, M_w and M_w/M_n respectively) of the distributions. Finally, M_w of HAox was determined by GPC Shimadzu 20A.

Differential scanning calorimetry (DSC) experiments were carried out on a micro-DSC-Illa (Setaram, France) to determine the glass transition temperature (T_g) of the polymers. Three heating-cooling cycles were analyzed under nitrogen atmosphere between 25 °C and 180 °C with a scanning rate of 10 °C/min, and T_g was determined as the midpoint of the transition of the second heating scan.

Thermogravimetric analysis (TGA) diagrams of the polymers were obtained in a thermogravimetric TGA Q500 (TA instruments) apparatus. Samples were analyzed in a range of 40-800 °C under nitrogen at a heating rate of 10 °C/min

The particle size distribution, mean hydrodynamic diameter (D_h) and particle dispersion index (PDI), and the zeta potential (ξ) of catechol functionalized NP suspensions were studied by dynamic light scattering (DLS) and laser doppler electrophoresis (LDE) respectively, using a Malvern Nanosizer NanoZS Instrument at r.t.

Morphology of catechol conjugated polymers films and nanoparticles was studied using a field emission scanning electron microscope (FE-SEM), Hitachi SU-8000, Japan. Light microscopy characterization of 3D printed scaffolds was performed with a stereomicroscope SMZ800N (Nikon, Germany) equipped with home-made bottom illumination, an optical microscope (Nikon SMZ800N, Germany) and camera (Samsung 13MPx). Surface morphology of conjugated polymer films, IPN hydrogel membranes and 3D printed scaffolds was performed using a multimode atomic force microscope (AFM) (Veeco Instruments, Santa Barbara, CA, USA) with a Nanoscope IVa control system (Plainview, NY, USA, software version 6.14r1) in tapping mode.

4.2. MECHANICAL CHARACTERIZATION

4.2.1. Bioadhesive strength tests

To test the bioadhesive properties of VCL_CEMA copolymers versus bone tissue hydrogels were prepared with gelatin and the copolymers to simulate the mussel adhesion proteins. The adhesion strength was determined in tension tests using a modification of the American Society for Testing and Materials (ASTM) F2258-05 method for chicken bones. Homogeneous plates of chicken keel were prepared. The hydrogel sample was deposited onto the transversal surface of the chicken bone plate, covered with another plate and clamped for 2 min to prevent motion. Tissue adhesion was examined using a universal testing machine (UTM, Instron model 3366) with a 100 N load cell and the adhesion data were collected by pulling metallic supports attached to the bones with a loading rate of 5 mm/min.

The adhesion strength of catechol conjugated polymers was examined on pig skin using a UTM (Instron model 3366, Norwood, MA, USA) equipped with a 100 N load cell. The protocol of the lap shear experiment was adapted from the ASTM standard F2255-05 (Reapproved 2015). Polymer and oxidation agent solutions were spread on the dermis surface of a porcine skin sample following an adapted protocol reported in literature.[282] Immediately, the sample was covered with the dermis part of another piece of skin (bonding area: 15 × 10 mm^2). Samples were allowed to cure for 30 min in moist conditions. Adhesion strength data were collected by pulling away the two skin pieces at a rate of 5 mm/min and calculated as the maximum force divided by the overlapping adhesion area.

Finally, the same ASTM lap shear method was used to test the bioadhesive property of the IPN membranes Ch/HAox/T/Fe to porcine skin. Maximum adhesion strength was tested using a UTM (Instron Frame model 5869, controller type 5800) equipped with a 100 N load cell. Membranes were deposited onto the dermis part of porcine skin samples and immediately covered with another dermis piece, obtaining an overlapping area of 15 × 10 mm^2. Test samples were stored at moist conditions for 12 h. Finally, samples were pulled to failure at a rate of 5 mm/min and maximum strength was calculated as the maximum force divided by the known adhesive overlap.

4.2.2. Rheological characterization

Viscoelastic properties of inks were studied by rheology to determine their suitability for printing. Rheological measurements were performed using a rotational rheometer (ARG2, TA Instruments) equipped with a parallel plate sand-blasted geometry of 25 mm of diameter, at controlled

temperature of 25 °C. A material volume of 150 µL was used for each measurement, and measuring gap was predefined at 300 µm.

Gelation times and material stiffness were analyzed in a time sweep experiment to study the crosslinking kinetics of the hydrogel precursors. Storage modulus (G′) and loss modulus (G′′) were recorded as a function of time (0-5 min) at a constant frequency of 1 Hz and 1% oscillatory strain. G′ and G′′ were recorded against frequency (1-200 Hz) at 1% strain in a frequency sweep experiment. Viscosity of the solutions was determined in a rotational flow sweep experiment at increasing shear rate from 0.1 to 150 1/s, to analyze the shear thinning behavior.

4.3. BIOACTIVE PROPERTIES

4.3.1. Antioxidant activity

In vitro antioxidant activity of VCL_CEMA copolymers was evaluated by measuring the radical scavenging activity (RSA) with 2-diphenyl-2-picrylhydrazil radical (DPPH) experiment. Ethanol solutions of VCL_CEMA copolymers were mixed with the same volume of a DPPH• ethanol solution and the decrease in absorbance at 515 nm was monitored using a Biotek Synergy HT detector. The RSA was calculated using the absorbance of the DPPH• either in the absence (A_0) or presence of antioxidant (A_1) using equation (1).

$$RSA\ (\%) = [(A_0 - A_1)/A_0] \times 100 \quad (1)$$

4.3.2. UV shielding

UV protective screen properties of the catechol polymer conjugates were evaluated based on the change in the wettability of porcine skin after UV irradiation. The wettability of porcine skin samples was measured by analyzing the water contact angle. Skin samples were covered with catechol conjugated polymer films and exposed to UV radiation generated using a UVP CL-1000 lamp with peak emission at 313 nm with an intensity of 0.95 W/m^2. The water contact angle of the skin below the terpolymer films was determined in order to compare and evaluate the UV protection of the catechol conjugated polymers on the porcine skin.

4.4. *IN VITRO* PERFORMANCE

4.4.1. Degradation

The *in vitro* degradation of the catechol conjugated polymer films, IPN hydrogel membranes and 3D printed scaffolds was examined gravimetrically under simulated physiological conditions. Briefly, the sample was initially dried and weighed (W_0). Weight loss was monitored as a function of incubation time in Dulbecco's modified Eagle's medium (DMEM) free of serum or phosphate buffered saline (PBS) (pH = 7.4) at 37 °C. At specific periods of time the samples were carefully withdrawn from the medium, washed with water, dried and weighed (W_t). Weight remaining (ΔW %) was determined using equation (2):

$$\Delta W(\%) = [1 - [(W_0 - W_t)/W_0]] \times 100 \quad (2)$$

Evaluation of surface morphology of dried samples of IPN membranes and 3D printed scaffolds after immersion in the simulated physiological medium for different periods of time was analyzed by SEM (Hitachi SU-8000), and microscope pictures (Nikon SMZ800N, Germany) respectively.

4.4.2. Swelling

Swelling of the IPN hydrogel membranes was measured gravimetrically. Dried samples accurately weighed (W_0) were immersed in PBS (pH=7.4) at 37 °C. At specific time points, hydrogels were taken out from the solution and weighed after absorbing the excess of water on the surface with a filter paper (W_t). Swelling degree was calculated using equation (3):

$$\text{Swelling degree } (\%) = [(W_t - W_0)/W_0] \times 100 \quad (3)$$

The 3D printed hydrogel scaffolds (2 layer square-based scaffolds) were incubated in PBS for 4 h and after gentle removal of excess of PBS, imaged using a stereomicroscope SMZ800N (Nikon, Germany). Swelling was evaluated by measuring strands widths in the scaffold with imageJ software, before and after incubation.

4.4.3. Catechol species release

Catechol species release from Ch/HAox/T and Ch/HAox/T/Fe hydrogels was analyzed under simulated physiological conditions. Dry membranes were weighed and immersed into PBS of pH 7.4 at 37 °C. At different time intervals, PBS samples were collected and catechol concentrations

were quantified by measuring the absorbance at 290 nm using a NanoDrop one (Thermo Fisher Scientific). A calibration curve of hydrocaffeic acid in PBS was used and cumulative release percentage was calculated for each sample and plotted as function of the release time.

Release of NP29 nanoparticles from CMChNP29/HAox-HA printed scaffolds was studied. Scaffolds were immersed into PBS of pH 7.4 and stored at 37 °C. The absorbance at 280 nm of the PBS taken at different time points was measured with NanoDrop One. Catechol NP concentration was quantified using a calibration curve of hydrocaffeic acid in PBS, and the cumulative release percentage was calculated for each sample.

4.5. *IN VITRO* BIOLOGICAL CHARACTERIZATION

4.5.1. Cytotoxicity

Cytotoxicity of the materials has been analyzed *in vitro* using cell cultures of different cell lines and standardized assays. Cytotoxicity of the VCL_CEMA copolymer samples and NP2 and NP29 nanoparticles was determined by incubating the cells in the presence of solutions/dispersions samples at different concentrations and using Alamar Blue (AB) assay. Human dermal fibroblasts (HDF, Innoprot) and murine RAW 264.7 macrophages (ECACC, Sigma) were used for copolymers and nanoparticle samples respectively. In all experiments, cells were seeded and incubated to confluence. After 24 h of incubation the medium was replaced with sample dilutions and incubated at 37 °C for 24 h. AB dye (10 % of AB solution in phenol red free DMEM medium) was added to the samples and plates were incubated at 37 °C for 3 h. The fluorescence emission was measured at 530 nm (excitation) and 600 nm (emission) using a UV multiplate reader (Biotek Synergy HT).

For the catechol conjugated polymer films and the IPN membranes, indirect cytotoxicity to human bone marrow mesenchymal stem cells (hBMSCs, Innoprot) was analyzed by incubating the cells with the samples extracts taken at different times. AB assay was performed according to ISO 10993–5 standard. Sterilized hydrogels were incubated in fetal bovine serum (FBS)-free supplemented DMEM at 37 °C. Cells were seeded at a density of 9 x 10^4 cells/mL in complete medium in a 96-well culture plate. After 24 h of incubation, the medium was replaced with aliquots of medium extracts taken at different times and further incubated for additional 24 h. Finally, medium was removed and AB assay was performed as described below.

4.5.2. Cell viability

In order to evaluate cell viability of L929 fibroblasts (ATCC, Germany) within the 3D bioprinted scaffolds over a 14 days-period, a live-dead assay was carried out staining with fluorescein diacetate (FDA) and propidium iodide (PI) to detect live and dead cells respectively. At different time points of incubation (1, 4, 7 and 14 days) the scaffolds were washed with PBS and incubated with FDA and PI and fluorescence images were taken using Nikon Ti-Ecllipse microscope (Nikon Instruments Europe B.V., Germany). Image analysis was performed using the Image-J 1.52p software counting both green and red cells with the function "find maxima". Cell viability percentage was calculated by quantifying the live cells between the total amount of cells in at least 5 images for 3 independent samples.

4.5.3. Cell proliferation

Cell viability of hBMSCs directly seeded on the IPN hydrogel membranes was analyzed by AB assay over a 14-days period. In the same way, cell viability of L929 fibroblasts within the 3D printed scaffolds was analyzed over a 14-days period. At specific time points, culture medium was removed and AB assay was performed as detailed in 4.5.1 section.

DNA quantification assay was performed in order to analyze cell proliferation of hBMSCs on the IPN membranes using Picogreen kit (Invitrogen) over a 14 days period. At specific time points, wells were washed with PBS and cells lysis was performed by freeze/thaw cycles. Total DNA quantification was determined according to the manufacturer's protocol. Fluorescence was read at excitation of 485/20 nm and emission of 528/20 nm using with a UV multiplate reader (Biotek Synergy HT).

4.5.4. Cell Staining

Cell morphology after culture on the IPN membranes was studied by confocal microscopy after phalloidin-tetramethylrhodamine B isocyanate staining (Sigma). Cells were fixed, permeabilized and incubated with a 50 μg/mL fluorescent phalloidin conjugate solution in PBS for 40 min at r.t. for cytoskeletal staining. Images were captured using a confocal laser scanning microscopy (CLSM, Leica TCS-SP5 RS AOBS), after excitation at 633 nm and collection of the emitted fluorescence in the range between 700 and 800 nm.

Immunostaining of the 3D bioprinted scaffolds was carried out at different times of culture. Cells were fixed, permeabilized and blocked. Then, they were incubated in 1:1000 vinculin rabbit

antibody (Thermofisher) for cytoskeleton labeling and 1:200 Alexa fluor-546 phalloidin (Thermofisher) for focal adhesion staining in phosphate buffered saline with Tween-20 (PBST) at r.t. for 1 hour. Then, they were incubated with secondary antibody Alexa flour-488 goat antirabbit (Thermofisher, 1:500 dilution) to stain cytoskeleton, and finally with 1:1000 4′,6-diamidino-2-phenylindole (DAPI, Thermofisher) in PBS for 20 min for nuclei staining. Finally, fluorescence imaging was carried out using a Zeiss LSM 880 confocal microscope.

4.5.5. Cell uptake

Endocytosis of NP2 and NP29 loaded with fluorescent coumarin-6 (C6NP2 and C6NP29 samples) was studied using RAW 264.7 macrophages. RAW 264.7 cells were seeded into a 96 well-plate at the density of 1 x 10^5 cells/mL in complete DMEM and incubated overnight. Afterward, medium was replaced by NP suspensions at different concentrations. Then, cells were washed and fixed, nuclei were stained with DAPI, and fluorescence images were taken at 60x magnification using a stereomicroscope (Nikon SMZ800N, Germany).

4.5.6. Intracellular ROS quantification

The ROS scavenging capacity of catechol conjugated films, IPN membranes and NP samples was evaluated fluorometrically using 2',7'-dichlorofluorescin diacetate (DCFH-DA, Sigma-Aldrich).[283,284] For the conjugated films and the IPN membranes studies, hBMSCs were directly seeded on the samples surfaces and cultured for 24 h to confluence. Then, they were washed with PBS and incubated with DCFH-DA solution in PBS for 30 min. Finally, they were treated with a H_2O_2 solution in order to activate the oxidative stress and samples solutions (samples extracts) were added. Relative fluorescence was measured at 485 nm excitation/580 nm emission with a UV multiplate reader (Biotek Synergy HT) and free radical relative content was determined by comparison. On the other hand, for the nanoparticle samples study RAW 264.7 macrophages were seeded on well-plates and cultured for 24 h to confluence. Medium was removed, replaced by NP2 and NP29 suspensions at different concentrations and cultured for 24 h more. Afterwards, the process continued as previously explained.

4.5.7. Anti-inflammatory properties

The nitric oxide (NO) inhibitory assay[285] was used to assess the anti-inflammatory activity of VCL_CEMA copolymers, catechol conjugated films and NP2 and NP29 nanoparticles using RAW 264.7 cells. Cells were seeded in 96-well plates at a density of 2 × 10^5 cells/mL and incubated at 37

°C for 24 h, except for the catechol conjugated films where cells were seeded on the top of the films. After 24 h of culture, medium was removed and 5 μg/mL of lipopolysaccharides from *E. coli* 055:B5 (LPS, Sigma) and the corresponding polymer solution were added. In the case of the nanoparticles, medium was first replaced by NP2 and NP29 dispersions, incubated for 24 h, and then LPS was added and incubated again for 24 h. NO concentration was determined by the Griess reaction.[286,287] Aliquots of the supernatant from RAW 264.7 cells were reacted with Griess reagent and the absorbance at 548 nm was measured. Cellular viability of RAW 264.7 cells in the presence of the different materials was evaluated in parallel by using the Alamar Blue assay (described in section 4.5.1.).

4.5.8. Interleukin IL-1β release

IL-1β release of cells seeded on the IPN hydrogel membranes was studied to gain more information about the anti-inflammatory activity of the samples. hBMSCs were seeded onto the IPN hydrogel membranes at a density of 6×10^4 cells/mL and incubated for 1 day. Cells were washed with PBS, oxidative stress was induced by incubation with H_2O_2 for 30 min,[288] cells were washed again, and samples extracts taken after 4 days of samples immersion in PBS were added and incubated with H_2O_2-damaged cells for 3 days. IL-1β release was measured by ELISA kit (Invitrogen) following the manufacturer's protocol.

4.5.9. Vascular endothelial growth factor (VEGF) release

VEGF or cells loaded into 3D printed scaffolds was studied in order to assess the neovascularization promoting activity of the samples. L929 fibroblasts were seeded into 16-well plates at 10^5 cells/mL. Cells were treated with serum-free medium for 2 h. Then, they were exposed to different concentrations of NP2 and NP29 dispersions in serum-free medium for 48 h. Medium supernatants were centrifuged for 1 min at 1400 r.p.m. and VEGF release was evaluated by ELISA experiment according to the manufacturer's instructions (Invitrogen, Thermo Scientific, San Diego, USA). The cell viability was determined using trypsin and a cell counter (Invitrogen) and results were normalized to 10^6 cells.

Endothelial cells (Invitrogen) in serum free medium were seeded on the top of the hydrogel bioink (with and without NP29) at 3 x 10^5 cells/mL. After 48 h of culture, medium supernatants were centrifuged for 1 min at 1400 r.p.m. and VEGF release was evaluated by ELISA experiment according to the manufacturer's instructions. DNA content of cells within the gels was analyzed by Picogreen assay and results were normalized to 10^6 pg DNA.

4.6. *IN VIVO* BIOCOMPATIBILITY STUDY

Animal experiments were performed to evaluate the *in vivo* biocompatibility of IPN hydrogel membranes. These experiments were also performed for the crosslinked hydrogel and the semi-IPN samples. As a commercial control a collagen membrane was used. The *in vivo* model consisted of a subcutaneous implantation of the samples in 21 male Albino Wistar rats with 250-300 g weight (Charles River, Barcelona, Spain). Four skin longitudinal incisions were done at the back of the rat (under general anesthesia) and four independent subcutaneous pockets were made by blunt dissection. Each rat received four membranes (1 cm, Ø), each one implanted in a separate pocket: control bovine collagen membrane (RCM6, ACE surgical supply co, USA) and the three studied hydrogel membranes Ch/HAox, Ch/HAox/T and Ch/HAox/T/Fe. Finally, each pocket was carefully sutured. After each predetermined implantation time period (1, 2 and 4 weeks) each animal (n=7) was euthanized. After dissection, each tissue sample was fixed in 4% neutral formol for standard histological tissue processing with paraffin embedding. Paraffin blocks were cut and microtome sections were stained with haematoxylin and eosin (H-E) technique. Tissue reaction was evaluated by presence and degree of the inflammatory reaction and cellular component. Appearance of the membrane sample, formation of fibrous tissue or fibrous capsule and vascularization degree were also examined.

2. REFERENCES

1. O'brien FJ. Biomaterials & scaffolds for tissue engineering. *Materials today.* 2011;14(3):88-95.

2. Khan F, Tanaka M, Ahmad SR. Fabrication of polymeric biomaterials: a strategy for tissue engineering and medical devices. *Journal of Materials Chemistry B.* 2015;3(42):8224-8249.

3. Bajaj P, Schweller RM, Khademhosseini A, West JL, Bashir R. 3D biofabrication strategies for tissue engineering and regenerative medicine. *Annual review of biomedical engineering.* 2014;16:247-276.

4. Atala A. Tissue engineering and regenerative medicine: concepts for clinical application. *Rejuvenation research.* 2004;7(1):15-31.

5. Naderi H, Matin MM, Bahrami AR. Critical issues in tissue engineering: biomaterials, cell sources, angiogenesis, and drug delivery systems. *Journal of biomaterials applications.* 2011;26(4):383-417.

6. Langer R, Vacanti J. Tissue engineering. Science 260: 920-926. *TISSUE ENGINEERING: THE UNION OF BIOLOGY AND ENGINEERING.* 1993;98.

7. Nerem RM. Cellular engineering. *Annals of biomedical engineering.* 1991;19(5):529-545.

8. Langer R. Biomaterials in drug delivery and tissue engineering: one laboratory's experience. *Accounts of Chemical Research.* 2000;33(2):94-101.

9. Bonassar LJ, Vacanti CA. Tissue engineering: the first decade and beyond. *Journal of cellular biochemistry.* 1998;72(S30–31):297-303.

10. Meyer U, Meyer T, Handschel J, Wiesmann HP. *Fundamentals of tissue engineering and regenerative medicine*: Springer; 2009.

11. Mano J, Silva G, Azevedo HS, et al. Natural origin biodegradable systems in tissue engineering and regenerative medicine: present status and some moving trends. *Journal of the Royal Society Interface.* 2007;4(17):999-1030.

12. Fisher MB, Mauck RL. Tissue engineering and regenerative medicine: recent innovations and the transition to translation. *Tissue Engineering Part B: Reviews.* 2013;19(1):1-13.

13. Vats A, Tolley N, Polak J, Gough J. Scaffolds and biomaterials for tissue engineering: a review of clinical applications. *Clinical Otolaryngology & Allied Sciences.* 2003;28(3):165-172.

14. Berthiaume F, Maguire TJ, Yarmush ML. Tissue engineering and regenerative medicine: history, progress, and challenges. *Annual review of chemical and biomolecular engineering.* 2011;2:403-430.

15. Ratner BD, Bryant SJ. Biomaterials: where we have been and where we are going. *Annu. Rev. Biomed. Eng.* 2004;6:41-75.

16. Langer R. Perspectives and challenges in tissue engineering and regenerative medicine. *Advanced materials.* 2009;21(32-33):3235-3236.

17. Kohane DS, Langer R. Polymeric biomaterials in tissue engineering. *Pediatric research.* 2008;63(5):487-491.

18. Asadi N, Del Bakhshayesh AR, Davaran S, Akbarzadeh A. Common Biocompatible Polymeric Materials for Tissue Engineering and Regenerative Medicine. *Materials Chemistry and Physics.* 2019:122528.

19. Furth ME, Atala A, Van Dyke ME. Smart biomaterials design for tissue engineering and regenerative medicine. *Biomaterials.* 2007;28(34):5068-5073.

20. Spicer CD. Hydrogel scaffolds for tissue engineering: the importance of polymer choice. *Polymer Chemistry.* 2020.

21. Acevedo CA, Sánchez E, Díaz-Calderón P, Blaker JJ, Enrione J, Quero F. Synergistic effects of crosslinking and chitosan molecular weight on the microstructure, molecular mobility, thermal and sorption properties of porous chitosan/gelatin/hyaluronic acid scaffolds. *Journal of Applied Polymer Science.* 2017;134(18).

22. Karageorgiou V, Kaplan D. Porosity of 3D biomaterial scaffolds and osteogenesis. *Biomaterials.* 2005;26(27):5474-5491.

23. Nair LS, Laurencin CT. Biodegradable polymers as biomaterials. *Progress in polymer science.* 2007;32(8-9):762-798.

24. Reya T, Morrison SJ, Clarke MF, Weissman IL. Stem cells, cancer, and cancer stem cells. *nature.* 2001;414(6859):105-111.

25. O'Connell G, Garcia J, Amir J. 3D Bioprinting: New Directions in Articular Cartilage Tissue Engineering. *ACS Biomaterials Science & Engineering.* 2017/01/17 2017.

26. Ozbolat IT. Bioprinting of osteochondral tissues: A perspective on current gaps and future trends. *International Journal of Bioprinting.* 2017;3(2).

27. Pedde RD, Mirani B, Navaei A, et al. Emerging Biofabrication Strategies for Engineering Complex Tissue Constructs. *Adv Mater.* May 2017;29(19).

28. Tibbitt MW, Anseth KS. Hydrogels as extracellular matrix mimics for 3D cell culture. *Biotechnology and bioengineering.* 2009;103(4):655-663.

29. Nolan K, Millet Y, Ricordi C, Stabler CL. Article Commentary: Tissue Engineering and Biomaterials in Regenerative Medicine. *Cell transplantation.* 2008;17(3):241-243.

30. Sanmartín-Masiá E, Poveda-Reyes S, Gallego Ferrer G. Extracellular matrix–inspired gelatin/hyaluronic acid injectable hydrogels. *International Journal of Polymeric Materials and Polymeric Biomaterials.* 2017;66(6):280-288.

31. Giancotti FG, Ruoslahti E. Integrin signaling. *science.* 1999;285(5430):1028-1033.

32. Denry I, Kelly J. Emerging ceramic-based materials for dentistry. *Journal of Dental Research.* 2014;93(12):1235-1242.

33. Zhang K, He S, Yan S, et al. Regeneration of hyaline-like cartilage and subchondral bone simultaneously by poly(l-glutamic acid) based osteochondral scaffolds with induced autologous adipose derived stem cells. *J. Mater. Chem. B.* 2016;4(15):2628-2645.

34. Han Y, Zeng Q, Li H, Chang J. The calcium silicate/alginate composite: Preparation and evaluation of its behavior as bioactive injectable hydrogels. *Acta Biomaterialia.* 2013/11/01/ 2013;9(11):9107-9117.

35. Zheng L, Jiang X, Chen X, Fan H, Zhang X. Evaluation of novel in situ synthesized nano-hydroxyapatite/collagen/alginate hydrogels for osteochondral tissue engineering. *Biomed Mater.* Oct 30 2014;9(6):065004.

36. Caló E, Khutoryanskiy VV. Biomedical applications of hydrogels: A review of patents and commercial products. *European Polymer Journal.* 2015;65:252-267.

37. Malda J, Visser J, Melchels FP, et al. 25th anniversary article: engineering hydrogels for biofabrication. *Advanced materials.* 2013;25(36):5011-5028.

38. Annabi N, Tamayol A, Uquillas JA, et al. 25th anniversary article: Rational design and applications of hydrogels in regenerative medicine. *Advanced materials.* 2014;26(1):85-124.

39. Eiselt P, Yeh J, Latvala RK, Shea LD, Mooney DJ. Porous carriers for biomedical applications based on alginate hydrogels. *Biomaterials.* 2000;21(19):1921-1927.

40. Albuquerque P, Coelho LC, Teixeira JA, Carneiro-da-Cunha MG. Approaches in biotechnological applications of natural polymers. 2016.

41. Pan Z, Ding J. Poly (lactide-co-glycolide) porous scaffolds for tissue engineering and regenerative medicine. *Interface focus.* 2012;2(3):366-377.

42. Hu J, Sun X, Ma H, Xie C, Chen YE, Ma PX. Porous nanofibrous PLLA scaffolds for vascular tissue engineering. *Biomaterials.* 2010;31(31):7971-7977.

43. Green DW, Ben-Nissan B, Yoon K-S, Milthorpe B, Jung H-S. Bioinspired materials for regenerative medicine: going beyond the human archetypes. *Journal of Materials Chemistry B.* 2016;4(14):2396-2406.

44. Brennan AB, Kirschner CM. *Bio-inspired materials for biomedical engineering*: Wiley Online Library; 2014.

45. Sanchez C, Arribart H, Guille MMG. Biomimetism and bioinspiration as tools for the design of innovative materials and systems. *Nature materials.* 2005;4(4):277-288.

46. Shin H, Jo S, Mikos AG. Biomimetic materials for tissue engineering. *Biomaterials.* 2003;24(24):4353-4364.

47. Hege CS, Schiller SM. New bioinspired materials for regenerative medicine. *Current Molecular Biology Reports.* 2015;1(2):77-86.

48. Cardoso V, Ribeiro C, Lanceros-Mendez S. Metamorphic biomaterials. *Bioinspired Materials for Medical Applications*: Elsevier; 2017:69-99.

49. Leiro V, Moreno P, Sarmento B, et al. Design and preparation of biomimetic and bioinspired materials. *Bioinspired Materials for Medical Applications*: Elsevier; 2017:1-44.

50. Montero de Espinosa L, Meesorn W, Moatsou D, Weder C. Bioinspired polymer systems with stimuli-responsive mechanical properties. *Chemical reviews.* 2017;117(20):12851-12892.

51. Trask R, Williams H, Bond I. Self-healing polymer composites: mimicking nature to enhance performance. *Bioinspiration & Biomimetics.* 2007;2(1):P1.

52. Mano JF. Stimuli-responsive polymeric systems for biomedical applications. *Advanced Engineering Materials.* 2008;10(6):515-527.

53. Wang W, Zhang Y, Liu W. Bioinspired fabrication of high strength hydrogels from non-covalent interactions. *Progress in Polymer Science.* 2017;71:1-25.

54. Girotti A, Orbanic D, Ibáñez-Fonseca A, Gonzalez-Obeso C, Rodríguez-Cabello JC. Recombinant technology in the development of materials and systems for soft-tissue repair. *Advanced healthcare materials.* 2015;4(16):2423-2455.

55. Chan B, Leong K. Scaffolding in tissue engineering: general approaches and tissue-specific considerations. *European spine journal.* 2008;17(4):467-479.

56. Kolesky DB, Homan KA, Skylar-Scott MA, Lewis JA. Three-dimensional bioprinting of thick vascularized tissues. *Proceedings of the National Academy of Sciences of the United States of America.* Mar 22 2016;113(12):3179-3184.

57. Dalby MJ, Gadegaard N, Tare R, et al. The control of human mesenchymal cell differentiation using nanoscale symmetry and disorder. *Nature materials.* Dec 2007;6(12):997-1003.

58. Johnson T, Bahrampourian R, Patel A, Mequanint K. Fabrication of highly porous tissue-engineering scaffolds using selective spherical porogens. *Bio-medical materials and engineering.* 2010;20(2):107-118.

59. Shen X, Chen L, Cai X, Tong T, Tong H, Hu J. A novel method for the fabrication of homogeneous hydroxyapatite/collagen nanocomposite and nanocomposite scaffold with hierarchical porosity. *Journal of Materials Science: Materials in Medicine.* 2011;22(2):299-305.

60. Lim JI, Lee Y-K, Shin J-S, Lim K-J. Preparation of interconnected porous chitosan scaffolds

by sodium acetate particulate leaching. *Journal of Biomaterials Science, Polymer Edition.* 2011;22(10):1319-1329.

61. Buttafoco L, Engbers-Buijtenhuijs P, Poot AA, et al. First steps towards tissue engineering of small-diameter blood vessels: preparation of flat scaffolds of collagen and elastin by means of freeze drying. *Journal of Biomedical Materials Research Part B: Applied Biomaterials: An Official Journal of The Society for Biomaterials, The Japanese Society for Biomaterials, and The Australian Society for Biomaterials and the Korean Society for Biomaterials.* 2006;77(2):357-368.

62. Faraj KA, Van Kuppevelt TH, Daamen WF. Construction of collagen scaffolds that mimic the three-dimensional architecture of specific tissues. *Tissue engineering.* 2007;13(10):2387-2394.

63. Pavinatto FJ, Caseli L, Oliveira Jr ON. Chitosan in nanostructured thin films. *Biomacromolecules.* 2010;11(8):1897-1908.

64. Boudou T, Crouzier T, Ren K, Blin G, Picart C. Multiple functionalities of polyelectrolyte multilayer films: new biomedical applications. *Advanced materials.* 2010;22(4):441-467.

65. Haynie DT, Zhang L, Zhao W, Rudra JS. Protein-inspired multilayer nanofilms: science, technology and medicine. *Nanomedicine: Nanotechnology, Biology and Medicine.* 2006;2(3):150-157.

66. Liu Y, Ren L, Long K, Wang L, Wang Y. Preparation and characterization of a novel tobramycin-containing antibacterial collagen film for corneal tissue engineering. *Acta biomaterialia.* 2014;10(1):289-299.

67. Wrobel S, Serra SC, Ribeiro-Samy S, et al. In vitro evaluation of cell-seeded chitosan films for peripheral nerve tissue engineering. *Tissue Engineering Part A.* 2014;20(17-18):2339-2349.

68. Yeh M-k, Liang Y-m, Cheng K-m, Dai N-T, Liu C-c, Young J-j. A novel cell support membrane for skin tissue engineering: Gelatin film cross-linked with 2-chloro-1-methylpyridinium iodide. *Polymer.* 2011;52(4):996-1003.

69. Chlapanidas T, Tosca M, Farago S, et al. Formulation and characterization of silk fibroin films as a scaffold for adipose-derived stem cells in skin tissue engineering. *International journal of immunopathology and pharmacology.* 2013;26(1_suppl):43-49.

70. Truckenmüller R, Giselbrecht S, Rivron N, et al. Thermoforming of film-based biomedical microdevices. *Advanced materials.* 2011;23(11):1311-1329.

71. Lammers G, Roth G, Heck M, et al. Construction of a microstructured collagen membrane mimicking the papillary dermis architecture and guiding keratinocyte morphology and gene expression. *Macromolecular bioscience.* 2012;12(5):675-691.

72. Tien LW, Gil ES, Park SH, Mandal BB, Kaplan DL. Patterned silk film scaffolds for aligned lamellar bone tissue engineering. *Macromolecular bioscience.* 2012;12(12):1671-1679.

73. Vieira A, Vieira J, Ferra J, Magalhães F, Guedes R, Marques A. Mechanical study of PLA–PCL fibers during in vitro degradation. *Journal of the mechanical behavior of biomedical materials.* 2011;4(3):451-460.

74. Murugan R, Ramakrishna S. Nano-featured scaffolds for tissue engineering: a review of spinning methodologies. *Tissue engineering.* 2006;12(3):435-447.

75. Milleret V, Simona B, Neuenschwander P, Hall H. Tuning electrospinning parameters for production of 3D-fiber-fleeces with increased porosity for soft tissue engineering applications. *Eur Cell Mater.* 2011;21(1473-2262):286-303.

76. Liu H, Li X, Zhou G, Fan H, Fan Y. Electrospun sulfated silk fibroin nanofibrous scaffolds for vascular tissue engineering. *Biomaterials.* 2011;32(15):3784-3793.

77. Kanokpanont S, Damrongsakkul S, Ratanavaraporn J, Aramwit P. Physico-chemical properties and efficacy of silk fibroin fabric coated with different waxes as wound dressing. *International journal of biological macromolecules.* 2013;55:88-97.

78. Billiet T, Vandenhaute M, Schelfhout J, Van Vlierberghe S, Dubruel P. A review of trends and limitations in hydrogel-rapid prototyping for tissue engineering. *Biomaterials.* 2012;33(26):6020-6041.

79. Ratheesh G, Venugopal JR, Chinappan A, Ezhilarasu H, Sadiq A, Ramakrishna S. 3D fabrication of polymeric scaffolds for regenerative therapy. *ACS Biomaterials Science & Engineering.* 2017;3(7):1175-1194.

80. Peltola SM, Melchels FP, Grijpma DW, Kellomäki M. A review of rapid prototyping techniques for tissue engineering purposes. *Annals of medicine.* 2008;40(4):268-280.

81. Rengier F, Mehndiratta A, Von Tengg-Kobligk H, et al. 3D printing based on imaging data: review of medical applications. *International journal of computer assisted radiology and surgery.* 2010;5(4):335-341.

82. Richards DJ, Tan Y, Jia J, Yao H, Mei Y. 3D printing for tissue engineering. *Israel Journal of Chemistry.* 2013;53(9-10):805-814.

83. Paten JA, Tilburey GE, Molloy EA, Zareian R, Trainor CV, Ruberti JW. Utility of an optically-based, micromechanical system for printing collagen fibers. *Biomaterials.* 2013;34(11):2577-2587.

84. Skoog SA, Goering PL, Narayan RJ. Stereolithography in tissue engineering. *Journal of Materials Science: Materials in Medicine.* 2014;25(3):845-856.

85. Chen C-H, Shyu VB-H, Chen J-P, Lee M-Y. Selective laser sintered poly-ε-caprolactone scaffold hybridized with collagen hydrogel for cartilage tissue engineering. *Biofabrication.* 2014;6(1):015004.

86. Mandrycky C, Wang Z, Kim K, Kim DH. 3D bioprinting for engineering complex tissues. *Biotechnol Adv.* Jul-Aug 2016;34(4):422-434.

87. Murphy SV, Atala A. 3D bioprinting of tissues and organs. *Nature biotechnology.* Aug 2014;32(8):773-785.

88. Cui H, Nowicki M, Fisher JP, Zhang LG. 3D Bioprinting for Organ Regeneration. *Advanced Healthcare Materials.* 2017;6(1):1601118.

89. Arslan-Yildiz A, Assal RE, Chen P, Guven S, Inci F, Demirci U. Towards artificial tissue models: past, present, and future of 3D bioprinting. *Biofabrication.* 2016;8(1):014103.

90. Mironov V, Reis N, Derby B. Bioprinting: a beginning. *Tissue engineering.* 2006;12(4):631-634.

91. Derby B. Printing and prototyping of tissues and scaffolds. *Science.* 2012;338(6109):921-926.

92. Radhakrishnan J, Subramanian A, Krishnan UM, Sethuraman S. Injectable and 3D Bioprinted Polysaccharide Hydrogels: From Cartilage to Osteochondral Tissue Engineering. *Biomacromolecules.* Jan 09 2017;18(1):1-26.

93. Daly AC, Freeman FE, Gonzalez-Fernandez T, Critchley SE, Nulty J, Kelly DJ. 3D Bioprinting for Cartilage and Osteochondral Tissue Engineering. *Adv Healthc Mater.* Aug 14 2017.

94. Fedorovich NE, Schuurman W, Wijnberg HM, et al. Biofabrication of osteochondral tissue equivalents by printing topologically defined, cell-laden hydrogel scaffolds. *Tissue Eng Part C Methods.* Jan 2012;18(1):33-44.

95. Bartnikowski M, Akkineni AR, Gelinsky M, Woodruff MA, Klein TJ. A Hydrogel Model Incorporating 3D-Plotted Hydroxyapatite for Osteochondral Tissue Engineering. *Materials (Basel).* Apr 14 2016;9(4).

96. Hollister SJ. Porous scaffold design for tissue engineering. *Nature materials.* 2005;4(7):518-524.

97. Ikada Y. Challenges in tissue engineering. *Journal of the Royal Society, Interface.* Oct 22 2006;3(10):589-601.

98. Tomasina C, Bodet T, Mota C, Moroni L, Camarero-Espinosa S. Bioprinting Vasculature: Materials, Cells and Emergent Techniques. *Materials.* 2019;12(17):2701.

99. Moroni L, Boland T, Burdick JA, et al. Biofabrication: a guide to technology and terminology. *Trends in biotechnology.* 2018;36(4):384-402.

100. Mandrycky C, Wang Z, Kim K, Kim D-H. 3D bioprinting for engineering complex tissues. *Biotechnology advances.* 2016;34(4):422-434.

101. Muller M, Ozturk E, Arlov O, Gatenholm P, Zenobi-Wong M. Alginate Sulfate-Nanocellulose Bioinks for Cartilage Bioprinting Applications. *Ann Biomed Eng.* Jan 2017;45(1):210-223.

102. Yang SS, Choi WH, Song BR, et al. Fabrication of an osteochondral graft with using a solid freeform fabrication system. *Tissue Engineering and Regenerative Medicine.* 2015;12(4):239-248.

103. Kang HW, Lee SJ, Ko IK, Kengla C, Yoo JJ, Atala A. A 3D bioprinting system to produce human-scale tissue constructs with structural integrity. *Nature biotechnology.* Mar 2016;34(3):312-319.

104. Zhang J, Allardyce BJ, Rajkhowa R, et al. 3D printing of silk particle-reinforced chitosan hydrogel structures and their properties. *ACS Biomaterials Science & Engineering.* 2018;4(8):3036-3046.

105. Wu Q, Therriault D, Heuzey M-C. Processing and properties of chitosan Inks for 3D printing of hydrogel microstructures. *ACS Biomaterials Science & Engineering.* 2018;4(7):2643-2652.

106. Li H, Tan YJ, Liu S, Li L. Three-dimensional bioprinting of oppositely charged hydrogels with super strong Interface bonding. *ACS applied materials & interfaces.* 2018;10(13):11164-11174.

107. Highley CB, Song KH, Daly AC, Burdick JA. Jammed microgel inks for 3D printing applications. *Advanced Science.* 2019;6(1):1801076.

108. Hinton TJ, Jallerat Q, Palchesko RN, et al. Three-dimensional printing of complex biological structures by freeform reversible embedding of suspended hydrogels. *Science advances.* 2015;1(9):e1500758.

109. Skardal A, Zhang J, McCoard L, Xu X, Oottamasathien S, Prestwich GD. Photocrosslinkable hyaluronan-gelatin hydrogels for two-step bioprinting. *Tissue Eng Part A.* Aug 2010;16(8):2675-2685.

110. Levato R, Webb WR, Otto IA, et al. The bio in the ink: cartilage regeneration with bioprintable hydrogels and articular cartilage-derived progenitor cells. *Acta biomaterialia.* Oct 01 2017;61:41-53.

111. Zhai X, Ma Y, Hou C, et al. 3D-Printed High Strength Bioactive Supramolecular Polymer/Clay Nanocomposite Hydrogel Scaffold for Bone Regeneration. *ACS Biomaterials Science & Engineering.* 2017;3(6):1109-1118.

112. Klotz BJ, Gawlitta D, Rosenberg AJ, Malda J, Melchels FP. Gelatin-Methacryloyl Hydrogels: Towards Biofabrication-Based Tissue Repair. *Trends Biotechnol.* May 2016;34(5):394-407.

113. Melchels FP, Domingos MA, Klein TJ, Malda J, Bartolo PJ, Hutmacher DW. Additive manufacturing of tissues and organs. *Progress in Polymer Science.* 2012;37(8):1079-1104.

114. Ramos T, Moroni L. Tissue Engineering and Regenerative Medicine 2019: The Role of Biofabrication—A Year in Review. *Tissue Engineering Part C: Methods.* 2020;26(2):91-106.

115. Qasaimeh MA, Gervais T, Juncker D. Microfluidic quadrupole and floating concentration gradient. *Nature communications.* 2011;2(1):1-8.

116. Huh D, Matthews BD, Mammoto A, Montoya-Zavala M, Hsin HY, Ingber DE. Reconstituting organ-level lung functions on a chip. *Science.* 2010;328(5986):1662-1668.

117. Leng L, McAllister A, Zhang B, Radisic M, Günther A. Mosaic hydrogels: one-step formation of multiscale soft materials. *Advanced materials.* 2012;24(27):3650-3658.

118. Annabi N, Selimović Š, Cox JPA, et al. Hydrogel-coated microfluidic channels for cardiomyocyte culture. *Lab on a Chip.* 2013;13(18):3569-3577.

119. Atala A, Kasper FK, Mikos AG. Engineering complex tissues. *Science translational medicine.* 2012;4(160):160rv112-160rv112.

120. Mironov V, Kasyanov V, Drake C, Markwald RR. Organ printing: promises and challenges. 2008.

121. Mironov V, Kasyanov V, Markwald RR. Organ printing: from bioprinter to organ biofabrication line. *Current opinion in biotechnology.* 2011;22(5):667-673.

122. Schnurrer J, Lehr C-M. Mucoadhesive properties of the mussel adhesive protein. *International journal of pharmaceutics.* 1996;141(1-2):251-256.

123. Waite JH, Qin X. Polyphosphoprotein from the adhesive pads of Mytilus edulis. *Biochemistry.* 2001;40(9):2887-2893.

124. Yu M, Hwang J, Deming TJ. Role of L-3, 4-dihydroxyphenylalanine in mussel adhesive proteins. *Journal of the American Chemical Society.* 1999;121(24):5825-5826.

125. Waite JH, Tanzer ML. Polyphenolic substance of Mytilus edulis: novel adhesive containing L-dopa and hydroxyproline. *Science.* 1981;212(4498):1038-1040.

126. Kord Forooshani P, Lee BP. Recent approaches in designing bioadhesive materials inspired by mussel adhesive protein. *Journal of Polymer Science Part A: Polymer Chemistry.* 2017;55(1):9-33.

127. Herrmann K, Nagel CW. Occurrence and content of hydroxycinnamic and hydroxybenzoic acid compounds in foods. *Critical reviews in food science & nutrition.* 1989;28(4):315-347.

128. Chandra S, Gonzalez de Mejia E. Polyphenolic compounds, antioxidant capacity, and quinone reductase activity of an aqueous extract of Ardisia compressa in comparison to mate (Ilex paraguariensis) and green (Camellia sinensis) teas. *Journal of agricultural and food chemistry.* 2004;52(11):3583-3589.

129. Floriolli RY, von Langen J, Waite JH. Marine surfaces and the expression of specific byssal adhesive protein variants in Mytilus. *Marine Biotechnology.* 2000;2(4):352-363.

130. Zhao H, Sun C, Stewart RJ, Waite JH. Cement proteins of the tube-building polychaete Phragmatopoma californica. *Journal of Biological Chemistry.* 2005;280(52):42938-42944.

131. Miserez A, Schneberk T, Sun C, Zok FW, Waite JH. The transition from stiff to compliant materials in squid beaks. *Science.* 2008;319(5871):1816-1819.

132. Sedó J, Saiz-Poseu J, Busqué F, Ruiz-Molina D. Biomimetics: Catechol-Based Biomimetic Functional Materials (Adv. Mater. 5/2013). *Advanced Materials.* 2013;25(5):792-792.

133. Yang J, Stuart MAC, Kamperman M. Jack of all trades: versatile catechol crosslinking mechanisms. *Chemical Society Reviews.* 2014;43(24):8271-8298.

134. Prasetyo EN, Kudanga T, Steiner W, Murkovic M, Nyanhongo GS, Guebitz GM. Antioxidant activity assay based on laccase-generated radicals. *Analytical and bioanalytical chemistry.* 2009;393(2):679.

135. Roleira FM, Tavares-da-Silva EJ, Varela CL, et al. Plant derived and dietary phenolic antioxidants: Anticancer properties. *Food Chemistry.* 2015;183:235-258.

136. Heleno SA, Martins A, Queiroz MJR, Ferreira IC. Bioactivity of phenolic acids: Metabolites versus parent compounds: A review. *Food chemistry.* 2015;173:501-513.

137. Fresco P, Borges F, Diniz C, Marques M. New insights on the anticancer properties of dietary polyphenols. *Medicinal research reviews.* 2006;26(6):747-766.

138. Nagababu E, Rifkind JM, Boindala S, Nakka L. Assessment of antioxidant activity of eugenol in vitro and in vivo. *Free Radicals and Antioxidant Protocols*: Springer; 2010:165-180.

139. Huber D, Grzelak A, Baumann M, et al. Anti-inflammatory and anti-oxidant properties of laccase-synthesized phenolic- O - carboxymethyl chitosan hydrogels. *New Biotechnology.* 2018;40:236-244.

140. Barclay LRC, Edwards C, Vinqvist MR. Media effects on antioxidant activities of phenols and catechols. *Journal of the American Chemical society.* 1999;121(26):6226-6231.

141. Justino GC, Correia CF, Mira L, et al. Antioxidant activity of a catechol derived from abietic acid. *Journal of agricultural and food chemistry.* 2006;54(2):342-348.

142. Silva MM, Santos MR, Caroço G, Rocha R, Justino G, Mira L. Structure-antioxidant activity relationships of flavonoids: a re-examination. *Free Radical Research.* 2002;36(11):1219-1227.

143. Heijnen CG, Haenen GR, Minou Oostveen R, Stalpers EM, Bast A. Protection of flavonoids against lipid peroxidation: the structure activity relationship revisited. *Free Radical Research.* 2002;36(5):575-581.

144. Boots AW, Haenen GR, den Hartog GJ, Bast A. Oxidative damage shifts from lipid peroxidation to thiol arylation by catechol-containing antioxidants. *Biochimica et Biophysica Acta (BBA)-Molecular and Cell Biology of Lipids.* 2002;1583(3):279-284.

145. Dileep KV, Tintu I, Mandal PK, Karthe P, Haridas M, Sadasivan C. Binding to PLA2 May Contribute to the Anti-Inflammatory Activity of Catechol. *Chemical biology & drug design.* 2012;79(1):143-147.

146. Zheng LT, Ryu G-M, Kwon B-M, Lee W-H, Suk K. Anti-inflammatory effects of catechols in lipopolysaccharide-stimulated microglia cells: inhibition of microglial neurotoxicity. *European journal of pharmacology.* 2008;588(1):106-113.

147. Larrosa M, Luceri C, Vivoli E, et al. Polyphenol metabolites from colonic microbiota exert anti-inflammatory activity on different inflammation models. *Molecular nutrition & food research.* 2009;53(8):1044-1054.

148. Huang J, de Paulis T, May JM. Antioxidant effects of dihydrocaffeic acid in human EA. hy926 endothelial cells. *The Journal of nutritional biochemistry.* 2004;15(12):722-729.

149. McDowell LM, Burzio LA, Waite JH, Schaefer J. Rotational echo double resonance detection of cross-links formed in mussel byssus under high-flow stress. *Journal of Biological Chemistry.* 1999;274(29):20293-20295.

150. Waite JH. Nature's underwater adhesive specialist. *International Journal of Adhesion and Adhesives.* 1987;7(1):9-14.

151. Lee H, Scherer NF, Messersmith PB. Single-molecule mechanics of mussel adhesion. *Proceedings of the National Academy of Sciences.* 2006;103(35):12999-13003.

152. Waite JH. The phylogeny and chemical diversity of quinone-tanned glues and varnishes. *Comparative Biochemistry and Physiology Part B: Comparative Biochemistry.* 1990;97(1):19-29.

153. Lee BP, Dalsin JL, Messersmith PB. Synthesis and gelation of DOPA-modified poly

(ethylene glycol) hydrogels. *Biomacromolecules.* 2002;3(5):1038-1047.

154. Catron ND, Lee H, Messersmith PB. Enhancement of poly (ethylene glycol) mucoadsorption by biomimetic end group functionalization. *Biointerphases.* 2006;1(4):134-141.

155. Waiter JH. Reverse engineering of bioadhesion in marine mussels. *Annals of the New York Academy of Sciences.* 1999;875(1):301-309.

156. Gallivan JP, Dougherty DA. A computational study of cation– π interactions vs salt bridges in aqueous media: implications for protein engineering. *Journal of the American Chemical Society.* 2000;122(5):870-874.

157. Das S, Rodriguez NRM, Wei W, Waite JH, Israelachvili JN. Peptide Length and Dopa Determine Iron-Mediated Cohesion of Mussel Foot Proteins. *Advanced functional materials.* 2015;25(36):5840-5847.

158. Pillai KV, Renneckar S. Cation– π interactions as a mechanism in technical lignin adsorption to cationic surfaces. *Biomacromolecules.* 2009;10(4):798-804.

159. Halake K, Cho S, Kim J, et al. Applications using the metal affinity of polyphenols with mussel-inspired chemistry. *Macromolecular Research.* 2018;26(2):93-99.

160. Tyson CA, Martell AE. Equilibriums of metal ions with pyrocatechol and 3, 5-di-tert-butylpyrocatechol. *Journal of the American Chemical Society.* 1968;90(13):3379-3386.

161. Sever MJ, Wilker JJ. Absorption spectroscopy and binding constants for first-row transition metal complexes of a DOPA-containing peptide. *Dalton Transactions.* 2006(6):813-822.

162. Barrett DG, Fullenkamp DE, He L, Holten-Andersen N, Lee KYC, Messersmith PB. pH-based regulation of hydrogel mechanical properties through mussel-inspired chemistry and processing. *Advanced functional materials.* 2013;23(9):1111-1119.

163. Higginson CJ, Malollari KG, Xu Y, Kelleghan AV, Ricapito NG, Messersmith PB. Bioinspired Design Provides High-Strength Benzoxazine Structural Adhesives. *Angewandte Chemie International Edition.* 2019;58(35):12271-12279.

164. Wu J, Zhang L, Wang Y, et al. Mussel-inspired chemistry for robust and surface-modifiable multilayer films. *Langmuir.* 2011;27(22):13684-13691.

165. Jenkins CL, Siebert HM, Wilker JJ. Integrating mussel chemistry into a bio-based polymer to create degradable adhesives. *Macromolecules.* 2017;50(2):561-568.

166. Lee BP, Huang K, Nunalee FN, Shull KR, Messersmith PB. Synthesis of 3, 4-dihydroxyphenylalanine (DOPA) containing monomers and their co-polymerization with PEG-diacrylate to form hydrogels. *Journal of Biomaterials Science, Polymer Edition.* 2004;15(4):449-464.

167. Lee H, Lee BP, Messersmith PB. A reversible wet/dry adhesive inspired by mussels and geckos. *Nature.* 2007;448(7151):338-341.

168. Meng H, Li Y, Faust M, Konst S, Lee BP. Hydrogen peroxide generation and biocompatibility of hydrogel-bound mussel adhesive moiety. *Acta biomaterialia.* 2015;17:160-169.

169. Skelton S, Bostwick M, O'Connor K, Konst S, Casey S, Lee BP. Biomimetic adhesive containing nanocomposite hydrogel with enhanced materials properties. *Soft Matter.* 2013;9(14):3825-3833.

170. Lee BP, Chao C-Y, Nunalee FN, Motan E, Shull KR, Messersmith PB. Rapid gel formation and adhesion in photocurable and biodegradable block copolymers with high DOPA content. *Macromolecules.* 2006;39(5):1740-1748.

171. Ryu JH, Hong S, Lee H. Bio-inspired adhesive catechol-conjugated chitosan for biomedical applications: A mini review. *Acta biomaterialia.* 2015;27:101-115.

172. Zhang H, Zhao T, Newland B, Liu W, Wang W, Wang W. Catechol functionalized hyperbranched polymers as biomedical materials. *Progress in Polymer Science.* 2018;78:47-55.

173. Guvendiren M, Messersmith PB, Shull KR. Self-assembly and adhesion of DOPA-modified methacrylic triblock hydrogels. *Biomacromolecules.* 2008;9(1):122-128.

174. Barrett DG, Bushnell GG, Messersmith PB. Mechanically robust, negative-swelling, mussel-inspired tissue adhesives. *Advanced healthcare materials.* 2013;2(5):745-755.

175. Zobrist C, Sobocinski J, Lyskawa J, et al. Functionalization of titanium surfaces with polymer brushes prepared from a biomimetic RAFT agent. *Macromolecules.* 2011;44(15):5883-5892.

176. Gao C, Li G, Xue H, Yang W, Zhang F, Jiang S. Functionalizable and ultra-low fouling zwitterionic surfaces via adhesive mussel mimetic linkages. *Biomaterials.* 2010;31(7):1486-1492.

177. Ye Q, Wang X, Li S, Zhou F. Surface-initiated ring-opening metathesis polymerization of pentadecafluorooctyl-5-norbornene-2-carboxylate from variable substrates modified with sticky biomimic initiator. *Macromolecules.* 2010;43(13):5554-5560.

178. Faure E, Falentin-Daudré C, Jérôme C, et al. Catechols as versatile platforms in polymer chemistry. *Progress in Polymer Science.* 2013;38(1):236-270.

179. Ringsdorf H. Structure and properties of pharmacologically active polymers. Paper presented at: Journal of Polymer Science: Polymer Symposia1975.

180. Elvira C, Gallardo A, Roman J, Cifuentes A. Covalent polymer-drug conjugates. *Molecules.* 2005;10(1):114-125.

181. Joshi A. *Design, synthesis, and characterization of nanoscale therapeutics and nanocomposites*, Rensselaer Polytechnic Institute; 2008.

182. Duncan R, Ringsdorf H, Satchi-Fainaro R. Polymer Therapeutics: Polymers as Drugs, Drug and Protein Conjugates and Gene Delivery Systems: Past, Present and Future Opportunities. *Polymer Therapeutics I*2006:1-8.

183. Statz AR, Meagher RJ, Barron AE, Messersmith PB. New peptidomimetic polymers for antifouling surfaces. *Journal of the American Chemical Society.* 2005;127(22):7972-7973.

184. Zeng H, Hwang DS, Israelachvili JN, Waite JH. Strong reversible Fe3+-mediated bridging between dopa-containing protein films in water. *Proceedings of the National Academy of Sciences.* 2010;107(29):12850-12853.

185. Lee BP, Messersmith PB, Israelachvili JN, Waite JH. Mussel-Inspired Adhesives and Coatings. *Annu Rev Mater Res.* Aug 1 2011;41:99-132.

186. Madhurakkat Perikamana SK, Lee J, Lee YB, et al. Materials from Mussel-Inspired Chemistry for Cell and Tissue Engineering Applications. *Biomacromolecules.* Sep 14 2015;16(9):2541-2555.

187. Moulay S. Dopa/catechol-tethered polymers: Bioadhesives and biomimetic adhesive materials. *Polymer Reviews.* 2014;54(3):436-513.

188. Scognamiglio F, Travan A, Borgogna M, et al. Enhanced bioadhesivity of dopamine-functionalized polysaccharidic membranes for general surgery applications. *Acta Biomater.* 2016;44:232-242.

189. Han L, Lu X, Liu K, et al. Mussel-Inspired Adhesive and Tough Hydrogel Based on Nanoclay Confined Dopamine Polymerization. *ACS Nano.* 2017;11(3):2561-2574.

190. GhavamiNejad A, Rajan Unnithan A, Ramachandra Kurup Sasikala A, et al. Mussel-Inspired Electrospun Nanofibers Functionalized with Size-Controlled Silver Nanoparticles for Wound Dressing Application. *ACS Applied Materials & Interfaces.* 2015;7(22):12176-12183.

191. Lu D, Wang H, Li Te, et al. Mussel-Inspired Thermoresponsive Polypeptide–Pluronic Copolymers for Versatile Surgical Adhesives and Hemostasis. *ACS applied materials & interfaces.* 2017;9(20):16756-16766.

192. Sato T, Aoyagi T, Ebara M, Auzély-Velty R. Catechol-modified hyaluronic acid: in situ-forming hydrogels by auto-oxidation of catechol or photo-oxidation using visible light. *Polym. Bull.* 2017;74(10):4069-4085.

193. Jeon EY, Choi B-H, Jung D, Hwang BH, Cha HJ. Natural healing-inspired collagen-targeting surgical protein glue for accelerated scarless skin regeneration. *Biomaterials.* 2017;134:154-165.

194. GhavamiNejad A, Park CH, Kim CS. In Situ Synthesis of Antimicrobial Silver Nanoparticles within Antifouling Zwitterionic Hydrogels by Catecholic Redox Chemistry for Wound Healing Application. *Biomacromolecules.* 2016;17(3):1213-1223.

195. Scognamiglio F, Travan A, Rustighi I, et al. Adhesive and sealant interfaces for general surgery applications. *Journal of Biomedical Materials Research Part B: Applied Biomaterials.* 2016;104(3):626-639.

196. Chen T, Chen Y, Rehman HU, et al. Ultratough, Self-Healing, and Tissue-Adhesive Hydrogel for Wound Dressing. *ACS applied materials & interfaces.* 2018;10(39):33523-33531.

197. Burke KA, Roberts DC, Kaplan DL. Silk fibroin aqueous-based adhesives inspired by mussel adhesive proteins. *Biomacromolecules.* 2016;17(1):237-245.

198. Ryu JH, Lee Y, Kong WH, Kim TG, Park TG, Lee H. Catechol-functionalized chitosan/pluronic hydrogels for tissue adhesives and hemostatic materials. *Biomacromolecules.* 2011;12(7):2653-2659.

199. Xu J, Soliman GM, Barralet J, Cerruti M. Mollusk glue inspired mucoadhesives for biomedical applications. *Langmuir.* 2012;28(39):14010-14017.

200. Mehdizadeh M, Weng H, Gyawali D, Tang L, Yang J. Injectable citrate-based mussel-inspired tissue bioadhesives with high wet strength for sutureless wound closure. *Biomaterials.* 2012;33(32):7972-7983.

201. Liu Y, Meng H, Messersmith PB, Lee BP, Dalsin JL. Biomimetic adhesives and coatings based on mussel adhesive proteins. *Biological adhesives*: Springer; 2016:345-378.

202. Lee H, Dellatore SM, Miller WM, Messersmith PB. Mussel-inspired surface chemistry for multifunctional coatings. *science.* 2007;318(5849):426-430.

203. Zhao Y, Wu Y, Wang L, et al. Bio-inspired reversible underwater adhesive. *Nature communications.* 2017;8(1):1-8.

204. Palivan CG, Goers R, Najer A, Zhang X, Car A, Meier W. Bioinspired polymer vesicles and membranes for biological and medical applications. *Chemical society reviews.* 2016;45(2):377-411.

205. Ye Q, Zhou F, Liu W. Bioinspired catecholic chemistry for surface modification. *Chem Soc Rev.* Jul 2011;40(7):4244-4258.

206. Quan WY, Hu Z, Liu HZ, et al. Mussel-Inspired Catechol-Functionalized Hydrogels and Their Medical Applications. *Molecules.* Jul 16 2019;24(14).

207. Ho C-C, Ding S-J. Structure, properties and applications of mussel-inspired polydopamine. *Journal of biomedical nanotechnology.* 2014;10(10):3063-3084.

208. García-Fernández L, Cui J, Serrano C, et al. Antibacterial Strategies from the Sea: Polymer-Bound Cl-Catechols for Prevention of Biofilm Formation. *Advanced materials.* 2013;25(4):529-533.

209. Sedo J, Saiz-Poseu J, Busque F, Ruiz-Molina D. Catechol-based biomimetic functional materials. *Adv Mater.* Feb 6 2013;25(5):653-701.

210. Ahn BK, Lee DW, Israelachvili JN, Waite JH. Surface-initiated self-healing of polymers in

aqueous media. *Nature materials.* 2014;13(9):867-872.

211. Ren Y, Zhao X, Liang X, Ma PX, Guo B. Injectable hydrogel based on quaternized chitosan, gelatin and dopamine as localized drug delivery system to treat Parkinson's disease. *International journal of biological macromolecules.* 2017;105:1079-1087.

212. Kim K, Kim K, Ryu JH, Lee H. Chitosan-catechol: A polymer with long-lasting mucoadhesive properties. *Biomaterials.* 2015;52:161-170.

213. Araujo PZ, Morando PJ, Blesa MA. Interaction of catechol and gallic acid with titanium dioxide in aqueous suspensions. 1. Equilibrium studies. *Langmuir.* 2005;21(8):3470-3474.

214. Black KC, Yi J, Rivera JG, Zelasko-Leon DC, Messersmith PB. Polydopamine-enabled surface functionalization of gold nanorods for cancer cell-targeted imaging and photothermal therapy. *Nanomedicine.* 2013;8(1):17-28.

215. Ono RJ, Lee ALZ, Voo ZX, et al. Biodegradable Strain-Promoted Click Hydrogels for Encapsulation of Drug-Loaded Nanoparticles and Sustained Release of Therapeutics. *Biomacromolecules.* Aug 14 2017;18(8):2277-2285.

216. Hasegawa U, Moriyama M, Uyama H, van der Vlies AJ. Catechol-bearing block copolymer micelles: Structural characterization and antioxidant activity. *Polymer.* 2015/06/01/ 2015;66:1-7.

217. Mao X, Liu L, Cheng L, et al. Adhesive nanoparticles with inflammation regulation for promoting skin flap regeneration. *Journal of Controlled Release.* 2019/03/10/ 2019;297:91-101.

218. Lee D, Park JP, Koh M-Y, et al. Chitosan-catechol: a writable bioink under serum culture media. *Biomaterials Science.* 2018;6(5):1040-1047.

219. Guo Z, Xia J, Mi S, Sun W. Mussel-Inspired Naturally Derived Double-Network Hydrogels and Their Application in 3D Printing: From Soft, Injectable Bioadhesives to Mechanically Strong Hydrogels. *ACS Biomaterials Science & Engineering.* 2020/03/09 2020;6(3):1798-1808.

220. Chouhan D, Dey N, Bhardwaj N, Mandal BB. Emerging and innovative approaches for wound healing and skin regeneration: Current status and advances. *Biomaterials.* Sep 2019;216:119267.

221. Boateng JS, Matthews KH, Stevens HN, Eccleston GM. Wound healing dressings and drug delivery systems: a review. *J Pharm Sci.* Aug 2008;97(8):2892-2923.

222. Chouhan D, Dey N, Bhardwaj N, Mandal BB. Emerging and innovative approaches for wound healing and skin regeneration: current status and advances. *Biomaterials.* 2019:119267.

223. Martin P. Wound healing--aiming for perfect skin regeneration. *Science.* 1997;276(5309):75-81.

224. Clark RA, Ghosh K, Tonnesen MG. Tissue engineering for cutaneous wounds. *Journal of Investigative Dermatology.* 2007;127(5):1018-1029.

225. Gosain A, DiPietro LA. Aging and wound healing. *World journal of surgery.* 2004;28(3):321-326.

226. Brem H, Stojadinovic O, Diegelmann RF, et al. Molecular markers in patients with chronic wounds to guide surgical debridement. *Molecular medicine.* 2007;13(1-2):30.

227. Gibson DJ, Schultz G. Chronic wound diagnostic for matrix metalloproteinase: chronic wounds. *Wound healing Southern Africa.* 2009;2(2):68-70.

228. Nyanhongo GS, Sygmund C, Ludwig R, Prasetyo EN, Guebitz GM. Synthesis of multifunctional bioresponsive polymers for the management of chronic wounds. *Journal of Biomedical Materials Research Part B: Applied Biomaterials.* 2013;101(5):882-891.

229. Bhardwaj N, Chouhan D, Mandal BB. 3D functional scaffolds for skin tissue engineering. *Functional 3D tissue engineering scaffolds*: Elsevier; 2018:345-365.

230. Klar AS, Güven S, Biedermann T, et al. Tissue-engineered dermo-epidermal skin grafts prevascularized with adipose-derived cells. *Biomaterials.* 2014;35(19):5065-5078.

231. Kumar JP, Mandal BB. Antioxidant potential of mulberry and non-mulberry silk sericin and its implications in biomedicine. *Free Radical Biology and Medicine.* 2017;108:803-818.

232. Marino D, Luginbühl J, Scola S, Meuli M, Reichmann E. Bioengineering dermo-epidermal skin grafts with blood and lymphatic capillaries. *Science translational medicine.* 2014;6(221):221ra214-221ra214.

233. Suarato G, Bertorelli R, Athanassiou A. Borrowing from Nature: biopolymers and biocomposites as smart wound care materials. *Frontiers in bioengineering and biotechnology.* 2018;6:137.

234. Moura LI, Dias AM, Carvalho E, de Sousa HC. Recent advances on the development of wound dressings for diabetic foot ulcer treatment—a review. *Acta biomaterialia.* 2013;9(7):7093-7114.

235. Lisovsky A, Chamberlain MD, Wells LA, Sefton MV. Cell Interactions with Vascular Regenerative MAA-Based Materials in the Context of Wound Healing. *Advanced healthcare materials.* 2015;4(16):2375-2387.

236. Rodrigues M, Kosaric N, Bonham CA, Gurtner GC. Wound healing: a cellular perspective. *Physiological reviews.* 2019;99(1):665-706.

237. Blázquez R, Sánchez-Margallo FM, Álvarez V, Usón A, Casado JG. Surgical meshes coated with mesenchymal stem cells provide an anti-inflammatory environment by a M2 macrophage polarization. *Acta biomaterialia.* 2016;31:221-230.

238. Guo J, Sun W, Kim JP, et al. Development of tannin-inspired antimicrobial bioadhesives. *Acta biomaterialia.* 2018;72:35-44.

239. Tao SC, Guo SC, Li M, Ke QF, Guo YP, Zhang CQ. Chitosan wound dressings incorporating exosomes derived from microRNA-126-overexpressing synovium mesenchymal stem cells provide sustained release of exosomes and heal full-thickness skin defects in a diabetic rat model. *Stem cells translational medicine.* 2017;6(3):736-747.

240. Niu Y, Li Q, Ding Y, Dong L, Wang C. Engineered delivery strategies for enhanced control of growth factor activities in wound healing. *Advanced drug delivery reviews.* 2019;146:190-208.

241. Gilotra S, Chouhan D, Bhardwaj N, Nandi SK, Mandal BB. Potential of silk sericin based nanofibrous mats for wound dressing applications. *Materials Science and Engineering: C.* 2018;90:420-432.

242. Kogelenberg Sv, Yue Z, Dinoro JN, Baker CS, Wallace GG. Three-dimensional printing and cell therapy for wound repair. *Advances in wound care.* 2018;7(5):145-156.

243. Yang JM, Olanrele OS, Zhang X, Hsu CC. Fabrication of hydrogel materials for biomedical applications. *Novel Biomaterials for Regenerative Medicine*: Springer; 2018:197-224.

244. Hu MS, Maan ZN, Wu JC, et al. Tissue engineering and regenerative repair in wound healing. *Ann Biomed Eng.* Jul 2014;42(7):1494-1507.

245. Lau K, Paus R, Tiede S, Day P, Bayat A. Exploring the role of stem cells in cutaneous wound healing. *Experimental dermatology.* 2009;18(11):921-933.

246. Chen L, Tredget EE, Wu PY, Wu Y. Paracrine factors of mesenchymal stem cells recruit macrophages and endothelial lineage cells and enhance wound healing. *PloS one.* 2008;3(4).

247. Badillo AT, Zhang L, Liechty KW. Stromal progenitor cells promote leukocyte

migration through production of stromal-derived growth factor 1α: a potential mechanism for stromal progenitor cell–mediated enhancement of cellular recruitment to wounds. *Journal of pediatric surgery.* 2008;43(6):1128-1133.

248. Shen Y-I, Song H-HG, Papa AE, Burke JA, Volk SW, Gerecht S. Acellular hydrogels for regenerative burn wound healing: translation from a porcine model. *Journal of Investigative Dermatology.* 2015;135(10):2519-2529.

249. Liu M, Duan X-P, Li Y-M, Yang D-P, Long Y-Z. Electrospun nanofibers for wound healing. *Materials Science and Engineering: C.* 2017;76:1413-1423.

250. Jiang S, Li SC, Huang C, Chan BP, Du Y. Physical properties of implanted porous bioscaffolds regulate skin repair: focusing on mechanical and structural features. *Advanced healthcare materials.* 2018;7(6):1700894.

251. Eke G, Mangir N, Hasirci N, MacNeil S, Hasirci V. Development of a UV crosslinked biodegradable hydrogel containing adipose derived stem cells to promote vascularization for skin wounds and tissue engineering. *Biomaterials.* 2017;129:188-198.

252. Loh QL, Choong C. Three-dimensional scaffolds for tissue engineering applications: role of porosity and pore size. *Tissue Engineering Part B: Reviews.* 2013;19(6):485-502.

253. Lokhande G, Carrow JK, Thakur T, et al. Nanoengineered injectable hydrogels for wound healing application. *Acta biomaterialia.* 2018;70:35-47.

254. Chouhan D, Lohe Tu, Samudrala PK, Mandal BB. In situ forming injectable silk fibroin hydrogel promotes skin regeneration in full thickness burn wounds. *Advanced healthcare materials.* 2018;7(24):1801092.

255. Chouhan D, Thatikonda N, Nilebäck L, Widhe M, Hedhammar M, Mandal BB. Recombinant spider silk functionalized silkworm silk matrices as potential bioactive wound dressings and skin grafts. *ACS applied materials & interfaces.* 2018;10(28):23560-23572.

256. Chouhan D, Chakraborty B, Nandi SK, Mandal BB. Role of non-mulberry silk fibroin in deposition and regulation of extracellular matrix towards accelerated wound healing. *Acta biomaterialia.* 2017;48:157-174.

257. Gil ES, Panilaitis B, Bellas E, Kaplan DL. Functionalized silk biomaterials for wound healing. *Advanced healthcare materials.* 2013;2(1):206-217.

258. Zhao L, Niu L, Liang H, Tan H, Liu C, Zhu F. pH and glucose dual-responsive injectable hydrogels with insulin and fibroblasts as bioactive dressings for diabetic wound healing. *ACS applied materials & interfaces.* 2017;9(43):37563-37574.

259. Griffin DR, Weaver WM, Scumpia PO, Di Carlo D, Segura T. Accelerated wound healing by injectable microporous gel scaffolds assembled from annealed building blocks. *Nature materials.* 2015;14(7):737-744.

260. Yu J, Huang TR, Lim ZH, et al. Production of hollow bacterial cellulose microspheres using microfluidics to form an injectable porous scaffold for wound healing. *Advanced healthcare materials.* 2016;5(23):2983-2992.

261. Michael S, Sorg H, Peck C-T, et al. Tissue engineered skin substitutes created by laser-assisted bioprinting form skin-like structures in the dorsal skin fold chamber in mice. *PloS one.* 2013;8(3).

262. Binder KW, Zhao W, Aboushwareb T, Dice D, Atala A, Yoo JJ. In situ bioprinting of the skin for burns. *Journal of the American College of Surgeons.* 2010;211(3):S76.

263. Koch L, Deiwick A, Schlie S, et al. Skin tissue generation by laser cell printing. *Biotechnology and bioengineering.* 2012;109(7):1855-1863.

264. Ho J, Walsh C, Yue D, Dardik A, Cheema U. Current Advancements and Strategies in Tissue Engineering for Wound Healing: A Comprehensive Review. *Adv Wound Care (New Rochelle).* Jun 1 2017;6(6):191-209.

265. Long J, Etxeberria AE, Nand AV, Bunt CR, Ray S, Seyfoddin A. A 3D printed chitosan-pectin hydrogel wound dressing for lidocaine hydrochloride delivery. *Materials Science and Engineering: C.* 2019;104:109873.

266. Hafezi F, Scoutaris N, Douroumis D, Boateng J. 3D printed chitosan dressing crosslinked with genipin for potential healing of chronic wounds. *International journal of pharmaceutics.* 2019;560:406-415.

267. Muwaffak Z, Goyanes A, Clark V, Basit AW, Hilton ST, Gaisford S. Patient-specific 3D scanned and 3D printed antimicrobial polycaprolactone wound dressings. *International journal of pharmaceutics.* 2017;527(1-2):161-170.

268. Pourmoussa A, Gardner DJ, Johnson MB, Wong AK. An update and review of cell-based wound dressings and their integration into clinical practice. *Annals of translational medicine.* 2016;4(23).

269. Caputo WJ, Vaquero C, Monterosa A, et al. A retrospective study of cryopreserved umbilical cord as an adjunctive therapy to promote the healing of chronic, complex foot ulcers with underlying osteomyelitis. *Wound Repair and Regeneration.* 2016;24(5):885-893.

270. Lavery LA, Fulmer J, Shebetka KA, et al. The efficacy and safety of Grafix® for the treatment of chronic diabetic foot ulcers: results of a multi-centre, controlled, randomised, blinded, clinical trial. *International wound journal.* 2014;11(5):554-560.

271. Zelen CM, Serena TE, Gould L, et al. Treatment of chronic diabetic lower extremity ulcers with advanced therapies: a prospective, randomised, controlled, multi-centre comparative study examining clinical efficacy and cost. *International wound journal.* 2016;13(2):272-282.

272. Seavey JG, Masters ZA, Balazs GC, et al. Use of a bioartificial dermal regeneration template for skin restoration in combat casualty injuries. *Regenerative medicine.* 2016;11(1):81-90.

273. Böttcher-Haberzeth S, Biedermann T, Schiestl C, et al. Matriderm® 1 mm versus Integra® Single Layer 1.3 mm for one-step closure of full thickness skin defects: a comparative experimental study in rats. *Pediatric surgery international.* 2012;28(2):171-177.

274. Nicoletti G, Brenta F, Bleve M, et al. Long-term in vivo assessment of bioengineered skin substitutes: a clinical study. *Journal of tissue engineering and regenerative medicine.* 2015;9(4):460-468.

275. Harding K, Sumner M, Cardinal M. A prospective, multicentre, randomised controlled study of human fibroblast-derived dermal substitute (Dermagraft) in patients with venous leg ulcers. *International wound journal.* 2013;10(2):132-137.

276. Wong VW, Gurtner GC. Tissue engineering for the management of chronic wounds: current concepts and future perspectives. *Exp Dermatol.* Oct 2012;21(10):729-734.

277. Chaudhari AA, Vig K, Baganizi DR, et al. Future Prospects for Scaffolding Methods and Biomaterials in Skin Tissue Engineering: A Review. *Int J Mol Sci.* Nov 25 2016;17(12).

278. Khorshidi S, Karkhaneh A. A self-crosslinking tri-component hydrogel based on functionalized polysaccharides and gelatin for tissue engineering applications. *Mater. Lett.* 2016;164:468-471.

279. Tan H, Chu CR, Payne KA, Marra KG. Injectable in situ forming biodegradable chitosan–hyaluronic acid based hydrogels for cartilage tissue engineering. *Biomaterials.* 2009;30(13):2499-2506.

280. Zhao H, Heindel ND. Determination of degree of substitution of formyl groups in polyaldehyde dextran by the hydroxylamine

hydrochloride method. *Pharmaceutical Research.* 1991;8(3):400-402.

281. Yan S, Wang T, Feng L, et al. Injectable in situ self-cross-linking hydrogels based on poly (L-glutamic acid) and alginate for cartilage tissue engineering. *Biomacromolecules.* 2014;15(12):4495-4508.

282. Paez JI, Ustahüseyin O, Serrano C, et al. Gauging and tuning cross-linking kinetics of catechol-PEG adhesives via catecholamine functionalization. *Biomacromolecules.* 2015;16(12):3811-3818.

283. Puertas-Bartolomé M, Vázquez-Lasa B, San Román J. Bioactive and Bioadhesive Catechol Conjugated Polymers for Tissue Regeneration. *Polymers.* 2018;10(7):768.

284. Wang H, Joseph JA. Quantifying cellular oxidative stress by dichlorofluorescein assay using microplate reader1. *Free Radical Biol. Med.* 1999;27(5-6):612-616.

285. Wang SY, Lan XY, Xiao JH, Yang JC, Kao YT, Chang ST. Antiinflammatory activity of Lindera erythrocarpa fruits. *Phytother. Res.* 2008;22(2):213-216.

286. Guevara I, Iwanejko J, Dembińska-Kieć A, et al. Determination of nitrite/nitrate in human biological material by the simple Griess reaction. *Clinica Chimica Acta.* 1998;274(2):177-188.

287. Choi MS, Lee SH, Cho HS, et al. Inhibitory effect of obovatol on nitric oxide production and activation of NF-κB/MAP kinases in lipopolysaccharide-treated RAW 264.7 cells. *Eur. J. Pharmacol.* 2007;556(1-3):181-189.

288. Lai Y-L, Lin Y-Y, Sadhasivam S, et al. Efficacy of Bletilla striata polysaccharide on hydrogen peroxide-induced apoptosis of osteoarthritic chondrocytes. *Journal of Polymer Research.* 2018;25(2).

CHAPTER

02

BIOCOMPATIBLE AND BIOADHESIVE LOW MOLECULAR WEIGHT POLYMERS CONTAINING LONG-ARM CATECHOL-FUNCTIONALIZED METHACRYLATE

María Puertas-Bartolomé[1,2], Mar Fernández-Gutiérrez[1,2], Luis García-Fernández[1,2,*], Blanca Vázquez-Lasa[1,2*] and Julio San Román[1,2]

[1] Institute of Polymer Science and Technology, ICTP-CSIC 28006 Madrid, Spain
[2] CIBER-BBN, Health Institute Carlos III. 28029 Madrid, Spain

European Polymer Journal 98 (2018) 47–55

Research Article

Biocompatible and bioadhesive low molecular weight polymers containing long-arm catechol-functionalized methacrylate

María Puertas-Bartolomé, Mar Fernández-Gutiérrez, Luis García-Fernández*, Blanca Vázquez-Lasa* and Julio San Román

European Polymer Journal 98 (2018) 47–55

DOI:10.1016/j.eurpolymj.2017.11.011

ABSTRACT

Excellent adherence properties of blue mussels have been attributed to a catechol-containing amino acid, L-3,4-dihydroxyphenylalanine. This natural form of adhesion has been a source of inspiration to develop bioadhesive polymers that adhere to biological interfaces. In this study, we describe a bioinspired approach for preparing bioadhesive and biocompatible materials based on synthetic low molecular weight copolymers of a flexible catechol-functionalized methacrylate (CEMA) and *N*-vinylcaprolactam. Copolymers with CEMA contents in the range 0.9 - 13.5 mole % were obtained by radical copolymerization. These systems show good biocompatibility and provide good antioxidant behavior and anti-inflammatory activity. Likewise, hydrogels prepared by mixture of a selected copolymer with gelatin possess good bone bioadhesive properties. These findings show that copolymer composition can be used as a tool for the preparation of biomedical systems with tunable properties and great potential for the development of drug delivery systems and bioactive gels that can be applied in tissue regeneration processes.

Keywords: *catechol polymers, antioxidant, anti-inflammatory, bioadhesion, tissue regeneration.*

CHAPTER

03

BIOACTIVE AND BIOADHESIVE CATECHOL CONJUGATED POLYMERS FOR TISSUE REGENERATION

María Puertas-Bartolomé[1,2], Blanca Vázquez-Lasa[1,2*] and Julio San Román[1,2]

[1] Institute of Polymer Science and Technology, ICTP-CSIC 28006 Madrid, Spain
[2] CIBER-BBN, Health Institute Carlos III. 28029 Madrid, Spain

Polymers 10 (2018) 768

Research Article

Bioactive and Bioadhesive Catechol Conjugated Polymers for Tissue Regeneration

María Puertas-Bartolomé, Blanca Vázquez-Lasa* and Julio San Román

Polymers 10 (2018) 768

DOI: 10.1016/j.msec.2019.110040

ABSTRACT

The effective treatment of chronic wounds constitutes one of the most common worldwide healthcare problem due to the presence of high levels of proteases, free radicals and exudates in the wound, which constantly activate the inflammatory system, avoiding tissue regeneration. In this study, we describe a multifunctional bioactive and resorbable membrane with in-built antioxidant agent catechol for the continuous quenching of free radicals as well as to control inflammatory response, helping to promote the wound-healing process. This natural polyphenol (catechol) is the key molecule responsible for the mechanism of adhesion of mussels providing also the functionalized polymer with bioadhesion in the moist environment of the human body. To reach that goal, synthesized statistical copolymers of *N*-vinylcaprolactam (V) and 2-hydroxyethyl methacrylate (H) have been conjugated with catechol bearing hydrocaffeic acid (HCA) molecules with high yields. The system has demonstrated good biocompatibility, a sustained antioxidant response, an anti-inflammatory effect, an ultraviolet (UV) screen, and bioadhesion to porcine skin, all of these been key features in the wound-healing process. Therefore, these novel mussel-inspired materials have an enormous potential for application and can act very positively, favoring and promoting the healing effect in chronic wounds.

Keywords: *wound healing, catechol, conjugated, antioxidant, anti-inflammatory, bioadhesion, ultraviolet (UV) shielding.*

3

CHAPTER

04

BIOADHESIVE FUNCTIONAL HYDROGELS: CONTROLLED RELEASE OF CATECHOL SPECIES WITH ANTIOXIDANT AND ANTI-INFLAMMATORY BEHAVIOR

María Puertas-Bartolomé[1,2], Lorena Benito-Garzón[3], Stephanie Fung[4], Joachim Kohn[4], Blanca Vázquez-Lasa[1,2*], Julio San Román[1,2]

[1] Institute of Polymer Science and Technology, ICTP-CSIC 28006 Madrid, Spain
[2] CIBER-BBN, Health Institute Carlos III. 28029 Madrid, Spain
[3] Faculty of Medicine, University of Salamanca 37007, Salamanca, Spain.
[4] Rutgers University, New Jersey Center for Biomaterials, 08854 Piscataway, NJ, USA.

Materials Science & Engineering C 105 (2019) 110040

Research Article

Bioadhesive functional hydrogels: Controlled release of catechol species with antioxidant and anti-inflammatory behavior

María Puertas-Bartolomé, Lorena Benito-Garzón, Stephanie Fung, Joachim Kohn, Blanca Vázquez-Lasa* and Julio San Román

Materials Science & Engineering C 105 (2019) 110040

DOI: 10.1016/j.msec.2019.110040

ABSTRACT

Chronic wounds are particularly difficult to heal and constitute an important global health care problem. Some key factors that make chronic wounds challenging to heal are attributed to the incessant release of free radicals, which activate the inflammatory system and impair the repair of the wound. Intrinsic characteristics of hydrogels are beneficial for wound healing, but the effective control of free radical levels in the wound and subsequent inflammation is still a challenge. Catechol, the key molecule responsible for the mechanism of adhesion of mussels, has been proven to be an excellent radical scavenger and anti-inflammatory agent. Our approach in this work lies in the preparation of a hybrid system combining the beneficial properties of hydrogels and catechol for its application as a bioactive wound dressing to assist in the treatment of chronic wounds. The hydrogel backbone is obtained through a self-covalent crosslinking between chitosan (Ch) and oxidized hyaluronic acid (HAox) in the presence of a synthetic catechol terpolymer, which is subsequently coordinated to Fe^{3+} to obtain an interpenetrated polymer network (IPN). The structural analysis, catechol release profiles, *in vitro* biological behavior and *in vivo* performance of the IPN is analyzed and compared with the semi-IPN (without Fe) and the Ch/HAox crosslinked hydrogels as controls. Catechol-containing hydrogels present high tissue adhesion strength under wet conditions, support growth, migration and proliferation of hBMSCs, protect cells against oxidative stress damage induce by ROS, and promote down-regulation of the pro-inflammatory cytokine IL-1β. Furthermore, *in vivo* experiments reveal their biocompatibility and stability, and histological studies indicate normal inflammatory responses and faster vascularization, highlighting the performance of the IPN system. The novel IPN design also allows for the *in situ* controlled and sustained delivery of catechol. Therefore, the developed IPN is a suitable ECM-mimic platform with high cell affinity and bioactive functionalities that, together with the controlled catechol release, will enhance the tissue regeneration process and has a great potential for its application as wound dressing.

Keywords: *chitosan, hyaluronic acid, catechol, antioxidant, anti-inflammatory, in vivo.*

4

CHAPTER

05

3D PRINTING OF A REACTIVE HYDROGEL BIOINK USING A STATIC MIXING TOOL

María Puertas-Bartolomé[1,2], Małgorzata K.Włodarczyk-Biegun[3], Aránzazu del Campo[3,4], Blanca Vázquez-Lasa[1,2]* and Julio San Román[1,2]

[1] *Institute of Polymer Science and Technology, ICTP-CSIC 28006 Madrid, Spain*
[2] *CIBER-BBN, Health Institute Carlos III. 28029 Madrid, Spain*
[3] *INM – Leibniz Institute for New Materials, 66123 Saarbrücken, Germany*
[4] *Chemistry Department, Saarland University, 66123 Saarbrücken, Germany*

In consideration for publication

Research Article

3D printing of a reactive hydrogel bioink using a static mixing tool

María Puertas-Bartolomé, Małgorzata K.Włodarczyk-Biegun, Aránzazu del Campo, Blanca Vázquez-Lasa* and Julio San Román

In consideration for publication

ABSTRACT

Hydrogel based bioinks have recently attracted much attention for 3D printing applications in tissue engineering due to their remarkable intrinsic properties, such as a cell supporting environment. However, their usually weak mechanical properties lead to poor printability and low stability of the obtained structures. To obtain good shape fidelity current approaches based on extrusion printing use high viscosity solutions, which can compromise cell viability. This paper presents a novel bioprinting methodology based on a dual-syringe system with a static mixing tool that allows in situ crosslinking of a two-component hydrogel-based ink in the presence of living cells. The reactive hydrogel system consists of carboxymethyl chitosan (CMCh) and partially oxidized hyaluronic acid (HAox) that undergo fast self-covalent crosslinking via Schiff base formation. This new approach allows using low viscosity solutions since in situ gelation provides the appropriate structural integrity to maintain the printed shape. The proposed bioink formulation was optimized to match crosslinking kinetics with the printing process and multi layered 3D bioprinted scaffolds were successfully obtained. Printed scaffolds showed moderate swelling, good biocompatibility with embedded cells and were mechanically stable after 14 days of cell culture. We envision that this straightforward, powerful and generalizable printing approach can be used for a wide range of materials, growth factors or cell types, to be employed for soft tissue regeneration.

Keywords: *3D-bioprinting, static mixer, reactive hydrogel, chitosan, hyaluronic acid.*

1. INTRODUCTION

3D bioprinting is a booming additive manufacturing technology that allows layer by layer deposition of a cell-laden material to fabricate 3D constructs with spatial control over scaffold design. This technology has been widely used in the last few years for tissue engineering and regenerative medicine applications as it allows the artificial reconstruction of the complexity of native tissues or organs.[1-3] To date, great efforts have been made to develop suitable bioinks to provide cell-laden scaffolds with good mechanical properties as well as high cell viability. Hydrogels are often used as supporting material in the bioink due to their favorable intrinsic properties for supporting cellular growth.[4-11] Their unique inherent properties similar to the extracellular matrix (EMC), such as porosity that allows nutrient and gaseous exchange, high water content, biodegradability and biocompatibility make them attractive for cell therapy applications.[12-14] Specifically, bioinks based on natural hydrogels, such as alginate, agarose, gelatin, collagen, chitosan or hyaluronic acid are regularly used.[4,15-21]

Extrusion is the most frequently used technique for 3D bioprinting with hydrogel precursors.[22,23] The minimal requirements that the hydrogel bioink has to fulfil for successful extrusion include: 1) bioink must easily flow through the needle during printing but retain the shape after extrusion; 2) printed strands should have a good structural integrity to provide self-supporting structures with good adhesion between layers; 3) bioink must ensure cell survival and proliferation within the printed scaffold.[24,25] Naturally derived hydrogels are still challenging to print due to their weak mechanical properties that lead to poor printing accuracy and low stability of the printed structures.[9,26-29] Traditional approaches based on increasing the polymer content and viscosity or the crosslinking density have been attempted to improve printability of naturally derived hydrogel bioinks and the mechanical performance of their printed scaffolds.[5,25] However, bioinks with high polymer contents or viscosities can compromise cell viability due to the high shear forces and lower nutrients transport through the printed constructs.[5,25,30] Thus, the development of low viscosity bioinks and suitable printing extrusion processes for biofabrication is still in demand.

In this paper, we present a methodology for printing homogeneous strands from a reactive, *in situ* crosslinking hydrogel using a dual syringe system with a static mixing tool coupled to an extrusion bioprinter. The two reactive hydrogel precursors are loaded into separate syringes, simultaneously extruded by mechanical displacement and transported to the static mixer in a 1:1 ratio. They are homogeneously mixed during the short residence time in the static mixer and the crosslinking reaction is initiated prior extrusion. The partially crosslinked hydrogel is then extruded from the printhead. This approach has several advantages for 3D extrusion printing: 1)

it uses low viscosity starting solutions of the hydrogel precursors and avoids high shear stress during extrusion; 2) *in situ* crosslinking provides appropriate structural integrity to the printed thread to maintain the printed shape obtain good shape fidelity; 3) it avoids postprinting cell seeding (cells are embedded in the ink), washing steps or additional physical factors that may complicate the fabrication process.

Two component systems have been used for 3D printing. Skardal *et al*[31] used methacrylated gelatin and methacrylated hyaluronic acid[31] to print scaffolds with gradient material properties, but exchange of the syringes during the printing process was required. Bakarich *et al*[22] and O'Connell *et al*[32] presented a two component extrusion printing system (alginate/polyacrylamide and an acrylated urethane,[22] or gelatin–methacrylamide and hyaluronic acid–methacrylate)[32] where materials were mixed prior to printing in a static nozzle or in the needle, and UV irradiation was required for stabilization of the printed structures. Reactive hydrogels have been also used in 3D printing. Gregor *et al*[33] and Zimmermann *et al*[34] prepared 3D scaffolds by fusion of individual droplets of two precursors (fibrinogen and thrombin[33] or thiol-terminated starPEG and maleimide-functionalized heparin),[34] and Lozano *et al*[35] used a hand-held system with a coaxial syringe tip to extrude precursors (gellan gum-RGD and $CaCl_2$). However, mixing and crosslinking takes place during droplet deposition, and scaffolds with spatially graded material properties were obtained.[34,35] Maiullari *et al*[36] used a microfluidic 3D printing approach where alginate/PEG-fibrinogen and $CaCl_2$ precursors were mixed after extrusion from a coaxial needle and an UV crosslinking step was needed to increase stability of the printed structure. Bootsma *et al*[37] used a mixing head in order to combine hydrogel precursors (alginate/acrylamide/*N,N*- methylenebisacrylamide/D-glucono-δ-lactone and alginate/$CaCO_3$/Irgacure 1173), though additional UV crosslinking was still necessary to induce covalent crosslinking. On the other hand, the static mixing tool has been used for different reactive hydrogel systems in several reported works. Deepthi *et al* prepared an injectable fibrin hydrogel containing alginate nanobeads using a double syringe connected to the static mixer.[38] Hozumi *et al* studied the gelation process through a static mixer of alginate hydrogels with Ca^{2+}.[39] Also, different studies have reported the use of static mixers in other hydrogel processing technologies, like in injectable[40-43] or moulding formulations,[44,45] but in all these examples shape fidelity has not been addressed. To our best knowledge, static mixers have not been explored for 3D bioprinting of reactive hydrogels with good shape fidelity and resolution.

In order to take advantage of a static mixer for 3D printing of a reactive two component ink, the gelation kinetics has to be carefully adjusted to the residence time in the tool. In this work, we used the naturally derived hydrogels chitosan[26,46-48] and hyaluronic acid[19,49-51] modified with reactive groups and formulated in two separate precursor solutions. Chitosan is a great

candidate for tissue engineering applications since it exhibits notable biological features such as great cytocompatibility and biodegradability, antibacterial, hemostatic, or mucoadhesive properties.[52,53] Specifically, carboxymethyl chitosan derivative (CMCh) was selected because of its good solubility at physiological pH, that allows straightforward encapsulation of cells in the bioink[54,55] and avoids any neutralization or washing steps, commonly used for pure chitosan-based printing.[26,47,56,57] Hyaluronic acid (HA) is an important component of the ECM what favors cell affinity and proliferation.[58,59] HA is not suitable by itself for 3D printing, but it can improve printability of the bioink due to its shear-thinning behavior,[50] and when it is in combination with chitosan it can counteract the brittle mechanical properties of the former.[52] Thus, when using a CMCh/HA ink, the free amines of CMCh can react with the aldehyde groups of partially oxidized hyaluronic acid (HAox)[60] after mixing, via Schiff base formation[54,61-63] giving rise to a hydrogel structure. This system has been demonstrated to allow viable cell encapsulation.[64] In this paper, this printing methodology has been optimized in order to fulfil the requirements for successful bioprinting to lead to cell laden 3D hydrogel constructs with good resolution and shape fidelity.

2. EXPERIMENTAL SECTION

2.1. MATERIALS

Carboxymethyl chitosan (CMCh) (degree of deacetylation 85 – 90 %, viscosity = 5-300 mPas, Chitoscience), sodium hyaluronan (HA) (Sigma Aldrich, ~1.5-1.8 x 10^6 Da), sodium periodate ($NaIO_4$) (Alfa Aesar), ethylene glycol (Sigma), hydroxylamine (Sigma-Aldrich), iron chloride (III) (Sigma-Aldrich) and phosphate buffered saline solution (PBS) 10 mM pH 7.4 (Gibco) were used as received. Sodium hyaluronan of low molecular weight ($M_w \sim 200$ kDa, Bioiberica) was oxidized (HAox) prior to use as reported elsewhere,[60] with a final oxidation degree of 48±3.2%.[65,66]

2.2. BIOINK FORMULATION

Hydrogel inks were formulated in two separate solutions. CMCh was dissolved in PBS (pH=7.4), unless otherwise noted. HAox or HAox with HA mixture was dissolved in 0.1 M NaCl. The final ink formulation is named CMChn/HAoxn-HAn, where the number (n) that follows the polysaccharide abbreviation means the weight percentage of the precursor solution. Initially, different CMCh/HAox and CMCh/HAox-HA compositions were tested for optimization of the printing process. Finally, 3D printed scaffolds were prepared with the optimized hydrogel formulation: CMCh2/HAox4-HA0.4. A 1:1 volume ratio of the two solutions was used for printing.

To increase in vitro stability of the printed scaffolds for longer term cell studies, a post-printing stabilization step was carried by immersion in a 20 mM $FeCl_3$ aqueous solution for 7 min.

2.3. 3D PRINTING WITH A STATIC MIXING TOOL

The 3D Discovery printer (RegenHu, Switzerland) was modified to accommodate a static mixing tool. The mixing tool system consists of two 1 mL disposable syringes coupled to a single disposable static mixer (2.5 mL length, helical screw inside) provided by RegenHu Company, and a printing needle (Figure 1A). To employ mixing system, the original high precision plunger dispenser of the printer was adjusted with a custom-made holder for the static mixing tool. The obtained dual extrusion printing head employs simultaneous mechanically driven movement of two syringes plungers using a single motor (Figure 1B). This leads to 1:1 mixing ratio of the liquids from the connected syringes that have the same dimensions. The plungers speed is controlled by the software, accordingly modified by RegenHu. The solutions are transported to the static mixer, and finally extruded through the connected needle (Figure 1C).

Printing and plunger speeds were optimized for each tested ink formulation. Values in the range 5-25 mm/s (print head movement speed) and 0.04-0.1mm/s (plunger speed) were tested, using a design of 4 cm long parallel lines. Conical polyethylene needle with an inner diameter of 200 μm was used. 3D scaffolds (2 or 4 layer grid square: 120 x 120 mm^2, 10 mm separation between strands) were printed with 15 mm/s printing speed and 0.06 mm/s plunger speed. Prior to start of the designed architecture printing, one sacrificial 4 cm long line was printed to allow material homogenization in the mixer. Scaffolds were printed onto glass coverslips.

2.4. BIOINK AND 3D PRINTED SCAFFOLDS CHARACTERIZATION

2.4.1. Rheological analysis

Rheology experiments were performed at controlled temperature of 25 °C, using a rheometer (ARG2, TA Instruments) equipped with a parallel plate sand-blasted geometry (25 mm diameter).

Gelation times were measured in oscillation mode in time sweep experiments. Storage modulus (G′) and loss modulus (G′′) were recorded at a frequency of 1 Hz and 1% strain over 5 min. 75 μL of CMCh solution was deposited on the lower plate. Then, the same volume of the corresponding HAox or HAox-HA solution was deposited on top, shortly mixed by pipetting, and the mixture

was immediately compressed between measuring plates (300 μm measuring gap). Different compositions were tested: CMCh1/HAox1, CMCh1/HAox2, CMCh2/HAox2, CMCh2/HAox4, CMCh3/HAox3, CMCh3/HAox6 and CMCh2/HAox4-HA0.4. Gelation time was defined as the time when G' crossed-over G''. Each sample was measured three times and the average gelation time value was given. Additionally, to determine final viscoelastic properties, frequency sweep experiment was performed for the optimized bioink formulation CMCh2/HAox4-HA0.4. Storage modulus (G') and loss modulus (G'') were recorded at 1% strain and increasing frequencies from 1 to 200 Hz.

Viscosities of 2 wt% CMCh, 4 wt% HAox, and HAox-HA blends (4 wt% HAox with 0.2, 0.4 or 0.6 wt% HA amounts) solutions were determined by rotational shear measurements at increasing shear rate from 1 to 500 1/s. Final viscosity of CMCh2/HAox4-HA0.4 hydrogel was measured at shear rates increasing from 0.1 to 150 1/s.

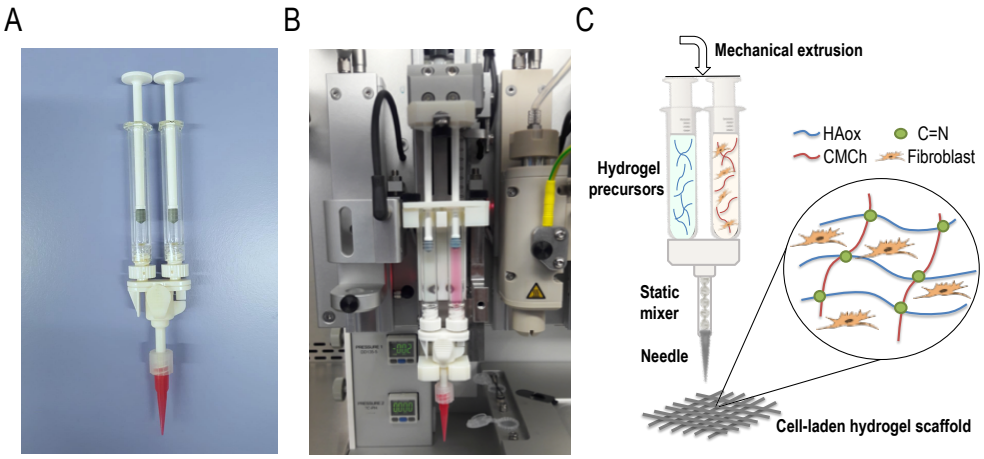

Figure 1. (A) Picture of the static mixing tool; (B) Static mixing tool coupled to the 3D printer; (C) Scheme of the bioprinting process using the mixing device coupled to the 3D printer.

2.4.2. ATR-FTIR spectroscopy

Attenuated Total Reflection Fourier Transform Infra-Red spectra of CMCh, HAox-HA and CMCh2/HAox4-HA0.4 samples were measured for structural characterization (ATR-FTIR, Perkin-Elmer Spectrum One).

2.4.3. Scaffolds morphology

Light microscopy characterization of printed formulations was performed with a stereomicroscope SMZ800N (Nikon, Germany) equipped with home-made bottom illumination and camera (Samsung 13MPx) for imaging.

2.4.4. *In vitro* swelling and degradation studies

Swelling and degradation *in vitro* were carried out in physiological (PBS pH=7.4 at 37 ºC) conditions to evaluate stability of just-printed scaffolds, and scaffolds with additional post-printing stabilization. Additional post-printing stabilization step was performed by immersion in a 20 mM $FeCl_3$ aqueous solution for 7 min. For the *in vitro* swelling experiments, printed samples (2 layer square-based scaffolds) were incubated in PBS for 4 h and, after gentle removal of excess of PBS, imaged using a stereomicroscope SMZ800N (Nikon, Germany). Swelling was evaluated by measuring strands widths in the scaffold with imageJ software, before and after incubation. A minimum of 4 replicates was analyzed and results were given as mean ± SD. In vitro degradation was qualitative analyzed by microscope pictures (Nikon SMZ800N, Germany) after 1, 4, 7, 14 and 21 days of incubation in PBS. Images were taken using a microscope Nikon Eclipse TE2000-S with camera NikonDS-Ri2.

2.5. CMCH2/HAOX4-HA0.4 BASED BIOPRINTING

2.5.1. Cell culture

L929 Fibroblasts (ATCC, Germany) were cultured in RPMI 1640 phenol red free medium (Gibco, 61870-010) supplemented with 20% fetal bovine serum (FBS, Gibco, 10270), 200 mM L-glutamine and 1% penicillin/streptomycin (Invitrogen). Incubation was carried out at 37 °C, 95% humidity and 5% CO_2. Cell culture media was changed every two days.

2.5.2. Bioink preparation

L929 Fibroblasts (ATCC, Germany) were loaded in the 2 wt% CMCh solution (prepared in RPMI 1640) at a 2 x 10^6 cells/mL concentration. Solutions of both hydrogel precursors (2 wt% CMCh loaded with L929, and 4 wt% HAox-0.4 wt% HA) were transferred into the printing syringes and 2 layer square-based (120 x 120 mm^2) scaffolds were printed at r.t. The final cell concentration in the scaffold was 1 x 10^6 cells/mL. Additional post-printing stabilization step was carried by

immersion in a 20 mM $FeCl_3$ aqueous solution for 7 min. After that time, solution was removed and samples were incubated in cell culture media.

2.5.3. Cell assays and staining

In order to evaluate cell viability within the hydrogel scaffold over a 14 days-period, staining with fluorescein diacetate (FDA) and propidium iodide (PI) was carried out to detect live and dead cells respectively. In brief, scaffolds were washed with PBS at different time points (1, 4, 7 and 14 days) and incubated with 20 μg/mL FDA and 6 μg/mL PI for 10 min at r.t. Then, samples were washed with PBS 3 x and fluorescence images were taken using Nikon Ti-Ecllipse microscope (Nikon Instruments Europe B.V., Germany). Quantification was performed by image analysis using the Image-J 1.52p software counting both green and red cells with the function "find maxima". Cell viability percentage was calculated by quantifying the live cells between the total amount of cells in at least 5 images for 3 independent samples. As a control, cell viability studies of cells encapsulated in bulk hydrogels without using the static mixer were performed at 1 day. Analysis of variance (ANOVA) using Tukey grouping method of the results for the printed samples was performed at each time with respect to the day 1 at significance level of *** $p < 0.05$, and with respect to non-printed samples at significance level of $^{\#\#\#}p<0.05$.

Fluorescence staining of nuclei was carried out to quantify cell proliferation within the 3D constructs over a 14-days period. Cells were fixed with PFA 3.7% w/v for 15 min at different time points (1, 4, 7 and 14 days), followed by permeabilization with 0.5% Triton -X 100 in PBS for 15 min and incubated with 1:1000 DAPI dilution in PBS for 20 min. Finally, samples were imaged using a Zeiss LSM 880 confocal microscope. Image analysis was performed using the Image-J 1.52p software using the functions "Z project" and "find maxima" to count the number of nuclei observed in all the z levels analyzed by confocal. Cell quantification with ImageJ was performed in 3 images per sample in a 425.1 x 425.1 μm tested area, and quantification obtained at day 1was normalized to 100%. Analysis of variance (ANOVA) using Tukey grouping method of the results for the printed samples was performed at each time point at significance level of * $p < 0.05$.

3. RESULTS AND DISCUSSION

3.1. 3D PRINTING WITH STATIC MIXING TOOL

The printing conditions to obtain stable threads from the two component hydrogel system using the static mixer tool were evaluated. Once the two components enter the static mixer, diffusion

and covalent reaction between the amine groups of CMCh and aldehyde groups of HAox is started. Non-covalent interactions such as hydrogen bonds or ionic interactions might further stabilize the gel[67-69] and can be beneficial for the extrusion process. For high fidelity printing without clogging the nozzle, the crosslinking kinetics must be adjusted to ensure adequate mixing and good printing quality. The polymer concentration and components ratio, the gelation kinetics and the viscosity of the inks are relevant parameters to adjust.

The matching between hydrogel crosslinking kinetics and extrusion speed is essential to obtain adequate crosslinking degree in the static mixer to allow flow while providing smooth and stable strands.[37,39] The crosslinking kinetics for different CMCh and HAox weight concentrations (CMCh1/HAox1, CMCh1/HAox2, CMCh2/HAox2, CMCh2/HAox4, CMCh3/HAox3 and CMCh3/HAox6) were studied in rheological experiments. Figure 2A presents the variation of the shear modulus G' and the loss modulus G" as a function of time for the CMCh/HAox formulations that gave a measurable gelation point. As the system began to crosslink through the formation of Schiff base linkages, G' increased at a faster speed than G'', indicating change in the viscoelastic behavior of the system to a more solid-like state. These differential growth speeds led to crossover point of G'and G'', defined as a gelation point, indicating that the 3D hydrogel network was formed.[64,70] The corresponding gelation time ranged from 0.90±0.06 to 4.68±0.10 min for the formulations studied (Figure 2B). Regarding ink composition, gelation time decreased with decreasing CMCh/HAox ratio and with increasing CMCh concentration. The printability of the ink formulations was evaluated by image analysis of printed threads (Figure 2C). Printed threads with 1 wt% CMCh were liquid, in agreement with the rheology data that did not show gel formation (undergelation). Broken lines with small gel blocks were visible for 3 wt% CMCh formulations. In these cases gel formation was faster than the residence time of the solution in the static mixer (overgelation), and the shear force needed to extrude the ink caused gel fracture. For the intermediate CMCh compositions (2 wt%), semi-solid printed strands were observed, so 2 wt% CMCh was considered a minimum concentration threshold for gel formation. The CMCh2/HAox2 formulation yielded broad lines with low shape fidelity. A feasible region was found for CMCh2/HAox4 formulation, which rendered smooth lines with shape fidelity. In this formulation the crosslinking degree achieved in the mixing head provided adequate viscosity for extrusion with enough mechanical stability for high fidelity printing. CMCh2/HAox4, with a gelation time of 3.64±0.43 min, was selected as the most appropriate ink for the subsequent experiments.

While printing the CMCh2/HAox4 mixture, bubbles were observed in the needle (Figure 3A, black arrows). In addition, the printed lines had an irregular shape (Figure 3A). We hypothesized that the different viscosity of the precursor solutions, due to the different molecular weights of

the polymers,[62,71] would be the reason for these features. Figure 3B shows that the viscosity of 2 wt% CMCh is 2 orders of magnitude higher than the viscosity of 4 wt% HAox. A different viscosity of the precursor's solutions is reported to lead to non-homogeneous mixtures due to their different flow through the mixer during extrusion.[37,39] Different strategies have been used in order to adjust viscosities of precursor solutions when using static mixers. For example, Hozumi et al[39] used carboxymethyl cellulose as thickening agent, and Bootsma et al[37] distributed the solution with largest impact on viscosity in the two syringes. In order to increase the viscosity of the HAox solution, we supplemented it with non-oxidized HA. The viscosity of different HAox-HA blends is also plotted in Figure 3B. All tested solutions presented a shear thinning behavior that facilitates extrusion and shape fidelity.[5] The addition of increasing amounts of HA to the HAox solution lead to a higher viscosity of the mixture. Based on the obtained results, addition of 0.4 wt% of HA to the 4 wt% HAox solution resulted in a similar viscosity to the 2 wt% CMCh solution. This addition did not influence crosslinking kinetics of the formulation (Figure S1). Printing test with CMCh2/HAox4-HA0.4 formulation (Figure 3C) showed regular and smooth lines without broken parts and no bubbles formed during the printing process. The CMCh2/HAox4-HA0.4 formulation provided stable filaments with low deviance from the needle geometry and minimized collapsing between the superposed layers visible in the cross-points (Figure 3C). These observations indicate that static mixing of solutions with comparable viscosities improves mixing performance, printing quality and resolution.

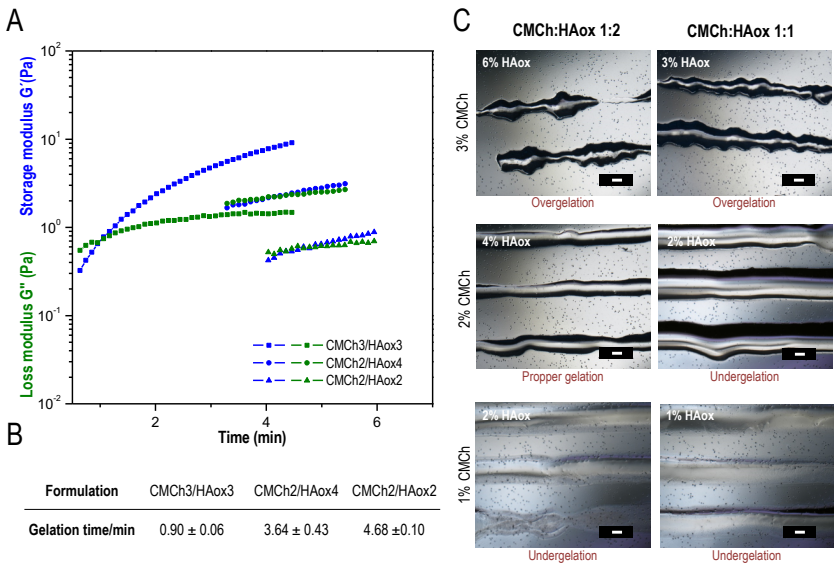

Figure 2. (A) Storage (G') and loss (G") moduli obtained in time sweep rheological experiments, (B) gelation times, defined as G' and G" crossover points and (C) light microscope pictures of printed samples of CMCh/HAox formulations with different weight concentrations of CMCh and HAox solutions. Scale bars in white color correspond to 500 μm.

The printing protocol described here allows high fidelity printing of hydrogel structures with low-viscosity ink solutions, which is favorable for cell laden scaffolds.[5,25,30] The hydrogel viscosity, flow rate and gelation kinetics of the components as they pass through the static mixer affect the mixing performance, homogeneity, and self-support capacity of the bioink.

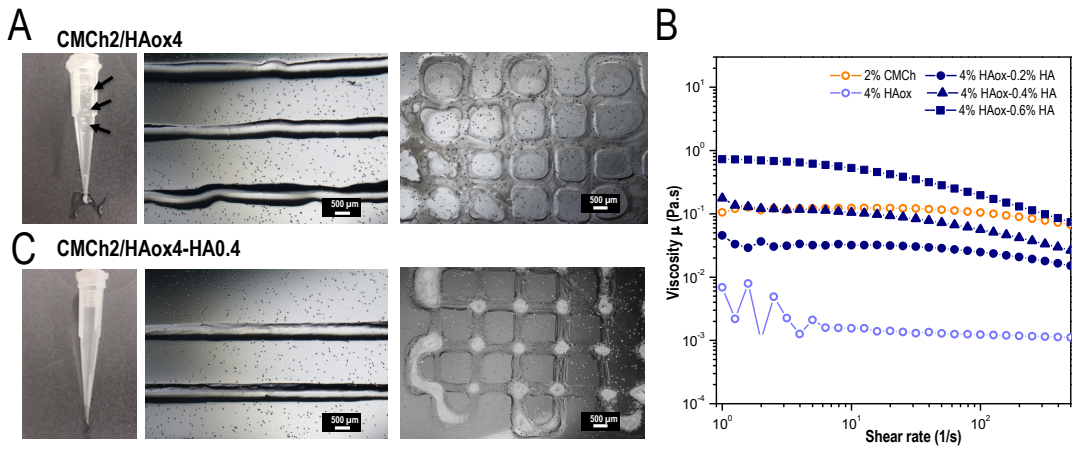

Figure 3. (A) Image of the needle during printing. Black arrows highlight bubbles inside the bioink. Light microscopy pictures of printed strands and 3D printed scaffolds using CMCh2/HAox4 formulation. (B)Viscosity measurements of 2 wt% CMCh, 4 wt% HAox and different HAox/HA blends. (C) Image of the needle during printing and light microscopy pictures of printed strands and 3D printed scaffolds using CMCh2/HAox4-HA0.4 formulation.

3.2. CHARACTERIZATION OF THE OPTIMIZED BIOINK

In order to confirm the formation of covalent crosslinks between the CMCh and HAox components of the printing mixture, the CMCh2/HAox4-HA0.4 formulation was characterized by FTIR spectroscopy (see Figure S2). The characteristic peaks corresponding to the functional groups of the CMCh and HAox/HA precursors were observed in the mixture,[54,55,60] together with a band at 1653 cm^{-1} which can be attributed to the stretching vibration of the C=N bond of the Schiff base formed by reaction of amine and aldehyde groups. This indicates that covalent crosslinking was successfully achieved.[61,62,72] Besides, a peak was observed at 885 cm^{-1}, corresponding to the hemiacetal structure obtained due to the unreacted aldehyde groups of HAox after crosslinking.[60] Intensity of this peak is lower than in the HAox spectrum, which indicates that the rest of the aldehyde groups had participated in the crosslinking reaction.

The viscoelastic properties of the crosslinked CMCh2/HAox4-HA0.4 hydrogel were studied by rheology in frequency sweep experiments. Hydrogel formation was corroborated since storage modulus was always higher than loss modulus. Additionally, a slight frequency-dependent viscoelastic behavior was observed. Presumably, the shear modulus values were mainly due to the covalent crosslinking of the CMCh and HAox functional groups, and HA did not influence crosslinking kinetics or final modulus (Figure S1). Gels were soft, with a shear modulus in the range of 50-100 Pa (Figure 4A). This value indicates that these hydrogel scaffolds are promising candidates for regeneration of soft tissues,[37] and is comparable to reported chitosan/hyaluronic acid injectable hydrogels with encapsulated cells for abdominal reparation and adhesion prevention.[37,61,72,73] The viscosity of the crosslinked CMCh2/HAox4-HA0.4 bioink vs. shear rate is plotted in Figure 4B. The ink viscosity found was relatively low, especially compared to air pressure-based extruded inks (in the range of 30–6 × 10^7 mPa),[1,2] which is a desirable feature since low-viscosity bioinks usually allow higher cell viability.[5,25,30] Solution behaved as a non-Newtonian fluid, where viscosity decreased linearly with increasing shear rate. This shear thinning behavior is a favorable property for printing. It implies a decrease in the viscosity when the shear stress increases inside the needle under applied pressure, followed by a sharp increase of viscosity after extrusion, facilitating both extrusion and shape fidelity.[5]

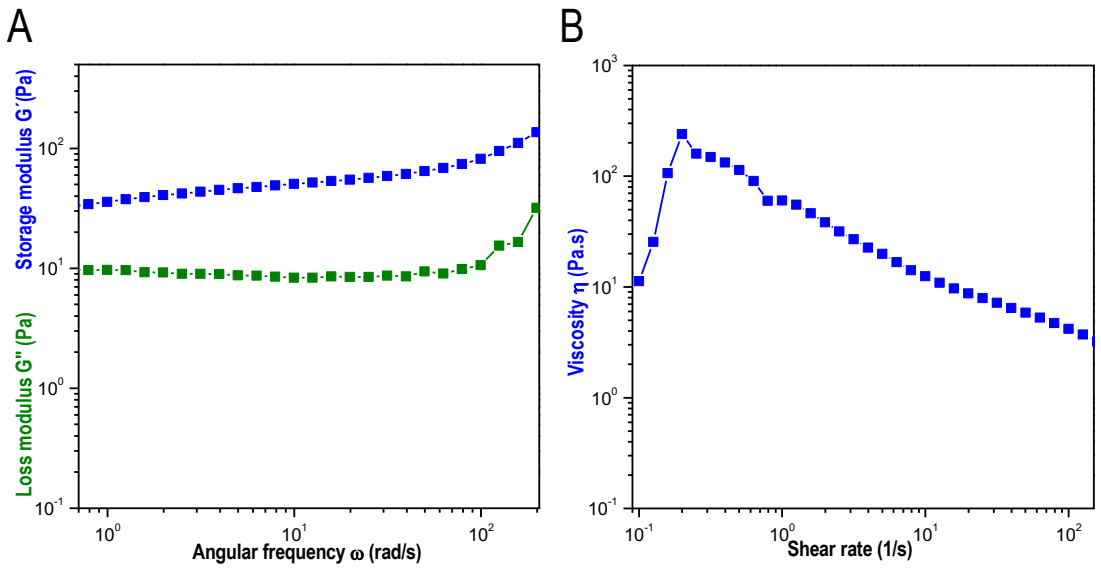

Figure 4. (A) Frequency sweep experiment and (B) viscosity analysis of CMCh2/HAox4-HA0.4 bioink formulation.

3.3. CHARACTERIZATION OF THE 3D PRINTED HYDROGEL SCAFFOLDS

2 and 4 layers grid square scaffolds (120 x 120 mm^2 printed area) were printed using the CMCh2/HAox4-HA0.4 formulation (Figure 5). Good printing accuracy and resolution was observed and stable scaffolds with filaments of uniform dimensions (diameter 357±58 μm) were obtained.

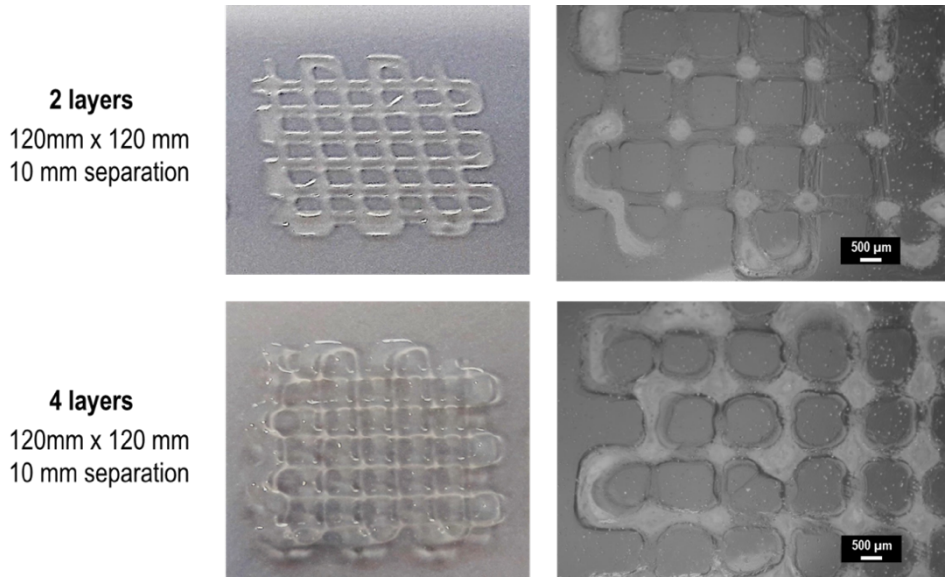

Figure 5. Camera pictures (left) and light microscopy pictures (right) of 2-layer and 4-layer square scaffolds printed using CMCh2/HAox4-HA0.4 formulation.

Swelling and degradation rates are relevant parameters when using hydrogels bioinks since they affect the fidelity and stability of the bioprinted scaffolds, as well as allow cellular ingrowth and tissue regeneration.[25,74,75] In this study, swelling and degradability of the printed scaffolds were analyzed by imaging the scaffolds after incubation in PBS for given times and by quantification of the width of the strands (Figures 6 A-C). Figure 6A shows the microscopy images of 2-layer printed scaffolds after 4 h immersion in PBS. A 49±9 % swelling was observed under these conditions (Figure 6A). A progressive and notable decrease in scaffold volume was observed with incubation time, up to nearly complete degradation after 7 days (Figure 6B). This degradation rate is slightly faster than previously reported for CMCh/HAox injectable hydrogels (10-14 days),[61,72,73] which can be assigned to the higher surface area and open structure of the grid

scaffold that makes them more sensitive for degradation. Schiff's base crosslinked hydrogels have low stability due to the dynamic nature of the bond.[55,76,77] Thus, to increase the long-term stability of the scaffolds a new crosslinking approach was proposed since stability directly related to the crosslinking degree of the hydrogel.[74,78,79] A post-printing crosslinking step was adopted by immersing the scaffold in 20 mM $FeCl_3$ for 7 min. Fe (III) forms coordination complexes with hyaluronic acid units at physiological pH,[80] which are expected to act as additional crosslinking points in the printed scaffold. Figure 6A shows lower swelling (19±8 %) of the printed scaffold after the second crosslinking step and 4 h swelling. Also, slower degradation of the scaffold was observed after postprinting stabilization (Figure 6C). The scaffold maintained its structural integrity up to 28 days of incubation, although signs of erosion were appreciated in the last stage. In conclusion, the treatment with iron (III) leads to 3D scaffolds with higher structural integrity and long-term stability. This reinforces the stability of Schiff's base crosslinked hydrogels which has remained a challenging issue.[43,76]

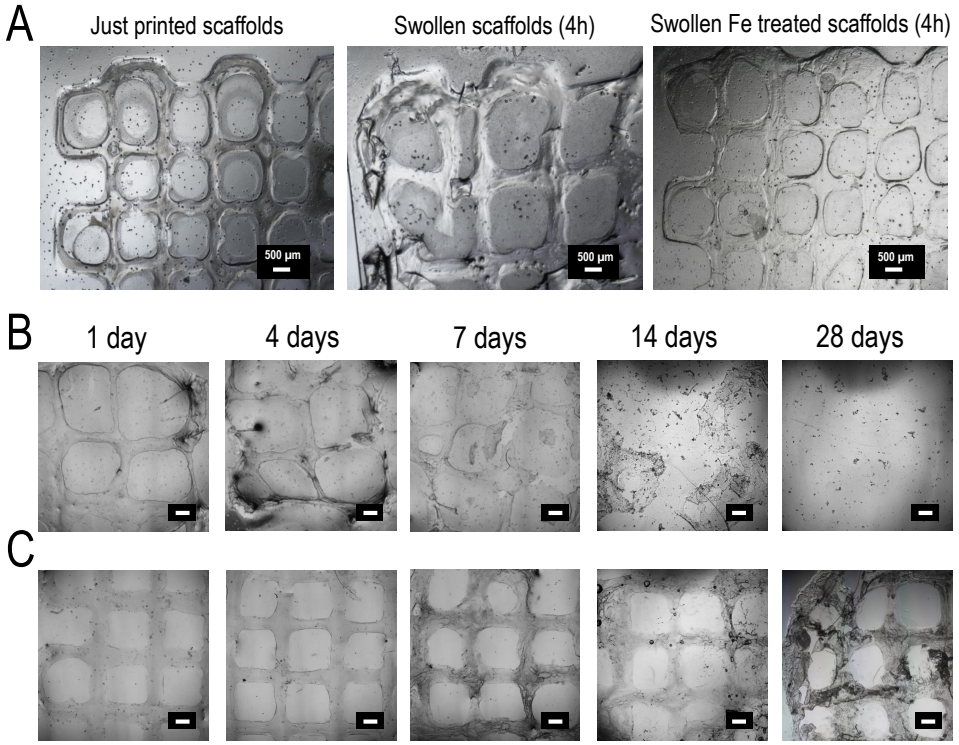

Figure 6. (A) Microscopy images of CMCh2/HAox4-HA0.4 printed scaffolds just after printing, after swelling in PBS for 4h, and after iron treatment and swelling in PBS for 4h. (B) Degradation study of CMCh2/HAox4-HA0.4 scaffolds with no

additional treatment after incubation in PBS and (C) after iron treatment and incubation in PBS at different time points. Scale bars correspond to 500 μm.

3.4. CMCH2/HAOX4-HA0.4 BASED BIOPRINTING

In general, 3D printed hydrogels have been demonstrated to protect cells from mechanical damage induced during the extrusion process, while providing an appropriate environment for the encapsulated cells after printing (by mimicking the ECM).[25,28] Nevertheless, it is a critical aspect in biofabrication to evaluate whether viscosity, *in situ* crosslinking and printing process are compatible with encapsulated living cells.[4,10] Thus, the ability of CMCh2/HAox4-HA0.4 formulation to be used as a bioink was tested by printing scaffolds with encapsulated L929 fibroblasts. Cell viability in the bioprinted scaffolds was studied during a 14 days-period. Live/dead staining allowed imaging of the cells in 2-layer printed scaffolds (Figure 7A). Abundance of cells homogeneously distributed in the scaffold were observed, which reflects the good mixing performance during the printing process. Additionally, cells were released from the hydrogel after 7 and 14 days of culture, which can be due to degradation rate of the scaffolds. This is a desirable characteristic for potential regenerative approaches for wound healing, where delivered cells would migrate out of the scaffold to heal the injured site.[4] Quantification of cell viability is displayed in Figure 7B, together with data from 3D cultures in non-printed hydrogels of the same formulation as controls. Cells in the printed or non-printed materials showed viability around 60-65 % after 1 day incubation. There are not significant differences between printed and non-printed formulation, which indicates that the printing process did not affect the cells short term viability. Cell viability in the printed scaffold increased at longer culture times and reached 96 and 95 % at 7 and 14 days of culture respectively, both significantly different from printed and non-printed formulations after 1 day of incubation. These data suggest that the neither the covalent reaction responsible of gelation, nor the shear stress produced by the printing process or the stabilization process with iron (III) cause adverse long-term effects on the cells. The proliferation rate of the cells in the scaffolds was analyzed after DAPI staining. Cell proliferation increased over the 14 days-period in the printed scaffolds (Figure 7C), and values reached after 14 days of incubation were significantly different from those found after 1 and 4 days of culture. Finally, the scaffolds maintained their structural integrity during the whole culture processes (Figure 7D), indicating that the optimized printed formula and the subsequent stabilization step with iron produced mechanically robust scaffolds with good biocompatibility.

These observations were consistent with other studies based on chitosan or hyaluronic acid bioprinting[15,49,81] For example, Akkineni *et al.* studied the encapsulation of endothelial cells in a low viscosity hydrogel core (1% gelatin and 3% alginate) obtaining cell viability values around

65% 1 day after printing, comparable to our results. A high viscosity shell composed of 10% alginate and 1% gelatin and a secondary crosslinking with $CaCl_2$ provided the structural integrity to the scaffold.[15] Also, Gu *et al.* presented the direct-write printing of stem cells within a polysaccharide-based bioink comprising alginate, carboxymethylchitosan, and agarose. The time course of dead cells content within the optimized bioink (containing 5% w/v of carboxymethylchitosan) demonstrated a relatively high (around 25%) cell death after printing subsequently decreasing to around a 10% by day 7, following a trend very similar to that of our work.[81] On the other hand, some reactive hydrogels have been reported for cell encapsulation such as: injectable hydrogels with proliferation trends similar to that found in our work;[40] layered platforms with constant cell viability values around 70% until 5 days;[35] or gradient formulations[34] where cell viability values slightly decrease with time until around 80% after 7 days. Based on the *in-vitro* studies, we conclude that the proposed printing technology and bioink formulation of this work are suitable as a 3D printing platform for potential biomedical applications as cell carriers in the tissue engineering field.

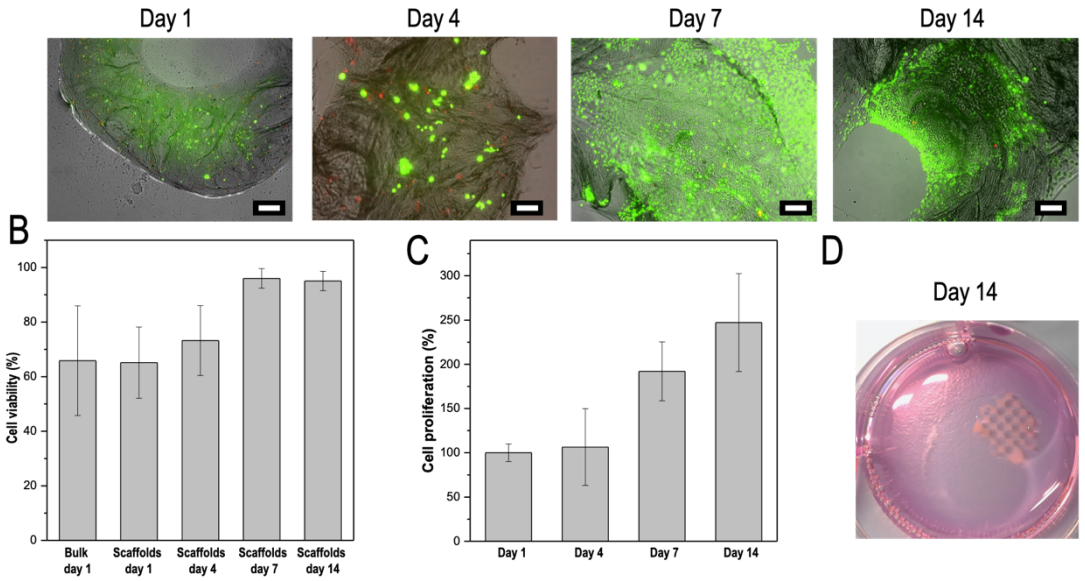

Figure 7. Biological results of CMCh2/HAox4-HA0.4 printed scaffolds loaded with L929 fibroblasts and treated with Fe over a 14 days period: (A) Fluorescence imaging of live/dead stained scaffolds at different culture days. (B) Quantification of live/dead results including bulk hydrogels at 1 day as control. Analysis of variance (ANOVA) of the results for the printed samples was performed at each time with respect to the day 1 at significance level of ***$p<0.05$, and with respect to non-printed samples at significance level of ###$p<0.05$. (C) Proliferation assay by quantification of nuclei after DAPI staining. Analysis of variance (ANOVA) of the results for the printed samples was performed at each time point at

significance level of **p<0.01. (D) Picture of a stable printed scaffold after 14 days of incubation. Scale bars correspond to 200 μm.

4. CONCLUSION

The present study describes the development of a reactive hydrogel bioink with an extrusion printing methodology based on a dual-syringe system with a static mixing tool. This method shows multiple advantages for 3D extrusion bioprinting. 1) Gelation during the extrusion process provides enough viscosity for printing with good shape fidelity while using low viscosity precursor solutions; 2) the crosslinking during extrusion provides enough structural integrity to retain the printed shape; 3) the stability of the scaffold, if required for long term culturing, can be increased in a simple incubation step. Bioprinted scaffolds obtained with our approach showed good biocompatibility, moderate swelling, and shape stability during 14 days of culture. Since precursors' concentrations and printing conditions can be easily varied, this printing approach offers high versatility and we envision that it can be adaptable to a wide range of reactive systems with appropriate crosslinking kinetics to be employed in future for broad applications in regenerative medicine and tissue-engineering.

ACKNOWLEDGMENTS

Authors thank CIBER-BBN (Spain) and the Spanish Ministry of Economy and Competitivity (M. Puertas-Bartolomé scholarship BES-2015-075161 and project MAT2017-84277-R) for supporting this work. The authors acknowledge RegenHu company, and particularly: Sandro Figi, Dominic Ernst, Michael Kuster and Andreas Scheidegger, for the fruitful collaboration, development and providing the mixing tool. The authors thank Dr. Emmanuel Terriac from INM, Germany, for assistance in the confocal imaging.

Supporting Information

3D printing of a reactive hydrogel bioink using a static mixing tool

María Puertas-Bartolomé, Małgorzata K.Włodarczyk-Biegun, Aránzazu del Campo, Blanca Vázquez-Lasa* and Julio San Román

In consideration for publication

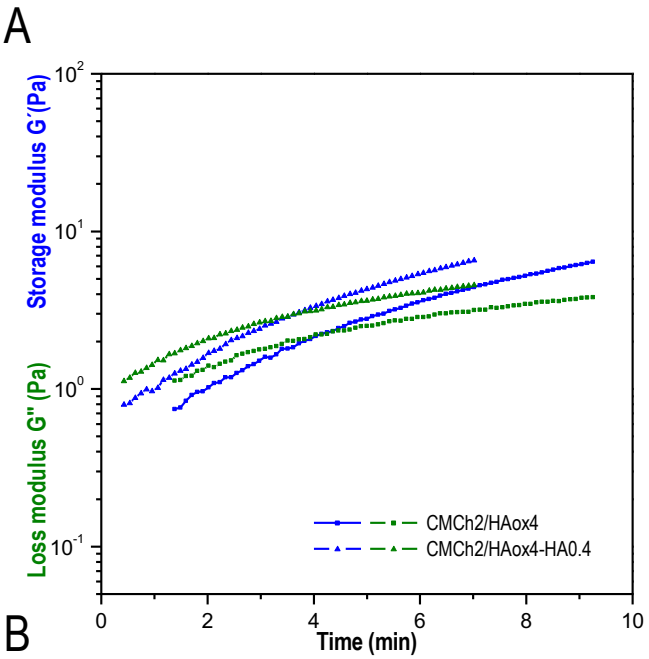

Formulation	CMCh2/HAox4	CMCh2HAox4-HA0.4
Gelation time/s	3.64 ± 0.43	3.65 ± 0.33

Figure S1. (A) Storage (G') and loss (G") moduli obtained in dynamic time sweep rheological experiments and (B) gelation times, defined as G' and G" crossover points, obtained for CMCh2/HAox4 and CMCh2/HAox4-HA0.4 formulations.

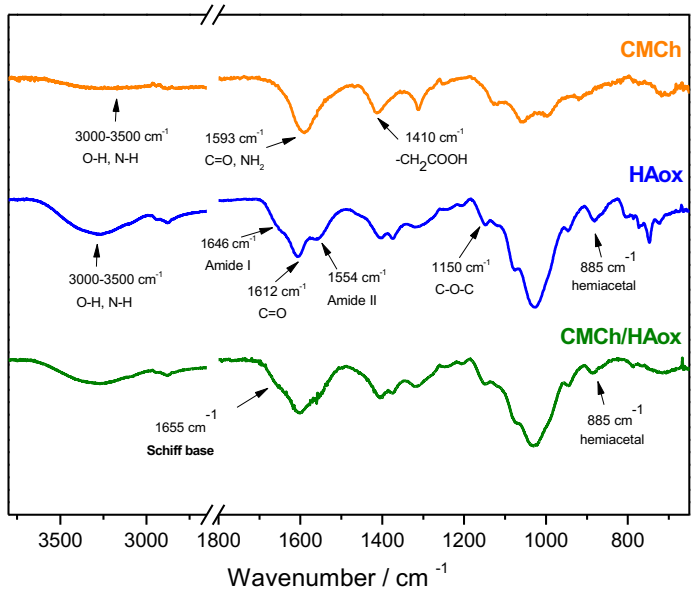

Figure S2. FTIR spectra of CMCh, HAox and CMCh/HAox reactive hydrogel.

REFERENCES

1. Derakhshanfar S, Mbeleck R, Xu K, Zhang X, Zhong W, Xing M. 3D bioprinting for biomedical devices and tissue engineering: A review of recent trends and advances. *Bioactive materials.* 2018;3(2):144-156.

2. Cui H, Nowicki M, Fisher JP, Zhang LG. 3D bioprinting for organ regeneration. *Advanced healthcare materials.* 2017;6(1):1601118.

3. Włodarczyk-Biegun MK, del Campo A. 3D bioprinting of structural proteins. *Biomaterials.* 2017;134:180-201.

4. Murphy SV, Skardal A, Atala A. Evaluation of hydrogels for bio-printing applications. *Journal of Biomedical Materials Research Part A.* 2013;101(1):272-284.

5. Malda J, Visser J, Melchels FP, et al. 25th anniversary article: engineering hydrogels for biofabrication. *Advanced materials.* 2013;25(36):5011-5028.

6. Hospodiuk M, Dey M, Sosnoski D, Ozbolat IT. The bioink: a comprehensive review on bioprintable materials. *Biotechnology advances.* 2017;35(2):217-239.

7. Chaudhari A, Vig K, Baganizi D, et al. Future prospects for scaffolding methods and biomaterials in skin tissue engineering: a review. *International journal of molecular sciences.* 2016;17(12):1974.

8. Mora-Boza A, Puertas-Bartolomé M, Vázquez-Lasa B, San Román J, Pérez-Caballer A, Olmeda-Lozano M. Contribution of bioactive hyaluronic acid and gelatin to regenerative medicine. Methodologies of gels preparation and advanced applications. 2017.

9. Zhang J, Allardyce BJ, Rajkhowa R, et al. 3D printing of silk particle-reinforced chitosan hydrogel structures and their properties. *ACS Biomaterials Science & Engineering.* 2018;4(8):3036-3046.

10. Aydogdu MO, Oner ET, Ekren N, et al. Comparative characterization of the hydrogel added PLA/β-TCP scaffolds produced by 3D bioprinting. *Bioprinting.* 2019;13:e00046.

11. Yan J, Wang Y, Zhang X, et al. Snakegourd root/Astragalus polysaccharide hydrogel preparation and application in 3D printing. *International journal of biological macromolecules.* 2019;121:309-316.

12. Annabi N, Tamayol A, Uquillas JA, et al. 25th anniversary article: Rational design and applications of hydrogels in regenerative medicine. *Advanced materials.* 2014;26(1):85-124.

13. Ratner BD, Bryant SJ. Biomaterials: where we have been and where we are going. *Annu. Rev. Biomed. Eng.* 2004;6:41-75.

14. Caló E, Khutoryanskiy VV. Biomedical applications of hydrogels: A review of patents and commercial products. *European Polymer Journal.* 2015;65:252-267.

15. Akkineni AR, Ahlfeld T, Lode A, Gelinsky M. A versatile method for combining different biopolymers in a core/shell fashion by 3D plotting to achieve mechanically robust constructs. *Biofabrication.* 2016;8(4):045001.

16. Roehm KD, Madihally SV. Bioprinted chitosan-gelatin thermosensitive hydrogels using an inexpensive 3D printer. *Biofabrication.* 2017;10(1):015002.

17. Huang J, Fu H, Wang Z, et al. BMSCs-laden gelatin/sodium alginate/carboxymethyl chitosan hydrogel for 3D bioprinting. *Rsc Advances.* 2016;6(110):108423-108430.

18. Park JY, Choi J-C, Shim J-H, et al. A comparative study on collagen type I and hyaluronic acid dependent cell behavior for osteochondral tissue bioprinting. *Biofabrication.* 2014;6(3):035004.

19. Haring AP, Thompson EG, Tong Y, et al. Process-and bio-inspired hydrogels for 3D bioprinting of soft free-standing neural and

glial tissues. *Biofabrication.* 2019;11(2):025009.

20. Li C, Wang K, Zhou X, et al. Controllable fabrication of hydroxybutyl chitosan/oxidized chondroitin sulfate hydrogels by 3D bioprinting technique for cartilage tissue engineering. *Biomedical Materials.* 2018.

21. Mora-Boza A, Włodarczyk-Biegun MK, del Campo A, Vázquez-Lasa B, Román JS. Glycerylphytate as an ionic crosslinker for 3D printing of multi-layered scaffolds with improved shape fidelity and biological features. *Biomaterials Science.* 2020.

22. Bakarich SE, Gorkin III R, Gately R, Naficy S, in het Panhuis M, Spinks GM. 3D printing of tough hydrogel composites with spatially varying materials properties. *Additive Manufacturing.* 2017;14:24-30.

23. Kirchmajer DM, Gorkin Iii R. An overview of the suitability of hydrogel-forming polymers for extrusion-based 3D-printing. *Journal of Materials Chemistry B.* 2015;3(20):4105-4117.

24. Kiyotake EA, Douglas AW, Thomas EE, Nimmo SL, Detamore MS. Development and quantitative characterization of the precursor rheology of hyaluronic acid hydrogels for bioprinting. *Acta biomaterialia.* 2019.

25. Hölzl K, Lin S, Tytgat L, Van Vlierberghe S, Gu L, Ovsianikov A. Bioink properties before, during and after 3D bioprinting. *Biofabrication.* 2016;8(3):032002.

26. Wu Q, Therriault D, Heuzey M-C. Processing and properties of chitosan Inks for 3D printing of hydrogel microstructures. *ACS Biomaterials Science & Engineering.* 2018;4(7):2643-2652.

27. Li H, Tan YJ, Liu S, Li L. Three-dimensional bioprinting of oppositely charged hydrogels with super strong Interface bonding. *ACS applied materials & interfaces.* 2018;10(13):11164-11174.

28. Highley CB, Song KH, Daly AC, Burdick JA. Jammed microgel inks for 3D printing applications. *Advanced Science.* 2019;6(1):1801076.

29. Hinton TJ, Jallerat Q, Palchesko RN, et al. Three-dimensional printing of complex biological structures by freeform reversible embedding of suspended hydrogels. *Science advances.* 2015;1(9):e1500758.

30. Aguado BA, Mulyasasmita W, Su J, Lampe KJ, Heilshorn SC. Improving viability of stem cells during syringe needle flow through the design of hydrogel cell carriers. *Tissue Engineering Part A.* 2011;18(7-8):806-815.

31. Skardal A, Zhang J, McCoard L, Xu X, Oottamasathien S, Prestwich GD. Photocrosslinkable hyaluronan-gelatin hydrogels for two-step bioprinting. *Tissue Engineering Part A.* 2010;16(8):2675-2685.

32. D O'Connell C, Di Bella C, Thompson F, et al. Development of the Biopen: a handheld device for surgical printing of adipose stem cells at a chondral wound site. *Biofabrication.* 2016;8(1):015019.

33. Gregor A, Hošek J. 3D printing methods of biological scaffolds used in tissue engineering. *Rom Rev Precis Mech Opt Mechatronics.* 2011;3:143-148.

34. Zimmermann R, Hentschel C, Schrön F, et al. High resolution bioprinting of multi-component hydrogels. *Biofabrication.* 2019.

35. Lozano R, Stevens L, Thompson BC, et al. 3D printing of layered brain-like structures using peptide modified gellan gum substrates. *Biomaterials.* 2015;67:264-273.

36. Maiullari F, Costantini M, Milan M, et al. A multi-cellular 3D bioprinting approach for vascularized heart tissue engineering based on HUVECs and iPSC-derived cardiomyocytes. *Scientific reports.* 2018;8(1):13532.

37. Bootsma K, Fitzgerald MM, Free B, et al. 3D printing of an interpenetrating network hydrogel material with tunable viscoelastic

properties. *Journal of the mechanical behavior of biomedical materials.* 2017;70:84-94.

38. Deepthi S, Jayakumar R. Alginate nanobeads interspersed fibrin network as in situ forming hydrogel for soft tissue engineering. *Bioactive materials.* 2018;3(2):194-200.

39. Hozumi T, Ohta S, Ito T. Analysis of the Calcium Alginate Gelation Process Using a Kenics Static Mixer. *Industrial & Engineering Chemistry Research.* 2015;54(7):2099-2107.

40. Zhang Y, Chen H, Zhang T, et al. Fast-forming BMSC-encapsulating hydrogels through bioorthogonal reaction for osteogenic differentiation. *Biomaterials science.* 2018;6(10):2578-2581.

41. Whitely M, Cereceres S, Dhavalikar P, et al. Improved in situ seeding of 3D printed scaffolds using cell-releasing hydrogels. *Biomaterials.* 2018;185:194-204.

42. Moglia RS, Whitely M, Dhavalikar P, et al. Injectable polymerized high internal phase emulsions with rapid in situ curing. *Biomacromolecules.* 2014;15(8):2870-2878.

43. Hozumi T, Kageyama T, Ohta S, Fukuda J, Ito T. Injectable hydrogel with slow degradability composed of gelatin and hyaluronic acid cross-linked by Schiff's base formation. *Biomacromolecules.* 2018;19(2):288-297.

44. Wu H-D, Yang J-C, Tsai T, et al. Development of a chitosan–polyglutamate based injectable polyelectrolyte complex scaffold. *Carbohydrate polymers.* 2011;85(2):318-324.

45. Kohn C, Klemens J, Kascholke C, et al. Dual-component collagenous peptide/reactive oligomer hydrogels as potential nerve guidance materials–from characterization to functionalization. *Biomaterials science.* 2016;4(11):1605-1621.

46. Caballero SSR, Saiz E, Montembault A, et al. 3-D printing of chitosan-calcium phosphate inks: rheology, interactions and characterization. *Journal of Materials Science: Materials in Medicine.* 2019;30(1):6.

47. Intini C, Elviri L, Cabral J, et al. 3D-printed chitosan-based scaffolds: An in vitro study of human skin cell growth and an in-vivo wound healing evaluation in experimental diabetes in rats. *Carbohydrate polymers.* 2018;199:593-602.

48. Demirtaş TT, Irmak G, Gümüşderelioğlu M. A bioprintable form of chitosan hydrogel for bone tissue engineering. *Biofabrication.* 2017;9(3):035003.

49. Noh I, Kim N, Tran HN, Lee J, Lee C. 3D printable hyaluronic acid-based hydrogel for its potential application as a bioink in tissue engineering. *Biomaterials research.* 2019;23(1):3.

50. Ouyang L, Highley CB, Rodell CB, Sun W, Burdick JA. 3D printing of shear-thinning hyaluronic acid hydrogels with secondary cross-linking. *ACS Biomaterials Science & Engineering.* 2016;2(10):1743-1751.

51. Mazzocchi A, Devarasetty M, Huntwork R, Soker S, Skardal A. Optimization of collagen type I-hyaluronan hybrid bioink for 3D bioprinted liver microenvironments. *Biofabrication.* 2018;11(1):015003.

52. Muxika A, Etxabide A, Uranga J, Guerrero P, de la Caba K. Chitosan as a bioactive polymer: Processing, properties and applications. *International journal of biological macromolecules.* Dec 2017;105(Pt 2):1358-1368.

53. Pellá MCG, Lima-Tenório MK, Tenório-Neto ET, Guilherme MR, Muniz EC, Rubira AF. Chitosan-based hydrogels: From preparation to biomedical applications. *Carbohydrate polymers.* Sep 15 2018;196:233-245.

54. Nguyen NT-P, Nguyen LV-H, Tran NM-P, Nguyen T-H, Huynh C-K, Van TV. Synthesis of cross-linking chitosan-hyaluronic acid based hydrogels for tissue engineering applications. Paper presented at: International Conference on the

Development of Biomedical Engineering in Vietnam2017.

55. Qian C, Zhang T, Gravesande J, Baysah C, Song X, Xing J. Injectable and self-healing polysaccharide-based hydrogel for pH-responsive drug release. *International journal of biological macromolecules.* 2019;123:140-148.

56. Ye K, Felimban R, Traianedes K, et al. Chondrogenesis of infrapatellar fat pad derived adipose stem cells in 3D printed chitosan scaffold. *PLoS One.* 2014;9(6).

57. Lee J-Y, Choi B, Wu B, Lee M. Customized biomimetic scaffolds created by indirect three-dimensional printing for tissue engineering. *Biofabrication.* 2013;5(4):045003.

58. Catoira MC, Fusaro L, Di Francesco D, Ramella M, Boccafoschi F. Overview of natural hydrogels for regenerative medicine applications. *J Mater Sci Mater Med.* Oct 10 2019;30(10):115.

59. Song R, Murphy M, Li C, Ting K, Soo C, Zheng Z. Current development of biodegradable polymeric materials for biomedical applications. *Drug design, development and therapy.* 2018;12:3117-3145.

60. Tan H, Chu CR, Payne KA, Marra KG. Injectable in situ forming biodegradable chitosan–hyaluronic acid based hydrogels for cartilage tissue engineering. *Biomaterials.* 2009;30(13):2499-2506.

61. Song L, Li L, He T, et al. Peritoneal adhesion prevention with a biodegradable and injectable N,O-carboxymethyl chitosan-aldehyde hyaluronic acid hydrogel in a rat repeated-injury model. *Sci Rep.* Nov 21 2016;6:37600.

62. Khorshidi S, Karkhaneh A. A self-crosslinking tri-component hydrogel based on functionalized polysaccharides and gelatin for tissue engineering applications. *Materials Letters.* 2016;164:468-471.

63. Puertas-Bartolomé M, Benito-Garzón L, Fung S, Kohn J, Vázquez-Lasa B, San Román J. Bioadhesive functional hydrogels: Controlled release of catechol species with antioxidant and antiinflammatory behavior. *Materials Science and Engineering: C.* 2019;105:110040.

64. Nguyen NT-P, Nguyen LV-H, Tran NM-P, et al. The effect of oxidation degree and volume ratio of components on properties and applications of in situ cross-linking hydrogels based on chitosan and hyaluronic acid. *Materials Science and Engineering: C.* 2019;103:109670.

65. Zhao H, Heindel ND. Determination of degree of substitution of formyl groups in polyaldehyde dextran by the hydroxylamine hydrochloride method. *Pharmaceutical Research.* 1991;8(3):400-402.

66. Yan S, Wang T, Feng L, et al. Injectable in situ self-cross-linking hydrogels based on poly (L-glutamic acid) and alginate for cartilage tissue engineering. *Biomacromolecules.* 2014;15(12):4495-4508.

67. Florczyk SJ, Wang K, Jana S, et al. Porous chitosan-hyaluronic acid scaffolds as a mimic of glioblastoma microenvironment ECM. *Biomaterials.* 2013;34(38):10143-10150.

68. Kim Y, Larkin AL, Davis RM, Rajagopalan P. The design of in vitro liver sinusoid mimics using chitosan–hyaluronic acid polyelectrolyte multilayers. *Tissue Engineering Part A.* 2010;16(9):2731-2741.

69. Wu J, Wang X, Keum JK, et al. Water soluble complexes of chitosan-g-MPEG and hyaluronic acid. *Journal of Biomedical Materials Research Part A.* 2007;80(4):800-812.

70. Weng L, Chen X, Chen W. Rheological characterization of in situ crosslinkable hydrogels formulated from oxidized dextran and N-carboxyethyl chitosan. *Biomacromolecules.* 2007;8(4):1109-1115.

71. Purcell BP, Lobb D, Charati MB, et al. Injectable and bioresponsive hydrogels for on-demand matrix metalloproteinase inhibition. *Nature materials.* 2014;13(6):653.

72. Deng Y, Ren J, Chen G, et al. Injectable in situ cross-linking chitosan-hyaluronic acid based hydrogels for abdominal tissue regeneration. *Scientific Reports.* 2017;7(1):2699.

73. Li L, Wang N, Jin X, et al. Biodegradable and injectable in situ cross-linking chitosan-hyaluronic acid based hydrogels for postoperative adhesion prevention. *Biomaterials.* 2014;35(12):3903-3917.

74. Huber D, Grzelak A, Baumann M, et al. Anti-inflammatory and anti-oxidant properties of laccase-synthesized phenolic-O-carboxymethyl chitosan hydrogels. *New biotechnology.* 2018;40:236-244.

75. Caliari SR, Burdick JA. A practical guide to hydrogels for cell culture. *Nature methods.* 2016;13(5):405.

76. Xin Y, Yuan J. Schiff's base as a stimuli-responsive linker in polymer chemistry. *Polymer Chemistry.* 2012;3(11):3045-3055.

77. Zhang ZP, Rong MZ, Zhang MQ. Polymer engineering based on reversible covalent chemistry: A promising innovative pathway towards new materials and new functionalities. *Progress in Polymer Science.* 2018;80:39-93.

78. Peng X, Peng Y, Han B, Liu W, Zhang F, Linhardt RJ. -stimulated crosslinking of catechol-conjugated hydroxyethyl chitosan as a tissue adhesive. *Journal of Biomedical Materials Research Part B: Applied Biomaterials.* 2018.

79. Barbucci R, Magnani A, Consumi M. Swelling behavior of carboxymethylcellulose hydrogels in relation to cross-linking, pH, and charge density. *Macromolecules.* 2000;33(20):7475-7480.

80. Mercê ALR, Carrera LCM, Romanholi LKS, Recio MaÁL. Aqueous and solid complexes of iron (III) with hyaluronic acid: potentiometric titrations and infrared spectroscopy studies. *Journal of inorganic biochemistry.* 2002;89(3-4):212-218.

81. Gu Q, Tomaskovic-Crook E, Lozano R, et al. Functional 3D neural mini-tissues from printed gel-based bioink and human neural stem cells. *Advanced healthcare materials.* 2016;5(12):1429-1438.

CHAPTER

06

3D PRINTED CONSTRUCT WITH CATECHOL FUNCTIONALIZED NANOPARTICLES FOR WOUND HEALING APPLICATIONS

María Puertas-Bartolomé[1,2], Małgorzata K.Włodarczyk-Biegun[3], Aránzazu del Campo[3,4], Blanca Vázquez-Lasa[1,2]* and Julio San Román[1,2]

[1] *Institute of Polymer Science and Technology, ICTP-CSIC 28006 Madrid, Spain*
[2] *CIBER-BBN, Health Institute Carlos III. 28029 Madrid, Spain*
[3] *INM – Leibniz Institute for New Materials, 66123 Saarbrücken, Germany*
[4] *Chemistry Department, Saarland University, 66123 Saarbrücken, Germany*

In consideration for publication

Research Article

3D printed construct with catechol functionalized nanoparticles for wound healing applications

María Puertas-Bartolomé, Małgorzata K.Włodarczyk-Biegun, Aránzazu del Campo, Blanca Vázquez-Lasa* and Julio San Román

In consideration for publication

ABSTRACT

The potential of 3D printing to manufacture complex structures with extraordinary control over geometry has demonstrated revolutionary progress in wound healing therapies, which constitute an important global health care problem. Hydrogels based bioinks have recently attracted much attention for skin tissue engineering due to their remarkable intrinsic properties favorable for the wound healing process, such as a cell supporting environment. Still, their weak mechanical properties make them challenging to print, and further studies are necessary to target specific events in the healing process to accelerate the tissue reparation in chronic wounds. Our approach in this work lies in the development of 3D printed hydrogel constructs containing novel catechol functionalized nanoparticles (NP) for its application in wound care management. This system combines the beneficial properties of the biomimetic hydrogels carboxymethyl chitosan and hyaluronic acid, with the bioactive properties of the catechol functionalized NP. A novel 3D bioprinting approach recently reported by our group based on reactive mixing has been used obtaining homogeneous scaffolds with good structural integrity and shape fidelity. The *in vitro* performance, rheological analysis, catechol NP release profile, and *in vitro* biological behavior of the bioink are investigated to assess its applicability for promoting wound healing. Bioink is demonstrated to support cell viability and proliferation over 14 days; while catechol functionalized NP protect cells against oxidative stress damage induced by radical oxygen species (ROS), regulate of the inflammatory response, and promote upregulation of the vascular endothelial growth factor (VEGF). We envision that NP loaded bioink presented in this work have promising applicability for wound healing therapies with several advantages: 1) the controlled release of the NP in the wound site provide localized bioactive wound promoting functions; 2) functionalized NP can act as nanocarriers for multiple hydrophobic drugs so the NP action could be extended with encapsulated drug; 3) printing approach used allows tailoring of geometry, materials and formulation doses based on patient requirements for wound specific treatments.

Keywords: *3D-bioprinting, catechol nanoparticles, chitosan, hyaluronic acid.*

1. INTRODUCTION

Wound healing is a complex process that requires the interaction of different types of cells, bioactive molecules and ECM as supporting platform to regenerate the damaged tissue. The wound healing process comprises four integrated stages: hemostasis, inflammation, proliferation and tissue remodeling. Several disease conditions such as diabetes can lead to the process malfunction and formation of chronic wounds, which represent an important global healthcare problem.[1-4] These kinds of wounds differ from the regular skin healing pattern and are especially difficult to heal. Therefore, the development of efficient wound dressings to assist and enhance the healing process in chronic wounds constitutes a significant target in regenerative medicine.[1,5-7]

3D printing is an advanced additive manufacturing technology that has demonstrated revolutionary progress in tissue engineering and regenerative medicine applications.[8-10] The potential of 3D printing to manufacture complex structures having extraordinary control over geometry can be utilized in developing 3D scaffolds for wound healing therapies. 3D printed scaffolds present numerous advantages for wound healing management: 1) facilitates the fabrication of wound dressings with well-defined dimensional properties such as thickness or pore size to match the defects; 2) fabrication can be achieved in a reproducible manner, since scaffolds can be designed by computer software and the process is automatized; 3) geometry, materials and formulation doses can be tailored based on patient requirements;[11-13] 4) cell-laden 3D scaffolds with homogeneous dispersion of encapsulated cells can be obtained. The last one is especially attractive, as cell therapy has emerged as a promising modality to enhance the wound healing process and restore the damaged tissue.[14-16]

Natural hydrogels have attracted much attention as potential printable materials for cell encapsulation (bioinks) due to their ability to provide an ECM-like biomimetic environment beneficial for cell migration, growth and proliferation.[17-21] Additionally, intrinsic properties of hydrogels are favorable for the wound healing process: 1) good biocompatibility and biodegradability; 2) high porosity and ability to swell, that allow nutrient and gaseous supply as well as waste exchange; and 3) high water content, which ensures a moisture environment in the wound proved to accelerate the re-epithelialization process.[22-24] However, the weak mechanical properties of hydrogels make them challenging to print.[25-29] Additionally, further developments in hydrogel-based bioinks bioactivity are necessary to target specific events in the healing process and accelerate the tissue reparation. In this way, nanomedicine tools, in particular the incorporation of bioactive nanoparticles (NP) to the hydrogel support, can improve wound

healing therapies.[30] NP can be co-printed with the supporting material to obtain a functional scaffold with precise control over scaffold's geometry and particles' distribution. In that manner, controlled release to the wound site would be obtained, increasing targeting precision, and avoiding side effects or usage of high drug doses.[30,31]

In this work, an advanced 3D printed hydrogel construct containing novel catechol functionalized NP has been developed and characterized for its use in wound care management. Hydrogel backbone consisted of the natural polysaccharides: carboxymethyl chitosan (CMCh) and hyaluronic acid (HA), with biomimetic physical structure. The association of the hydrogel matrix and the NP allows synergistic action between the beneficial properties of hydrogel and the bioactive function of the NP. A novel 3D bioprinting approach recently optimized by our group has been used to print the cell-laden NP-hydrogel system overcoming its intrinsic weak mechanical properties and obtaining homogeneous scaffolds with good resolution. The controlled and localized release of the catechol functionalized NP in the wound site is expected to regulate the radical oxygen species (ROS) production, control the constant activation of the inflammatory response, facilitate the neovascularization,[32] and consequently, promote the proliferation and tissue modeling. Moreover, functionalized NP can act as nanocarriers; therefore drug delivery strategies can be developed to combine NP effect with a drug release. Thus, the biologically active bioink designed in this work will allow engineering 3D scaffolds to target specific points and enhancing treatment efficiency in the chronic wound healing therapies.

2. EXPERIMENTAL

2.1. MATERIALS

3,4-dihydroxyhydrocinnamic acid or hydrocaffeic acid (Sigma-Aldrich), thionyl chloride (Scharlau), N,N-dimethylformamide (DMF) (Scharlau), toluene (Merck), dimethyl sulfoxide (DMSO) (Scharlau), N-vinylcaprolactam (Sigma-Aldrich), 1,4-dioxane (Panreac), triethylamine (Scharlau), ethanol (VWR Chemicals), carboxymethyl chitosan (Chitoscience, 85 – 90 % degree of deacetylation, viscosity = 5-300 mPas), sodium hyaluronan (HA) (M_w ~1.5-1.8 x 10^6 Da, Sigma Aldrich,), sodium periodate ($NaIO_4$) (Alfa Aesar), ethylene glycol (Sigma), hydroxylamine (Sigma-Aldrich), iron chloride (III) (Sigma-Aldrich), phosphate buffered saline solution (PBS) (10 mM pH 7.4, Gibco), esterase from porcine liver (Sigma- Aldrich), acetone (Scharlau), coumarin-6 (Sigma-Aldrich), and tween 80 (Fluka), were used as received. 2-Hydroxyethyl methacrylate (Sigma-Aldrich) was previously purified according to the literature.[33] Azobisisobutyronitrile (AIBN) (Sigma-Aldrich) was crystallized in methanol (Sigma-Aldrich)

prior to use. Oxidized sodium hyaluronan (HAox) was prepared as reported elsewhere,[34] with a final oxidation degree of 48±3.2 %.[35,36]

2.2. CATECHOL BEARING NP PREPARATION AND CHARACTERIZATION

2.2.1. Catechol NP preparation

Two terpolymers based on vinylcaprolactam, 2-hydroxyethylmethacrylate and conjugated catechol moieties were obtained and characterized as described previously.[37] Catechol fractions of 2 and 29 mol % were obtained (terpolymers designated as T2 and T29, respectively) quantified by UV spectroscopy (Figure S1).

Subsequently, self-assembled NP of the two amphiphilic terpolymers (T2 and T29) were obtained by the nanoprecipitation method. Briefly, the corresponding terpolymer was solved in ethanol/acetone 1:1 at 5 mg/mL, and added dropwise into a 0.003 M NaCl aqueous solution under continuous magnetic stirring, without any surfactant. The mixture was stirred at r.t. for 24 h in order to remove the organic solvent, obtaining a final NP concentration of 1 mg/mL. Finally, NP suspensions were sterilized by filtration through 0.22 μM poly(ether sulfone) membranes (PES, Millipore Express, Millex GP) and stored at 4 °C until used. Herein, these NP are designated by the catechol composition as NP2 and NP29.

NP of both compositions were loaded with the model drug coumarin-6 (C6) applying the described methodology except that 2 wt-% C6 respect to the polymer content was added to the terpolymer solution during the nanoprecipitation. These NP are designated as C6NP2 and C6NP29 (for T2 and T29, respectively).

2.2.2. NP characterization

The hydrodynamic properties of NP suspensions at 1mg/mL (i.e. particle size distribution and zeta potential (ξ)) were determined by Dynamic Light Scattering (DLS) and laser Doppler electrophoresis (LDE), respectively, using a Malvern Nanosizer NanoZS Instrument at r.t. For each sample, the statistical average and standard deviation of mean hydrodynamic diameter (D_h) and particle dispersion index (PDI) were calculated from 6 measurements of 11 runs, while the zeta statistical average and standard deviation were calculated from 6 measurements of 20 runs each. The morphology of the nanostructures was characterized by Scanning Electron Microscopy (SEM) using a Hitachi SU8000 TED, cold-emission FE-SEM microscope (accelerating voltage 2 kV) at 0.02 mg/mL concentration. The stability of aqueous NP suspensions was studied by

storing at 4 °C for 3 weeks. At different time points (1 day, 1 week and 3 weeks) the D_h, PDI and zeta potential were measured by DLS and LDE techniques.

2.2.3. C6 encapsulation efficiency and release

To calculate the encapsulation efficiency (EE) for coumarin-6, C6NP (C6NP2 or C6NP29) were prepared in water, freeze-dried, and dissolved in ethanol/acetone 1:1 mixture for 12 h, to dissolve both the self-assembled structure and the drug. Samples were analyzed by UV at 450 nm using a NanoDrop One spectrophotometer (Thermo Scientific, Spain). A calibration curve of C6 in the ethanol/acetone 1:1 mixture was used to calculate C6 concentration, and absorbance of the corresponding non-loaded NP (NP22 or NP29) were subtracted. EE was calculated as the percentage ratio of C6 concentration detected experimentally and the one initially added in the nanoprecipitation procedure. A minimum of three replicates of each composition were analyzed and results given as mean ± SD.

Esterase-mediated release kinetic of C6 from the nanoparticles was analyzed. To that end, 4 mL of aqueous suspensions of C6NP (C6NP2 or C6NP29) prepared in water with 15 u/mL esterase concentration were dialyzed (membrane molecular weight cutoff, 3.5 kDa) against 15 mL of 0.5 % tween 80 aqueous solution at 37 °C. At different time points (1, 4, 7, 14 and 21 days) 1 mL of the dialyzing medium was withdrawn and replenished by fresh medium. The absorbance of samples was analyzed by UV at 450 nm using NanoDrop One spectrophotometer. C6 release from the NP was calculated using a calibration line of C6 in the same solvent (0.5 % tween 80 aqueous solution) and absorbance of corresponding non-loaded NP (NP2 or NP29) were subtracted. Release data were calculated as the percentage ratio of C6 concentration detected experimentally and the one loaded in the NP. A minimum of three replicates of each composition were analyzed and results given as mean ± SD.

2.3. 3D PRINTING OF NP LOADED HYDROGEL BIOINK

2.3.1. Bioink formulation

NP29 loaded bioink, further denoted as CMChNP29/HAox-HA, was formulated as follows. Two hydrogel precursors solutions (A and B) were prepared separately: A) NP29 suspension at 1mg/mL was added into a 2 wt-% CMCh solution in PBS (pH=7.4); B) 4 wt-% HAox and 0.4 wt-% HA were solved in 0.1 M NaCl solution. Both solutions were mixed in a 1:1 volume ratio during the printing process giving a final NP29 concentration of 0.25 mg/mL. For cell-laden scaffolds, L929 fibroblasts (ATCC, Germany) were suspended in the precursor A (2 wt-% CMCh/NP29

solution) prepared in RPMI 1640 (Gibco) instead of PBS, giving a final cell concentration of 1 x 10^6 cells/mL. As a control blank formulation without NP (CMCh/HAox-HA) was prepared.

2.3.2. 3D printing methodology with static mixing tool

All 3D scaffolds were fabricated using a printing methodology previously developed by our group in which the 3D Discovery printer (RegenHu, Switzerland) was modified to adapt a static mixing tool (RegenHu, Switzerland). Briefly, two 1 ml syringes (RegenHu, Switzerland) were loaded with the hydrogel precursors solutions (A and B). The solutions were simultaneously extruded by mechanical printer motor into the static mixing tool in a 1:1 ratio, where they were mixed and immediately began to crosslink. Finally, the crosslinked hydrogel was extruded through the needle.

3D scaffolds were fabricated onto glass cover slips using a 2 layer grid square design: 120 x 120 mm^2, 10 mm separation between strands. One sacrificial 4 cm line was printed before the scaffold for material homogenization in the static mixer. Scaffolds were printed using a print head movement speed of 15 mm/s and a plunger speed of 0.06 mm/s, both processes were controlled by the software modified by RegenHu. A conical polyethylene needle with an inner diameter of 200 μm was used. A cytocompatible post-printing stabilization step was carried out by immersion of the printed scaffolds in a 20 mM $FeCl_3$ aqueous solution for 7 min. After that time, solution was removed and samples were incubated in cell culture media.

Light microscopy characterization of stabilized printed scaffolds was performed with an optical microscope (Nikon SMZ800N, Germany) and camera (Samsung 13MPx). Surface morphology was analyzed with Multimode AFM (Veeco Instruments).

2.4. 3D PRINTED SCAFFOLDS CHARACTERIZATION

2.4.1. Mechanical properties

Rheological measurements were performed using a rotational rheometer (ARG2, TA Instruments) equipped with a parallel plate sand-blasted geometry of 25 mm of diameter, at controlled temperature of 25 °C. A material volume of 150 μL was used for each measurement, and measuring gap was predefined at 300 μm. CMChNP29/HAox-HA and CMCh/HAox-HA ink formulations (without cells) were analyzed. All experiments were performed at least three times.

Gelation points and material stiffness were analyzed in a time sweep experiment. Storage modulus (G′) and loss modulus (G′′) were recorded in time (0-5 min) at a constant frequency of 1 Hz and 1% oscillatory strain. 75 µL of the CMCh solution (with or without NP29) was deposited on the lower plate, followed by deposition of 75 µL of the HAox-HA solution on top. Solutions were quickly mixed by pipetting, and compressed between the measuring plates. G′ and G′′ were recorded against frequency (1-300 Hz) at 1 % strain in a frequency sweep experiment. Viscosity of the solutions was determined in a rotational flow sweep experiment at increasing shear rate from 0.2 to 500 1/s, to analyze the shear thinning behavior.

2.4.2. *In vitro* stability

In vitro swelling and degradation assays were performed in physiological conditions (PBS pH=7.4 at 37 °C) for CMChNP29/HAox-HA and CMCh/HAox-HA printed scaffolds. 2 layer scaffolds were printed using a grid design (120 x 120 mm^2, 10 mm separation) and stabilization step with Fe^{3+} was carried out as explained in section 2.3.2. For swelling experiments, freshly printed scaffolds were weighed (W_d) and incubated in 3 mL of PBS for different times (0.5, 1, 4 and 18 h). At each time point, scaffolds were removed from PBS, carefully dried with tissue paper and weighed again (W_t). The water uptake was calculated using the following equation:

$$\text{Water uptake (\%)} = [(W_t - W_d)/W_d] \times 100$$

For degradation analysis, scaffolds were dried at 60 °C, weighed (W_0) and incubated in PBS for different times (1, 4, 7, 14 and 28 days). At the specific time points scaffolds were washed with distilled water, dried at 60 °C, and weighed again (W_t). Weight loss was calculated at each time gravimetrically and weight remaining of the samples was defined as following equation:

$$\text{Weight remaining (\%)} = [1-[(W_0-W_t)/W_0]]\times 100$$

A minimum of four replicates of each sample was analyzed for the experiments and results given as mean ± SD. Surface morphology of printed scaffolds after incubation in PBS for 1 to 28 days was qualitatively analyzed by optical microscope (Nikon SMZ800N, Germany).

2.4.3. *In vitro* NP release kinetics from 3D scaffolds

Release of NP29 nanoparticles from 2-layer CMChNP29/HAox-HA and CMCh/HAox-HA printed scaffolds (120 x 120 mm^2) was evaluated. The release of NP29 from hydrogel films of the same compositions (CMChNP29/HAox-HA and CMCh/HAox-HA) prepared by solvent-casting was also evaluated for comparison purposes. Freshly printed scaffolds or films were immersed into 3 mL

of PBS pH 7.4 after stabilization step with Fe^{3+} (explained in section 2.3.2.) and stored at 37 °C. At different time points (1, 4, 7 and 14 days), catechol NP concentration was quantified by measuring the absorbance of the PBS at 280 nm using a NanoDrop One (Thermo Fisher Scientific). A calibration curve of hydrocaffeic acid in PBS was used, and the cumulative release percentage was calculated for each sample. A minimum of 4 replicates was analyzed for each time point and results given as mean ± SD.

2.5. BIOLOGICAL CHARACTERIZATION

2.5.1. Cell cultures

For biological experiments L929 fibroblasts (ATCC, Germany), human dermal fibroblasts (HDF, Innoprot) murine RAW 264.7 macrophages (ECACC, Sigma) and human umbilical vein endothelial cells (HUVEC, Innoprot) were used. L929 Fibroblasts were cultured in RPMI 1640 phenol red free medium (Gibco, 61870-010) supplemented with 20 % fetal bovine serum (FBS, Gibco, 10270), 200 mM L-glutamine and 1 % penicillin/streptomycin (Invitrogen). HDF and RAW cells were cultured in Dulbecco's modified Eagle's medium (DMEM) supplemented with 4-(2-hydroxyethyl)-1-piperazineethanesulfonic acid (HEPES) for HDF cells or sodium pyruvate (110 mg/L) for RAW 264.7 cells; 10 % fetal bovine serum (FBS), 100 units/mL penicillin, 100 µg/mL streptomycin and 200 mM L-glutamine. Endothelial cells were cultured in endothelial cell medium (ECM, Innoprot) supplemented with 5% FBS, 1 % endothelial cell growth supplement and 1 % penicillin/streptomycin solution. Incubation was carried out at 37 °C, 95 % humidity and 5 % CO_2. The culture medium was changed every two days.

2.5.2. Cell uptake of C6-loaded NP

RAW 264.7 cells were selected to investigate endocytosis of C6NP2 and C6NP29 systems. RAW 264.7 cells were seeded into a 96 well-plate at the density of 1 x 10^5 cells/mL in complete DMEM and incubated overnight. Afterward, the medium was replaced by the corresponding NP solution (1:1 NP suspension/DMEM to give final particle concentrations from 0.0156 to 0.25 mg/mL) and incubated for 24 h. Then, cells were washed with PBS and fixed with paraformaldehyde solution in PBS (3.7 w/v %). Nuclei were stained with DAPI (Thermofisher) and fluorescence images were taken at 60x amplification using a stereomicroscope (Nikon SMZ800N, Germany).

2.5.3. NP Cytotoxicity

Cell viability was analyzed in the presence of different concentrations of NP2 and NP29. RAW 264.7 cells were seeded in a 96 well-plate at 2.5 x 10^5 cells/mL density and incubated overnight. The medium was replaced by the corresponding NP solution (1:1 NP suspension/DMEM to give final particle concentrations from 0.0156 to 0.5 mg/mL). After 24h of culture, cell viability was determined by Alamar Blue assay by measuring absorbance at 570 nm using a Multi-Detection Microplate Reader Synergy HT (BioTek Instruments; Vermont, USA). A minimum of 6 replicates was analyzed for each composition. Results were normalized to the control (cells seeded without NP) and expressed as a mean percentage of relative cell viability ± SD. Analysis of variance (ANOVA) using Tukey grouping method of the results for loaded and non-loaded NP, and for NP2 and NP29 compositions at the concentrations from 0.0156 to 0.25 mg/mL was performed at significant level *$p < 0.05$.

2.5.4. NP Antioxidant activity

Antioxidant properties of NP2 and NP29 were evaluated. For that, ROS quantification of RAW 264.7 macrophages in the presence of NP2 and NP29 at different concentrations was carried out using 2',7'-dichlorofluorescin diacetate (DCFH-DA). RAW 264.7 were seeded at 2.5 x 10^5 cells/mL density and incubated for 24 h in complete medium. The medium was removed and replaced by the corresponding NP solution (1:1 NP suspension/DMEM to give final particle concentrations from 0.0156 to 0.25 mg/mL). After 24 h of culture, cells were washed 3 times with PBS and 100 µL of a 40 mM DCFH-DA in PBS were added to the cells. Cells were incubated at 37 °C for 30 min, and washed again 3 times with PBS. Then, 100 µL of H_2O_2 solution in PBS (100 mM) were added to the wells. Well-plate was incubated for 15 min and fluorescence was measured at 485 nm excitation/580 nm emission with a UV multiplate reader (Biotek Synergy HT, Winooski, VT, USA). Analysis of variance (ANOVA) using Tukey grouping method of the results for NP2 and NP29 treated-cells was performed in comparison with the positive control of cells treated with H_2O_2 at significant level *$p < 0.05$, **$p < 0.01$ and ***$p < 0.001$.

2.5.5. NP Anti-inflammatory behavior

The anti-inflammatory activity of NP2 and NP29 nanoparticles was evaluated using the nitric oxide (NO) inhibitory assay.[38] RAW 264.7 cells were seeded in 96-well plates at a density of 2.5 x 10^5 cells/mL and incubated at 37 °C for 24 h. Afterward, the medium was removed and replaced by the corresponding NP solution (1:1 NP suspension/DMEM to give final particle concentrations from 0.0156 to 0.25 mg/mL). After 24 h of culture, medium was removed again

and 5 μg/mL of lipopolysaccharides from E. coli 055:B5 (LPS, Sigma) were added to half of the samples. These samples were incubated for next 24 h, either with or without LPS. NO concentration was determined by the Griess reaction.[39,40] Aliquots (100 μL) of supernatants were mixed with the Griess reagent (Sigma-Aldrich) (100 μL) and after 10 min, absorbance at 548 nm was measured. A minimum of 6 replicates was analyzed and data were expressed as the percentage of NO production and cell viability, and given as mean ± SD. Analysis of variance (ANOVA) using Tukey grouping method of the results for NP2 and NP29 treated-cells was performed in comparison with the positive control of cells treated with LPS at significant level *$p < 0.05$, **$p < 0.01$ and ***$p < 0.001$. Cell viability of RAW 264.7 cells in the presence of LPS and the different concentrations of NP2 and NP29 was evaluated in parallel by Alamar Blue assay as explained in section 2.5.3.

2.5.6. Live/dead assay in bioprinted scaffolds

Cell viability of L929 fibroblasts within the NP-loaded hydrogel scaffolds was evaluated after bioprinting using fluorescein diacetate (FDA, Sigma-Aldrich) and propidium iodide (PI, Sigma Aldrich) staining, to detect live and dead cells, respectively. L929 fibroblasts encapsulated in bulk hydrogel (no printing) after 1 day of culture were used as control. Stabilization step with Fe^{3+} (explained in section 2.3.2.) was performed for both printed and non-printed formulations. At different time points of culture (1, 4, 7 and 14 days) scaffolds were washed with PBS and incubated with FDA (20 μg/mL) and PI (6 μg/mL) for 10 min at r.t. Samples were washed 3 times with PBS and fluorescence images were taken with Nikon Ti-Ecllipse microscope (Nikon Instruments Europe B.V., Germany). To calculate the percentage of viable cells, live and dead cells were quantified in a minimum of 5 images for 3 independent samples using the Image-J software. Analysis of variance (ANOVA) using Tukey grouping method of the results for printed scaffolds at different time points was performed in comparison with the non-printed sample at significant level *$p < 0.05$, **$p < 0.01$ and ***$p < 0.001$.

2.5.7. Immunostaining of bioprinted scaffolds

Immunostaining of the 3D constructs was carried out at different times of culture (1, 4, 7 and 14 days). At each specific time point, cells were fixed with PFA 3.7 % w/v for 15 min, permeabilized with 0.5% Triton -X 100 in PBS for 15 min, and blocked with 0.1% Triton -X 100 and 5% w/v BSA (PBST solution) for 20 min. Scaffolds were incubated in 1:1000 vinculin rabbit antibody (Thermofisher) for cytoskeleton labeling and 1:200 Alexa fluor-546 Phalloidin (Thermofisher) for focal adhesion staining in PBST at r.t. for 1 hour. Samples were rinsed 3 times with PBST and

incubated with secondary antibody Alexa flour-488 goat antirabbit (Thermofisher, 1:500 dilution) to stain cytoskeleton. They were rinsed twice with PBST, incubated with 1:1000 DAPI (Thermofisher) in PBS for 20 min for nuclei staining, and rinsed twice in PBS. Finally, fluorescence imaging was carried out using a Zeiss LSM 880 confocal microscope, and fluorescence images of nuclei staining with DAPI were taken at 2x amplification using a stereomicroscope (Nikon SMZ800N, Germany).

2.5.8. Alamar Blue of bioprinted scaffolds

Alamar Blue assay (Sigma-Aldrich) was carried out to quantify cell proliferation of L929 fibroblasts within the printed scaffolds over a 14-days period by measuring absorbance at 570 nm using a Multi-Detection Microplate Reader Synergy HT (BioTek Instruments; Vermont, USA). A minimum of 6 replicates of 4 independent samples was analyzed for each scaffold composition. Results were normalized to the control (hydrogel without NP after 1 day of culture). Results were expressed as the mean percentage of relative cell viability ± SD. Analysis of variance (ANOVA) using Tukey grouping method of the results for CMChNP29/HAox-HA sample was performed in comparison with the CMCh/HAox-HA control sample at significant level *$p < 0.05$, **$p < 0.01$ and ***$p < 0.001$.

2.5.9. VEGF production quantification

L929 fibroblasts were seeded into 16-well plates at 100.000 cells/mL. Cells were treated with serum-free medium for 2 h. Then, they were exposed to different concentrations of NP2 and NP29 prepared in serum-free medium (0.25, 0.125 and 0.0625 mg/mL) for 48 h. After that time, medium supernatants were centrifuged for 1 min at 1400 r.p.m. and VEGF release was evaluated by ELISA experiment according to the manufacturer's instructions (Invitrogen, Thermo Scientific, San Diego, USA). The cell viability was determined using trypsin and a cell counter (Innoprot) and results were normalized to 10^6 cells. Cells without NP treatment were used as control. Analysis of variance (ANOVA) using Tukey grouping method of the results for NP2 and NP29 treated-cells was performed in comparison with the cells control at significant level *$p < 0.05$, **$p < 0.01$ and ***$p < 0.001$.

VEGF release by endothelial cell lines was also evaluated. Endothelial cells in serum free medium were seeded on the top of hydrogels of CMChNP29/HAox-HA and CMCh/HAox-HA compositions (directly prepared in 12-well plates right before seeding) at 300.000 cells/mL. After 48 h of culture, medium supernatants were centrifuged for 1 min at 1400 r.p.m. and VEGF release was evaluated by ELISA experiment according to the manufacturer's instructions. DNA content was analyzed by Picogreen assay of cells within the gels and results were normalized to 10^6 pg DNA.

Analysis of variance (ANOVA) using Tukey grouping method of the results for CMChNP29/HAox-HA sample was performed in comparison with CMCh/HAox-HA sample at significant level *$p < 0.05$, **$p < 0.01$ and ***$p < 0.001$.

3. RESULTS AND DISCUSSION

The purpose of this work was the fabrication of a functional 3D printed hydrogel scaffold with cells and bioactive NP for improved wound healing. We have developed the bioink consisting of a hydrogel supportive material loaded with cells and nanoparticles functionalized with catechol groups. The scaffolds were produced using a printing technology based on reactive mixing previously presented by our group. The hydrogel scaffolds were characterized to assess their applicability for promoting wound healing.

3.1. PREPARATION AND CHARACTERIZATION OF CATECHOL FUNCTIONALIZED NP

NP were fabricated using two amphiphilic terpolymers with different catechol compositions, i.e. 2 and 29 molar %. Terpolymers were obtained by statistical copolymerization of an acrylic and a vinyl monomer, and the subsequent conjugation of the catechol moieties which provided long-arm catechol side groups in the polymer chain.[37] The different reactivity ratios of the monomers (previously studied by Jansen et al.)[41] lead to the formation of blocky monomeric sequences that offered an appropriate hydrophilic/hydrophobic balance and allowed forming core-shell nanostructures by a self-assembling process. Micelles were obtained in aqueous media by nanoprecipitation method (Figure 1A).

Spherical and monodispersed nanoparticles were observed by scanning electron microscopy (SEM) (Figure 1B). Based on SEM images, the mean particle sizes of dried NP were 81.3±0.8 nm for NP2 and 69.0±1.0 nm for NP29, respectively. The DLS analysis revealed narrow unimodal size distributions (Figure 1C) presenting hydrodynamic diameters (D_h) of 109±6.6 nm for NP2 and 72±8.7 nm for NP29, and low PDI values (Table 1) which indicates the obtaining of homogeneous populations. DLS measurements differed somewhat from those observed by SEM; the observed differences in size can be explained by the fact that SEM measurements were performed for NP in the dry state, whereas DLS provided the hydrodynamic diameter of NP in water. Zeta potential values of -20.8±2.1 and -24.9±1.1 mV were obtained for NP2 and NP29 respectively (Table 1), which were negative enough to ensure stability. The difference in the negative surface charge of the NP suggests that the catechol groups were distributed at the NP

surface. This will give rise to a higher availability of the catechol groups and contribute to the action of their beneficial bioactive properties.[32,42-45] Aqueous dispersions of NP2 were stable in the medium until 3 weeks of storage at 4ºC, showing a relatively low increase in the D_h and zeta potential values during this storage time (Table S1). However, NP29 showed macroscopic aggregates after 3 weeks. This fact can be probably due to an "auto-oxidation" process of the catechol groups located at the surface, as previously explored by other groups.[46,47]

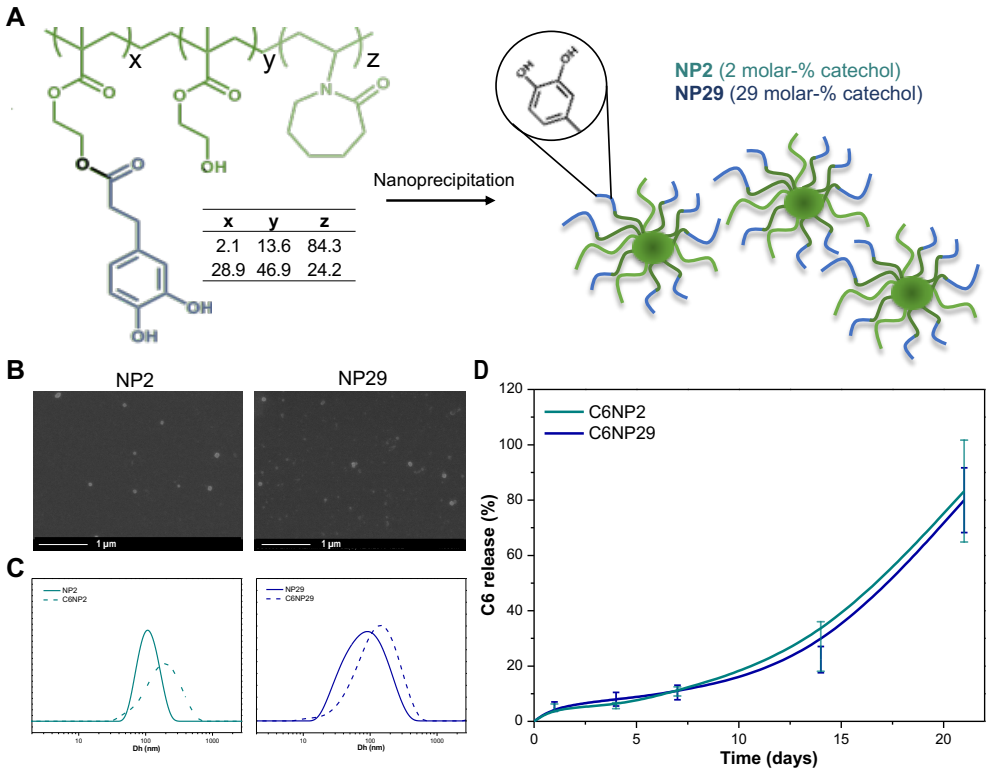

Figure 1. (A) Scheme of NP preparation on the basis on T2 and T29 amphiphilic catechol functionalized terpolymers. (B) SEM images of NP2 and NP29. (C) Graph of the particle size distribution of NP and the C6-loaded NP obtained by DLS. (D) C6 esterase mediated cumulative release from C6NP2 and C6NP29.

In order to test NP applicability as a drug carrier, coumarin-6 was used as a model of hydrophobic drug and it was encapsulated into the core during the self-assembly process. The encapsulation efficiency and controlled release properties of the C6NP were evaluated. Drug encapsulation was successfully performed with efficiency values around 70 % for both NP compositions (NP2 and NP29) giving C6NP nanoparticles with a slightly bigger size (Table 1 and Figure 1C). Subsequently, the C6 release from the NP was studied *in vitro* by an esterase-mediated dialysis

method. The drug release profile (Figure 1D) showed a sustained release with zero order kinetics during the first 14 days and exponential release for longer periods. An initial sustained release of the drug is a very important feature as a premature release can result in dangerous side effects and low effectiveness of the therapy.[48] We can conclude that NP2 and NP29 are expected to serve as nano-vehicles to carry other hydrophobic drugs that can be cytotoxic when they are administered systemically (not locally), such as some antimicrobial drugs, frequently applied in the treatment of skin injures.[49]

Table 1. Mean hydrodynamic diameter (D_h), polydispersity index (PDI) and zeta potential (ξ) of nude and C6-loaded NP, along with C6 encapsulation efficiency (EE) values.

Sample	D_h (nm)	PDI	ξ (mV)	EE (%)
NP2	109±6.6	0.07±0.02	-20.8±2.1	-
C6NP2	153±2.9	0.27±0.04	-	66.1±2.9
NP29	72±8.7	0.42±0.07	-24.9±1.1	-
C6NP29	107±2.2	0.42±0.06	-	74.5±7.0

3.2. FABRICATION OF NP-LOADED 3D SCAFFOLDS

The designed bioink was formulated in two different solutions containing the hydrogel precursors: CMCh and HAox. A chitosan and hyaluronic acid hydrogel were used, as they can form naturally derived hydrogels, due to their intrinsic ECM mimicking properties, thus, favoring cellular growth during tissue regeneration.[17-21,25,50,51] The soluble chitosan derivative carboxymethyl chitosan (CMCh) allows cell encapsulation in the bioink,[52,53] contrary to the non-modified chitosan, which is soluble at acidic conditions. Oxidized hyaluronic acid bearing aldehyde groups can undergo fast Schiff base reaction with the free amine groups of CMCh.[34] Therefore, these polysaccharides are linked by a self-covalent reaction when they are in contact, without the need of any additional crosslinker.[32,52,54,55] Moreover, any neutralization or washing steps are not needed, which is a common strategy used for pure chitosan-based printing.[26,56-58] NP29 were selected to be loaded into the hydrogel scaffolds because of its higher catechol content which presumably will enhance scaffolds' bioactivity (demonstrated in section 3.5). NP29 were added to the CMCh solution and the electrostatic interactions between the negatively charged NP and the cationic polymer contributed to form homogeneous NP dispersion.[59] On the

other hand, the HAox solution was mixed with non-modified HA in order to match viscosities of both precursor solutions (CMCh and HAox) and therefore to get a homogeneous mixing of the bioink during the printing process.

The NP loaded hydrogel scaffolds were obtained applying a new 3D printing methodology previously optimized by our group. Figure 2A shows the schematic setup of the printing system. Hydrogel precursor solutions in different syringes are simultaneously extruded by the printer through a static mixing tool, where they are mixed and covalent reaction is initiated. A partially crosslinked hydrogel is extruded from the printhead. To allow bioink's flow and providing good printing quality hydrogel crosslinking kinetics have to be adjusted to the residence time in the static mixer (this will be discussed in section 3.3). Applied printing methodology allowed us continuously printing with high speed (15 mm/s) using the CMChNP29/HAox-HA formulation and 2 layers grid square design-scaffolds (120x120 mm^2) were obtained as a model structure (Figure 2B). Structures up to 4 layers were prepared in the previous work using this printing approach, however, further adjustment of the mixing printhead will allow building up bigger constructs in the future. The morphology of the scaffolds was studied by light microscopy (Figure 2C). The images showed scaffolds with good printing quality: they maintained the design shape, showed stable structural integrity and presented smooth filaments of expected uniform dimensions (diameter 360±34 μm). Moreover, the microstructure of the hydrogel studied by AFM (Figure 2D) showed that NP were uniformly distributed in the hydrogel framework, presenting good integration between NP and the hydrogel matrix, what can be attributed to the homogeneity of the bioink.

This 3D printing approach has several advantages: *in situ* gelation while printing provides the necessary viscosity to obtain adequate structural integrity and shape fidelity; the use of additional physical factors like irradiation after extrusion to introduce post-printing stabilization can be avoided; the use of low viscosity solutions allows avoiding high shear stress of the encapsulated cells. Furthermore, this printing approach has also some benefits for wound management, since formulation or dimensions of the scaffolds can be tailored to match individual's needs.

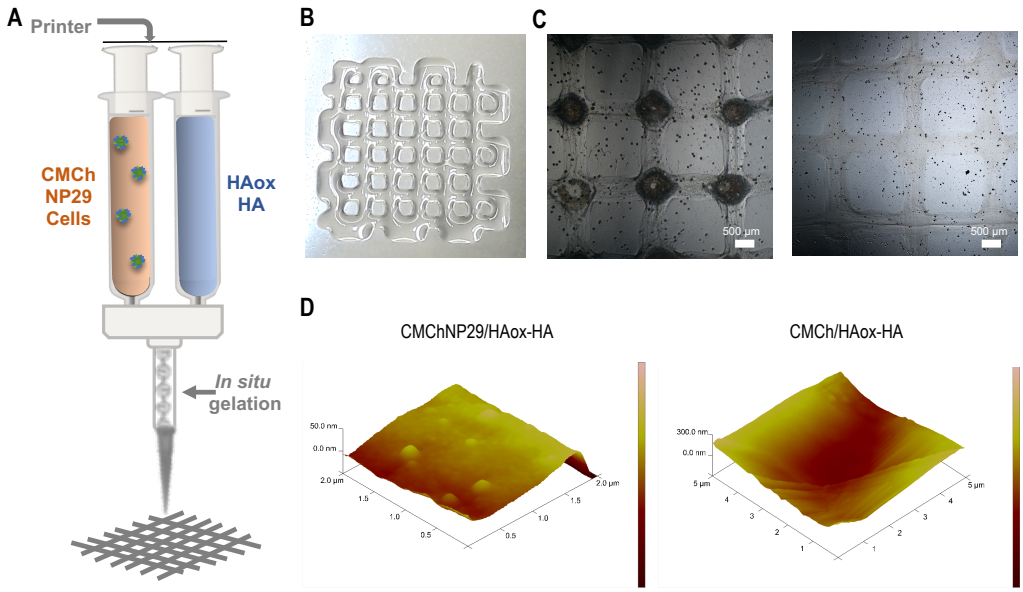

Figure 2. (A) Schematic illustration of the printing methodology. (B) Camera picture of a 2 layer grid square scaffold (120 x 120 mm², 10 mm separation between strands) using CMChNP29/HAox-HA formulation. (C) Light microscopy pictures of dried scaffold (left) and scaffold in PBS (right) using CMChNP29/HAox-HA formulation. (D) AFM microscopy of scaffold strand surface printed using CMChNP29/HAox-HA and CMCh/HAox-HA formulations.

3.3. RHEOLOGICAL STUDY

Viscoelastic properties of CMChNP29/HAox-HA formulation were studied by rheology to determine bioink suitability for printing. The CMCh/HAox-HA formulation (no particles added) was used as control. Time sweep experiments were performed to study the crosslinking kinetics of CMCh and HAox solutions in the presence or absence of the catechol NP. Figure 3A represents the variation of storage (G') and loss (G'') moduli as a function of time. It can be observed that both G' and G'' considerably increased with time due to the formation of Schiff base linkages in the system, what lead to a crossover point of G' and G'' indicating the hydrogel network formation.[60,61] Printing with static mixer tool requires that hydrogel crosslinking kinetics match the residence time in the static mixer, allowing ink flow during extrusion and good shape fidelity after printing. Gelation kinetics of CMCh/NP29HAox-HA formulation (3.32±0.53 min of gelation time) was optimal for printing, providing smooth and homogenous strands. Gelation time obtained for nude hydrogel (3.65±0.33 min) was in the same order of magnitude, what indicates that the presence of dispersed NP29 nanoparticles does not impair printing with static mixing tool.

Frequency sweep experiments (Figure 3B) corroborated hydrogel network formation at all tested frequency range (from 1 till 300 rad/s) since storage modulus was higher than loss modulus. Frequency sweep plots with small slope were obtained for CMChNP29/HAox-HA and CMCh/HAox-HA formulations. This behavior usually correlates with weak hydrogels with shear thinning behavior.[16] Storage modulus for NP loaded hydrogel is slightly higher than for hydrogel without NP. This effect might be attributed to the formation of electrostatic interactions between NP and hydrogel network. However, the difference is small, which implies that mainly the covalent crosslinking between hydrogel precursors contributed to the network formation. Results showed shear modulus values in the range of 50-150 Pa at frequencies between 2 and 300 rad/s, analogous to those reported for other cell-laden chitosan and hyaluronic acid hydrogels.[54,62-64] This result indicates that hydrogel scaffolds are soft, and suitable for soft tissues regeneration.[63]

The shear thinning behavior was investigated by measuring viscosity over increasing shear rate during continuous rotation (Figure 3C). Both formulations, CMCh/NP29HAox-HA and CMCh/HAox-HA, presented a clear shear-thinning where viscosity linearly decreased with increasing shear rate. The shear thinning behavior is a favorable characteristic for printing since ensures that hydrogel viscosity decreases under applied deformation facilitating the flow of the material during extrusion, and it increases when deformation ceases, enabling shape fidelity.[18,65] Viscosity of both studied solutions was relatively low compared to air pressure-based extruded inks (in the range of 30–6 × 10^7 mPa).[8,9] The NP's presence and their possible interactions with the hydrogel network did not influence viscosity values. Low viscosity of the ink and the shear thinning behavior contribute to the reduction of the shear stress to which cells are exposed during extrusion, which favors cell viability.[18,66-68]

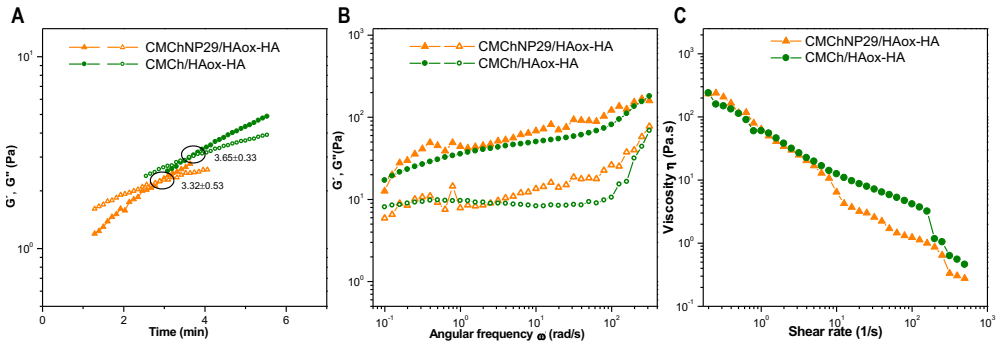

Figure 3. Rheological curves of CMChNP29/HAox-HA bioink formulation compared to the formulation without NP (CMCh/HAox-HA). (A) G' (full symbols) and G" (open symbols) moduli recorded as a function of time at a constant frequency of 1 Hz and 1 % oscillatory strain. Gelation times were determined as G' and G" crossover points. (B) G' (full

symbols) and G" (open symbols) moduli recorded as a function of angular frequency at 1 % strain. (C) Viscosity analysis of the bioinks as a function of shear rate.

3.4. SCAFFOLDS *IN VITRO* PERFORMANCE

Swelling and biodegradability are intrinsic properties of hydrogels, relevant in the wound repair process since influence scaffolds' *in vivo* performance. Thus, the study of hydrogel scaffold stability is of great importance for wound healing applications.[67,69,70] Swelling and degradation studies of 2 layer printed scaffolds of CMChNP29/HAox-HA formulation were performed and compared to CMCh/HAox-HA control. Figure 4A shows that both hydrogel formulations presented similar swelling behavior in *in vitro* physiological conditions; the presence of NP in the hydrogel did not affect the swelling properties of the network. A maximum swelling degree was obtained after 30 min of incubation (around 30 %), and then swelling decreased and stabilized to reach the equilibrium state (around 5 %) after 4 h. Figure 4B presents the scaffolds degradation profiles determined by monitoring the weight loss after different incubation times in physiological conditions. Both formulations presented a gradual degradation pattern. However, after 28 days degradation was relatively higher for the NP loaded formulation (68±9 % of weight loss) compared to the blank (53±12 % of weight loss). This effect might be attributed to the fact that the NP entrapped into the network influence the degradation mechanism of the hydrogel matrix. Anyway, scaffolds maintained their structural integrity after 28, though erosion signs can be appreciated in the optical microscopy visualization (Figure 4C) at that time point.

Swelling and degradation properties are related to the crosslinking of the network.[69,71,72] The dynamic intrinsic character of the Schiff base dynamic linkages may influence on the long-term stability of the printed scaffolds.[53,73-75] Therefore, a straightforward stabilization step of scaffolds incubation in $FeCl_3$ was applied. Stabilization with $FeCl_3$ has been proven to moderate swelling and to increase scaffolds stability via formation of coordination complexes of Fe (III) with hyaluronic acid.[76] NP29 are expected to form electrostatic interactions with the polysaccharides, and they may also form coordination complexes with Fe (III) in the scaffold surface.[47,59] During degradation, the release of NP29 from the scaffold may contribute to breakage of the described interactions, leading to slightly faster degradation in comparison to the control scaffolds without NP. Nevertheless, the small difference between both degradation patterns indicates that covalent reaction between polysaccharides seems to be the predominant crosslinking mechanism that influenced network stability behavior. The moderate swelling range of the scaffolds can be considered adequate for wound management since it can ensure a moisture environment in the wound, and a moist wound environment has been demonstrated to accelerate the re-epithelialization process.[11,64,69,70] Also, the gradual degradation of the scaffolds can match tissue

regeneration rate, allowing the progressive degradation of the scaffold while the new tissues are formed, and a complete resorption is expected *in vivo* due to the presence of proteases, lipases, and other enzymes.[69]

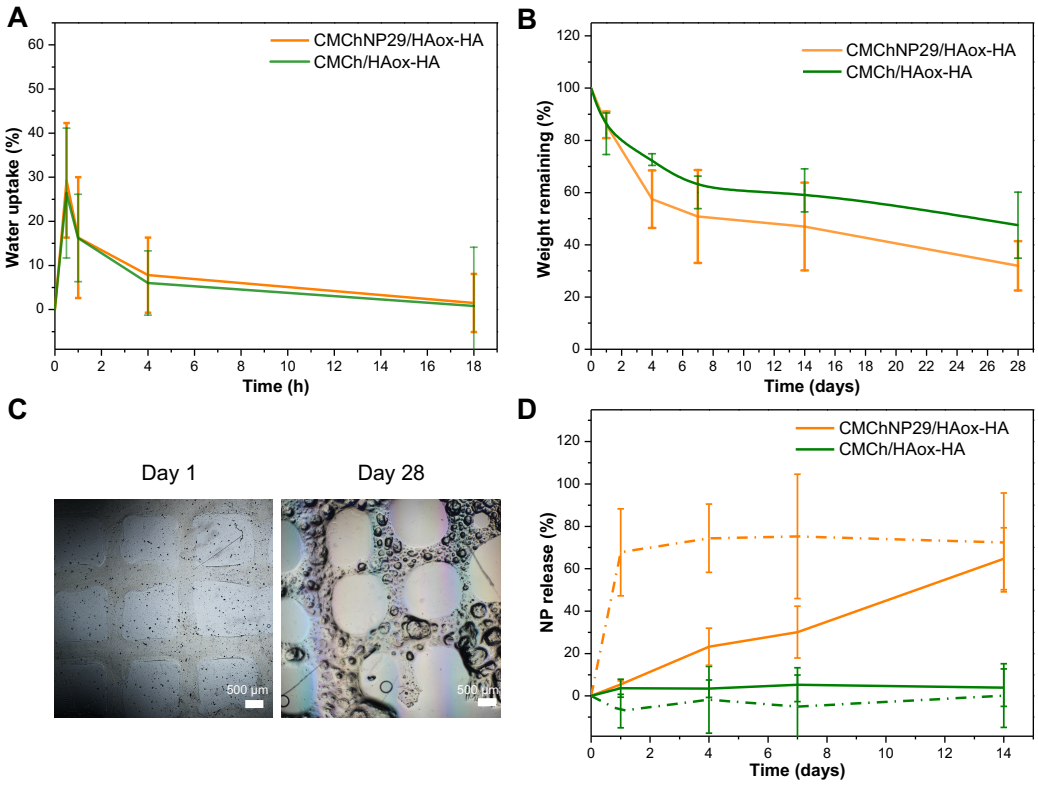

Figure 4. (A) In vitro water uptake and (B) degradation kinetics of CMChNP29/HAox-HA and CMCh/HAox-HA scaffolds in simulated physiological conditions. (C) Microscopic images at 2x magnification of dried scaffolds using CMChNP29/HAox-HA formulation after 1 and 28 days of incubation in PBS at 37 °C. (D) Cumulative NP29 release from 3D hydrogel scaffolds (continuous lines) and films (dot lines) of similar composition as a function of time.

Catechol functionalized NP release from the CMChNP29/HAox-HA printed scaffold and hydrogel films was studied in simulated physiological conditions (Figure 4D). Hydrogel films were tested in order to analyze the NP release profile from supports with very different morphologies. The cumulative release of catechol NP from the printed scaffolds presented a continuous and sustained profile releasing around 65 % of the initial NP amount in 21 days. Release from hydrogel films was faster; a burst release of 65 % was noticed at day 1 and a plateau value of around 70 % was reached after 4 days. This different release performance can be associated with the difference in the physical properties of the supports with different shapes.[51] Printed grid

scaffolds allow better entrapment of NP and present a higher contact surface with the medium so they facilitate progressive NP release. However, hydrogel films releases the NP located at the surface very fast, while they does not favor the release of NP trapped inside. Obtained results suggest that NP release rate from a printed hydrogel could be controlled by changing the 3D printed structure design, which is a very interesting feature for drug release strategies. Patient specific 3D printed scaffolds can offer a sustained release of the NP to the implantation site. Moreover, as previously proved, NP can serve as nanocarriers for different hydrophobic drugs that have low bioavailability and side effects when systemically administered, so the NP action could be extended to other encapsulated drugs.

3.5. BIOLOGICAL BEHAVIOR

In order to evaluate the potential of the 3D printed scaffolds bearing catechol functionalized NP for wound repair, bioactive properties of the system were evaluated in *in-vitro* studies. Firstly, the bioactivity of the catechol NP was examined. RAW 264.7 macrophages line was chosen for this study, since these cells have a key role in the regulation of the inflammatory reaction of chronic wounds.[77] Coumarin-6 was used as a fluorescent tracer to visualize the cellular uptake process of C6-loaded NP by RAW264.7 macrophages. Figure 5A shows microscope images of the cells exposed to different concentrations of the fluorescent C6NP after 24 h of culture. It can be observed that green fluorescent NP of both compositions (C6NP2 and C6NP29) were clearly located inside the cells, presumably internalized by endocytosis process according to the NP size.[78] It must be highlighted that cell uptake can be appreciated even for the lowest NP concentration (0.0156 mg/mL). These results corroborate that: (1) NP2 and NP29 were able to encapsulate the fluorescent model drug coumarin-6 into the core suggesting that they can serve as nano-vehicles for other hydrophobic drugs; and (2) NP were easily internalized by cells, where they will be able to reveal their bioactive action and release the encapsulated drug by digestion of the nanocarrier. Cytotoxicity of C6-loaded and non-loaded NP was also tested using macrophages line (Figure 5B). Results demonstrated that cell viability was lower for the highest tested concentration (0.5 mg/mL) of both loaded and non-loaded NP after 24 h of incubation although it was still around 70 %. However, for all other tested concentrations high cell viability (around 90%) was observed: no significant differences ($p<0.05$) were noticed comparing loaded and non-loaded NP, neither NP2 and NP29 compositions with each other, at the concentrations from 0.0156 to 0.25 mg/mL.

It has been demonstrated that polyphenols like catechol possess excellent antioxidant properties.[7,79-83] A cellular based assay was carried out to determine the catechol functionalized NP capacity to reduce intracellular ROS production of macrophages previously subjected to

oxidative stress with H_2O_2. In the Figure 5C it can be observed that both NP2 and NP29 were able to significantly decrease ROS production (compared to H_2O_2 treated macrophages without NP) at concentrations in the range 0.125-0.25 mg/mL. This reduction was more prominent for NP29, which were able to moderate ROS production at concentrations from 0.0625 to 0.25 mg/mL. These results clearly suggest that antioxidant activity of the nanoparticles is due to the content of catechol groups at their structure. The higher the catechol molar content of NP, the greater the ability to quench the intracellular production of ROS. ROS are continuously generated by cells as a normal metabolic byproduct.[84,85] In chronic wounds, ROS production generally exceeds the capability of the endogenous antioxidant defense.[86-91] This uncontrolled ROS overproduction induces oxidative stress, severe tissue damage and activates the inflammatory response.[5,6,84,86,90-94] Consequently, the wound remains in the inflammatory phase for too long, which hinders tissue regeneration and healing.[7,46,95] At sight of the antioxidant activity of catechol groups, the sustained release of the catechol NP embedded into the printed scaffold would provide a continuous source of ROS scavenger to the wound, beneficial for the wound healing process.

To assess the anti-inflammatory activity of the catechol NP, the NO inhibitory assay was used. NO acts as an intermediary and regulator in inflammatory reactions.[38,96] NO reduction by the materials indicates their anti-inflammatory properties. The ability of uptaken NP to inhibit NO production of macrophages exposed to the pro-inflammatory agent LPS was evaluated. NO production of LPS-treated macrophages with different cytocompatible concentrations of NP, as well as the corresponding cell viability values are displayed in Figure 5D. Both NP formulations showed a NO inhibition effect in a dose-depended manner. NP2 were able to significantly reduce NO production from 0.25 to 0.0625 mg/mL, compared to the positive control of LPS-treated macrophages without NP. For NP29 formulation, significant NO inhibition was observed for concentrations from 0.25 to 0.0313 mg/mL. Therefore, NO inhibition of LPS-treated macrophages was more efficient for NP29 formulation, following a similar trend to that of the ROS production. These results suggest that the anti-inflammatory activity of NP must be directly related to the catechol composition, as previously reported.[97-100] There are two reported strategies through which catechol groups can reduce NO production: (1) by inhibiting the LPS signaling and (2) by directly quenching the NO,[98] which demonstrates the potential of catechol to mitigate inflammatory damage. NO inhibition found for catechol functionalized NP together with their sustained release from the scaffold would guarantee a prolonged anti-inflammatory effect on the wound. This anti-inflammatory activity is especially desirable in the treatment of chronic wounds, when the inflammatory stage is too long and inhibits tissue regeneration.[7,82,90]

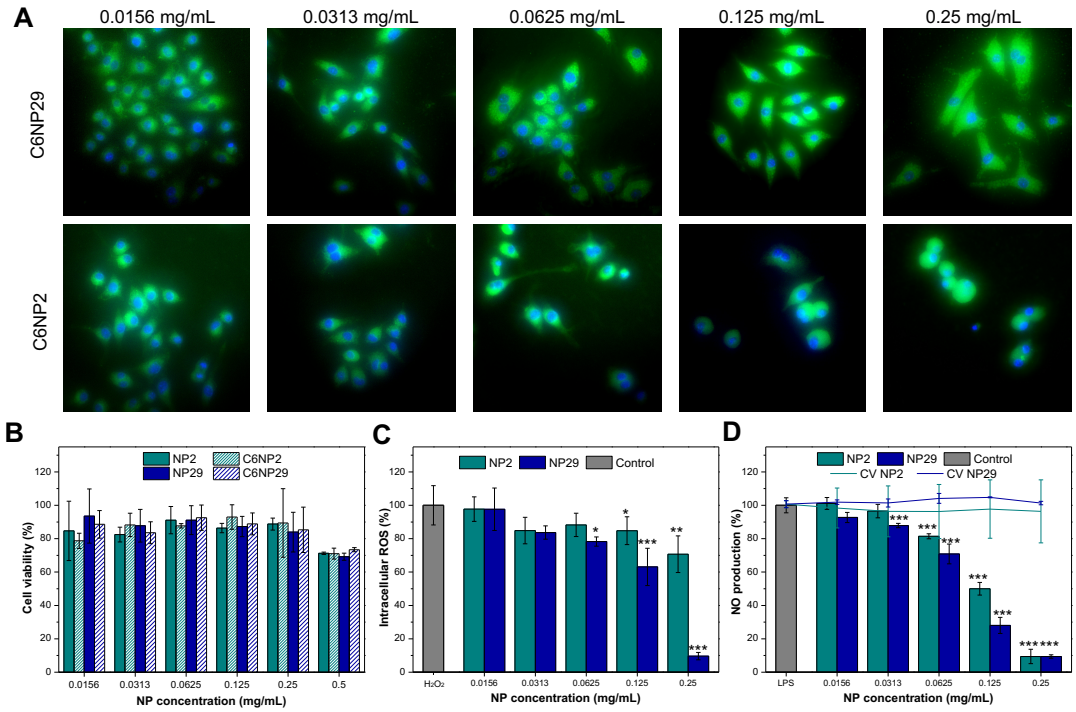

Figure 5. Biological assay of NP using RAW 264.7 macrophages: (A) Microscope images of RAW exposed to different concentrations of C6NP2 and C6NP29 for 24h. (B) Statistical Cytotoxicity of C6-loaded and non-loaded NP2 and NP29. ANOVA of the results for loaded and non-loaded NP, and for NP2 and NP29 compositions at the concentrations from 0.0156 to 0.25 mg/mL was performed at significant level *p < 0.05. (C) ROS production by RAW after treatment with H_2O_2 and different concentrations of NP2 and NP29. (D) NO production of LPS-treated RAW with different concentrations of NP, as well as the corresponding cell viability (CV) values. ANOVA of the results for NP2 and NP29 treated-cells was performed in comparison with the positive control of cells treated with H_2O_2 or LPS at significant level *p < 0.05, **p < 0.01 and ***p < 0.001.

The suitability of NP-loaded bioink to support L929 fibroblasts viability was evaluated. L929 fibroblasts viability within the bioprinted hydrogel scaffolds was assessed over 14 days. Fluorescence images using live/dead staining (Figure 6A) showed that cells were homogeneously distributed within the scaffold, due to the effective mixing in the static mixer during the extrusion process. Additionally, confocal images confirmed the abundance of cells homogeneously dispersed within the scaffold (Figure 6B). Figure 6B also showed that cells maintained a rounded morphology, due to the low stiffness of the hydrogel material. Actin cytoskeleton is specially appreciated, which is an important fact since actin is involved in important processes such as cell mobility.[101] Moreover, based of nuclei staining (Figure 6C) it can be concluded that the scaffolds maintained dimensional stability after the 14 days of culture.

Most probably it can be assigned to the stabilization step with Fe^{3+} that provides mechanical and structural integrity to the scaffolds.

Quantification of the cell viability in the bioprinted constructs after 1 day of culture (Figure 6D) was determined from live-dead assay. Results showed non-significant differences compared to the non-printed material. These results suggest that shear stress produced during the printing process did not have any negative effect on the short time cell viability. The viability of fibroblasts within the printed scaffolds significantly increased after 7 days and remained stable until 14 days of culture, showing values between 85 and 97 % respectively. High cell viability values at long times indicate that the NP release and the polysaccharides degradation products did not negatively influence the cells. Obtained results indicate that the NP loaded-hydrogel protected the cells from mechanical damage during the printing process and provided a suitable environment for the encapsulated cells after printing supporting long-term cell survival.

Metabolic activity of fibroblasts encapsulated into the bioprinted constructs was quantified over time using Alamar Blue assay. NP loaded scaffolds were compared to the printed hydrogel materials without NP (Figure 6E). NP loaded constructs supported a more stable cell growth rate than controls, showing significantly higher viability values at 4, 7 and 14 days of culture. This different biological response was attributed to the incorporation of the catechol groups of NP in the polysaccharide matrix. Catechol has been proposed as an activator of cell proliferation in several studies.[95,102,103] Fluorescence values for NP loaded hydrogels after 14 days of culture were over 2.5-fold higher compared to the immediate value after printing.

Results obtained for cell studies of the bioprinted scaffolds are consistent with other reported systems based on chitosan or hyaluronic acid bioprinted scaffolds.[104-106] We can conclude that *in vitro* studies demonstrate the wound healing promoting activities of the catechol functionalized nanoparticles as well as the ability of NP loaded hydrogel bioink to support cell proliferation, indicating that this bioink is a promising material for application in tissue regeneration processes.

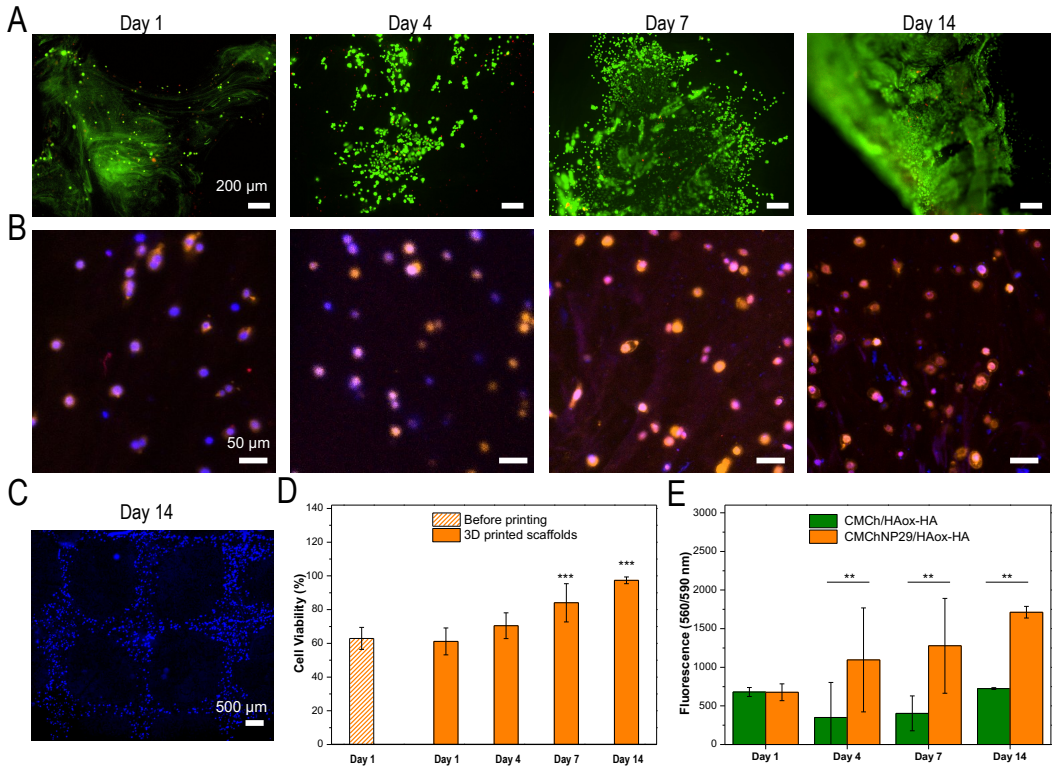

Figure 6. (A) Fluorescence images using live/dead staining and (B) confocal images of immunostaining of L929 fibroblasts embedded into CMChNP29/HAox-HA bioprinted scaffolds over 14 days of culture. (C) Fluorescence image of nuclei staining with DAPI of L929 fibroblasts in a CMChNP29/HAox-HA bioprinted scaffold after 14 days of culture taken by stereomicroscope. (D) Quantification of L929 fibroblasts viability in the non-printed hydrogels at 1 day and in the printed constructs over 14 days for CMChNP29/HAox-HA formulation. ANOVA of the results for printed scaffolds at different time points was performed in comparison with the non-printed sample at significant levels *$p < 0.05$, **$p < 0.01$ and ***$p < 0.001$. (E) Metabolic activity of L929 fibroblasts encapsulated into CMChNP29/HAox-HA and CMCh/HAox-HA printed constructs quantified over time using Alamar Blue assay. ANOVA of the results for CMChNP29/HAox-HA sample was performed in comparison with the CMCh/HAox-HA control sample at significant levels of *$p < 0.05$, **$p < 0.01$ and ***$p < 0.001$.

Angiogenesis or neovascularization plays an important role in tissue regeneration processes. New blood vessel formation provides nutrients and oxygen supply, removes metabolic waste and reduces the risk of infection, essential for the reparation of damaged tissues.[107-110] However, rapid angiogenesis is still a challenge in skin regeneration.[109,111] The neovascularization process is usually induced by growth factors released by cells. Among them, vascular endothelial growth factor (VEGF) is the most potent angiogenic growth factor that plays a critical role in the

regulation of wound angiogenesis.[112-114] In this study, the direct effects of catechol nanoparticles on the *in vitro* VEGF expression of cells were examined. VEGF expression of 2D fibroblasts culture exposed to 3 different concentrations of NP2 or NP29 was evaluated by ELISA assay (Figure 7A). In can be appreciated that NP29 prominently enhanced the VEGF expression of fibroblasts at 0.25 mg/mL concentration. However, VEGF expression of fibroblasts treated with NP2 was maintained at a basal level similar to the control. To further evaluate the effect of NP29 on the angiogenic activity of cells, endothelial cells were seeded on CMCh/HAox-HA and CMChNP29/HAox-HA hydrogels, and VEGF secretion was again analyzed by ELISA (Figure 7B). VEGF production of endothelial cells in the NP-loaded hydrogel was significantly higher respect to the non-loaded hydrogel. These findings corroborate with those reported by the authors on the *in vivo* response of catechol containing IPN membranes, where catechol functionalized chitosan/hyaluronic acid hydrogels demonstrated to promote *in vivo* blood vessels formation,[32] and with previously reported observations of other authors that suggested the pro-angiogenesis capacity of catechol containing polymers. For example, Shin et al.[102] and Park et al.[115] demonstrated the enhanced *in vivo* angiogenesis capacity of stem cells encapsulated in hyaluronic acid derivatives functionalized with catechol groups, for the treatment of ischemic diseases. Also, Xu et al. showed the upregulating capacity of catechol/ε-poly-L-lysine polymers in an *in-vivo* full-thickness cutaneous wound model.[116] Therefore, we envision that NP-loaded hydrogels studied in this work will facilitate the neovascularization process in the wound site upregulating the expression of VEGF, and consequently, accelerating the proliferative stage of the healing process.

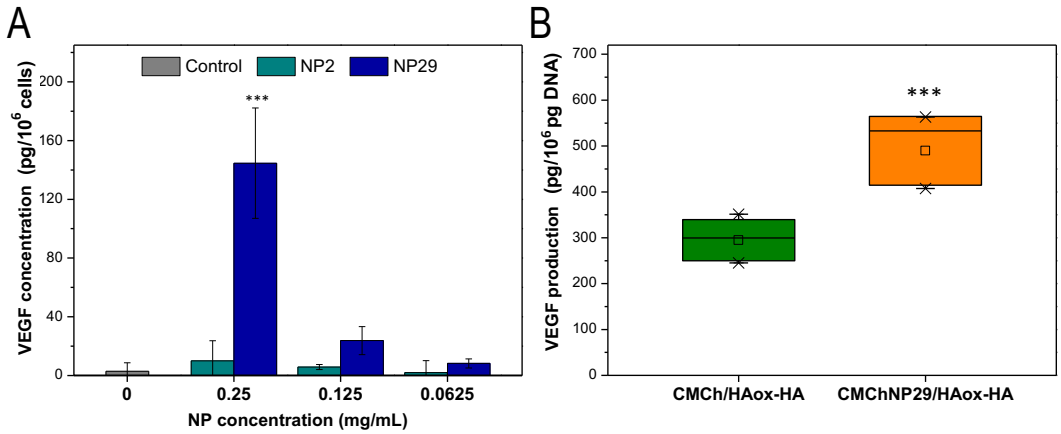

Figure 7. (A) VEGF expression of 2D fibroblasts culture exposed to different concentrations of NP2 or NP29 and evaluated by ELISA assay. ANOVA of the results for NP2 and NP29 treated-cells was performed in comparison with the cells control at significant level *p < 0.05, **p < 0.01 and ***p < 0.001. (B) VEGF secretion of endothelial cells seeded on

CMCh/HAox-HA and CMChNP29/HAox-HA gels analyzed by ELISA. ANOVA of the results for CMChNP29/HAox-HA sample was performed in comparison with CMCh/HAox-HA sample at significant level *p < 0.05, **p < 0.01 and ***p < 0.001.

4. CONCLUSIONS

In the present work, 3D printed hydrogel constructs containing novel catechol functionalized nanoparticles (NP) have been developed. The synergistic action between the biomimetic hydrogel network (composed of carboxymethyl chitosan and hyaluronic acid) and the bioactive function of the NP have been explored for its use in wound care management. A novel 3D bioprinting approach, previously optimized by our group, based on reactive mixing has been used overcoming the intrinsic weak mechanical properties of hydrogels. 2 layers grid square scaffolds have been successfully obtained with good resolution and shape fidelity. Further adjustment of the mixing printhead would allow to build up bigger constructs in follow up studies. Moreover, NP were uniformly distributed in the hydrogel framework. *In vitro* studies have demonstrate the ability of the bioink to support cell proliferation, and the wound healing promoting activities of the catechol functionalized nanoparticles: regulation of the radical oxygen species production, anti-inflammatory response and upregulation of vascular endothelial growth factor expression. Therefore, we envision that NP loaded bioink developed in this work has promising applicability for wound healing therapies with several advantages: 1) the controlled release of the NP in the wound site provides localized bioactive function; 2) functionalized NP can act as nanocarriers for multiple hydrophobic drugs; 3) printing approach used allows tailoring the geometry of the materials and formulation doses based on patient requirements for wound specific treatments.

ACKNOWLEDGMENTS

Authors thank CIBER-BBN (Spain) and the Spanish Ministry of Economy and Competitivity (M. Puertas-Bartolomé scholarship BES-2015-075161 and project MAT2017-84277-R) for supporting this work. The authors acknowledge RegenHu company, and particularly: Sandro Figi, Dominic Ernst, Michael Kuster and Andreas Scheidegger, for the fruitful collaboration, development and providing the mixing tool. The authors thank Dr. Emmanuel Terriac from INM, Germany for assistance in the confocal imaging

Supporting information

3D printed construct with catechol functionalized nanoparticles for wound healing applications

María Puertas-Bartolomé, Małgorzata K.Włodarczyk-Biegun, Aránzazu del Campo, Blanca Vázquez-Lasa* and Julio San Román

In consideration for publication

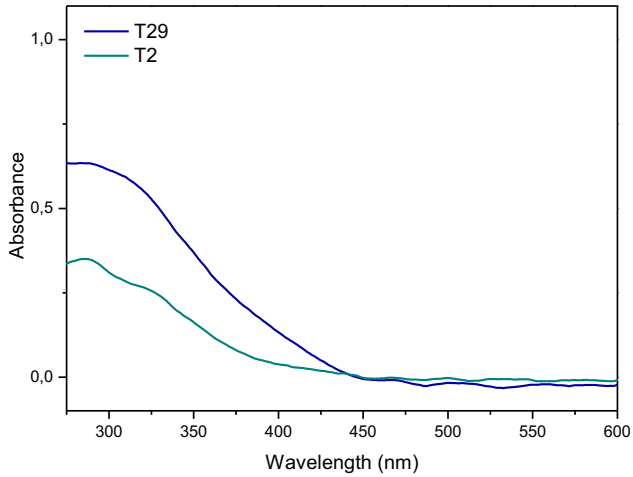

Figure S1. (A) UV spectra of T2 and T29 amphiphilic terpolymers.

Table S1. Mean hydrodynamic diameter (D_h), polydispersity index (PDI), and zeta potential (ξ) of NP2 and NP29 dispersions stored at 4ºC for different times.

	Day 1			**1 week**			**3 weeks**		
	D_h (nm)	PDI	ξ(mV)	D_h (nm)	PDI	ξ(mV)	D_h (nm)	PDI	ξ(mV)
NP2	109±6.6	0.07±0.02	-20.8±2.1	126±4.8	0.05±0.02	-21.7±0.9	133±7.3	0.05±0.02	23.3±1.2
NP29	72±8.7	0.42±0.07	-24.9±1.1	76±9.9	0.41±0.08	-24.1±1.9	-	-	-

REFERENCES

1. Chouhan D, Dey N, Bhardwaj N, Mandal BB. Emerging and innovative approaches for wound healing and skin regeneration: current status and advances. *Biomaterials.* 2019:119267.

2. Martin P. Wound healing--aiming for perfect skin regeneration. *Science.* 1997;276(5309):75-81.

3. Clark RA, Ghosh K, Tonnesen MG. Tissue engineering for cutaneous wounds. *Journal of Investigative Dermatology.* 2007;127(5):1018-1029.

4. Gosain A, DiPietro LA. Aging and wound healing. *World journal of surgery.* 2004;28(3):321-326.

5. Brem H, Stojadinovic O, Diegelmann RF, et al. Molecular markers in patients with chronic wounds to guide surgical debridement. *Molecular medicine.* 2007;13(1-2):30.

6. Gibson DJ, Schultz G. Chronic wound diagnostic for matrix metalloproteinase: chronic wounds. *Wound healing Southern Africa.* 2009;2(2):68-70.

7. Nyanhongo GS, Sygmund C, Ludwig R, Prasetyo EN, Guebitz GM. Synthesis of multifunctional bioresponsive polymers for the management of chronic wounds. *Journal of Biomedical Materials Research Part B: Applied Biomaterials.* 2013;101(5):882-891.

8. Derakhshanfar S, Mbeleck R, Xu K, Zhang X, Zhong W, Xing M. 3D bioprinting for biomedical devices and tissue engineering: A review of recent trends and advances. *Bioactive materials.* 2018;3(2):144-156.

9. Cui H, Nowicki M, Fisher JP, Zhang LG. 3D bioprinting for organ regeneration. *Advanced healthcare materials.* 2017;6(1):1601118.

10. Włodarczyk-Biegun MK, del Campo A. 3D bioprinting of structural proteins. *Biomaterials.* 2017;134:180-201.

11. Long J, Etxeberria AE, Nand AV, Bunt CR, Ray S, Seyfoddin A. A 3D printed chitosan-pectin hydrogel wound dressing for lidocaine hydrochloride delivery. *Materials Science and Engineering: C.* 2019;104:109873.

12. Hafezi F, Scoutaris N, Douroumis D, Boateng J. 3D printed chitosan dressing crosslinked with genipin for potential healing of chronic wounds. *International journal of pharmaceutics.* 2019;560:406-415.

13. Muwaffak Z, Goyanes A, Clark V, Basit AW, Hilton ST, Gaisford S. Patient-specific 3D scanned and 3D printed antimicrobial polycaprolactone wound dressings. *International journal of pharmaceutics.* 2017;527(1-2):161-170.

14. Kogelenberg Sv, Yue Z, Dinoro JN, Baker CS, Wallace GG. Three-dimensional printing and cell therapy for wound repair. *Advances in wound care.* 2018;7(5):145-156.

15. Yang JM, Olanrele OS, Zhang X, Hsu CC. Fabrication of hydrogel materials for biomedical applications. *Novel Biomaterials for Regenerative Medicine*: Springer; 2018:197-224.

16. Hsiao S-H, Hsu S-h. Synthesis and characterization of dual stimuli-sensitive biodegradable polyurethane soft hydrogels for 3D cell-laden bioprinting. *ACS applied materials & interfaces.* 2018;10(35):29273-29287.

17. Murphy SV, Skardal A, Atala A. Evaluation of hydrogels for bio-printing applications. *Journal of Biomedical Materials Research Part A.* 2013;101(1):272-284.

18. Malda J, Visser J, Melchels FP, et al. 25th anniversary article: engineering hydrogels for biofabrication. *Advanced materials.* 2013;25(36):5011-5028.

19. Hospodiuk M, Dey M, Sosnoski D, Ozbolat IT. The bioink: a comprehensive review on bioprintable materials. *Biotechnology advances.* 2017;35(2):217-239.

20. Chaudhari A, Vig K, Baganizi D, et al. Future prospects for scaffolding methods and biomaterials in skin tissue engineering: a review. *International journal of molecular sciences.* 2016;17(12):1974.

21. Mora-Boza A, Puertas-Bartolomé M, Vázquez-Lasa B, San Román J, Pérez-Caballer A, Olmeda-Lozano M. Contribution of bioactive hyaluronic acid and gelatin to regenerative medicine. Methodologies of gels

preparation and advanced applications. 2017.

22. Annabi N, Tamayol A, Uquillas JA, et al. 25th anniversary article: Rational design and applications of hydrogels in regenerative medicine. *Advanced materials.* 2014;26(1):85-124.

23. Ratner BD, Bryant SJ. Biomaterials: where we have been and where we are going. *Annu. Rev. Biomed. Eng.* 2004;6:41-75.

24. Caló E, Khutoryanskiy VV. Biomedical applications of hydrogels: A review of patents and commercial products. *European Polymer Journal.* 2015;65:252-267.

25. Zhang J, Allardyce BJ, Rajkhowa R, et al. 3D printing of silk particle-reinforced chitosan hydrogel structures and their properties. *ACS Biomaterials Science & Engineering.* 2018;4(8):3036-3046.

26. Wu Q, Therriault D, Heuzey M-C. Processing and properties of chitosan Inks for 3D printing of hydrogel microstructures. *ACS Biomaterials Science & Engineering.* 2018;4(7):2643-2652.

27. Li H, Tan YJ, Liu S, Li L. Three-dimensional bioprinting of oppositely charged hydrogels with super strong Interface bonding. *ACS applied materials & interfaces.* 2018;10(13):11164-11174.

28. Highley CB, Song KH, Daly AC, Burdick JA. Jammed microgel inks for 3D printing applications. *Advanced Science.* 2019;6(1):1801076.

29. Hinton TJ, Jallerat Q, Palchesko RN, et al. Three-dimensional printing of complex biological structures by freeform reversible embedding of suspended hydrogels. *Science advances.* 2015;1(9):e1500758.

30. Berthet M, Gauthier Y, Lacroix C, Verrier B, Monge C. Nanoparticle-based dressing: the future of wound treatment? *Trends in biotechnology.* 2017;35(8):770-784.

31. Frachini EC, Petri DF. Magneto-Responsive Hydrogels: Preparation, Characterization, Biotechnological and Environmental Applications. *Journal of the Brazilian Chemical Society.* 2019;30(10):2010-2028.

32. Puertas-Bartolomé M, Benito-Garzón L, Fung S, Kohn J, Vázquez-Lasa B, San Román J. Bioadhesive functional hydrogels: Controlled release of catechol species with antioxidant and antiinflammatory behavior. *Materials Science and Engineering: C.* 2019;105:110040.

33. Fort R, Polyzoidis T. Intrinsic viscosity-molecular weight relationships for poly (2-hydroxyethyl methacrylate). *European Polymer Journal.* 1976;12(9):685-689.

34. Tan H, Chu CR, Payne KA, Marra KG. Injectable in situ forming biodegradable chitosan–hyaluronic acid based hydrogels for cartilage tissue engineering. *Biomaterials.* 2009;30(13):2499-2506.

35. Zhao H, Heindel ND. Determination of degree of substitution of formyl groups in polyaldehyde dextran by the hydroxylamine hydrochloride method. *Pharm. Res.* 1991;8(3):400-402.

36. Yan S, Wang T, Feng L, et al. Injectable in situ self-cross-linking hydrogels based on poly (L-glutamic acid) and alginate for cartilage tissue engineering. *Biomacromolecules.* 2014;15(12):4495-4508.

37. Puertas-Bartolomé M, Vázquez-Lasa B, San Román J. Bioactive and Bioadhesive Catechol Conjugated Polymers for Tissue Regeneration. *Polymers.* 2018;10(7):768.

38. Wang SY, Lan XY, Xiao JH, Yang JC, Kao YT, Chang ST. Antiinflammatory activity of Lindera erythrocarpa fruits. *Phytother. Res.* 2008;22(2):213-216.

39. Guevara I, Iwanejko J, Dembińska-Kieć A, et al. Determination of nitrite/nitrate in human biological material by the simple Griess reaction. *Clinica Chimica Acta.* 1998;274(2):177-188.

40. Choi MS, Lee SH, Cho HS, et al. Inhibitory effect of obovatol on nitric oxide production and activation of NF-κB/MAP kinases in lipopolysaccharide-treated RAW 264.7 cells. *Eur. J. Pharmacol.* 2007;556(1-3):181-189.

41. Jansen JF, Houben EE, Tummers PH, Wienke D, Hoffmann J. Real-time

infrared determination of photoinitiated copolymerization reactivity ratios: application of the Hilbert transform and critical evaluation of data analysis techniques. *Macromolecules.* 2004;37(6):2275-2286.

42. Chen T, Chen Y, Rehman HU, et al. Ultratough, Self-Healing, and Tissue-Adhesive Hydrogel for Wound Dressing. *ACS applied materials & interfaces.* 2018;10(39):33523-33531.

43. Han L, Lu X, Liu K, et al. Mussel-inspired adhesive and tough hydrogel based on nanoclay confined dopamine polymerization. *ACS nano.* 2017;11(3):2561-2574.

44. Kim BJ, Oh DX, Kim S, et al. Mussel-mimetic protein-based adhesive hydrogel. *Biomacromolecules.* 2014;15(5):1579-1585.

45. Brubaker CE, Kissler H, Wang L-J, Kaufman DB, Messersmith PB. Biological performance of mussel-inspired adhesive in extrahepatic islet transplantation. *Biomaterials.* 2010;31(3):420-427.

46. Hasegawa U, Moriyama M, Uyama H, van der Vlies AJ. Catechol-bearing block copolymer micelles: Structural characterization and antioxidant activity. *Polymer.* 2015;66:1-7.

47. Yang J, Stuart MAC, Kamperman M. Jack of all trades: versatile catechol crosslinking mechanisms. *Chemical Society Reviews.* 2014;43(24):8271-8298.

48. Tan JPK, Voo ZX, Lim S, et al. Effective encapsulation of apomorphine into biodegradable polymeric nanoparticles through a reversible chemical bond for delivery across the blood–brain barrier. *Nanomedicine: Nanotechnology, Biology and Medicine.* 2019;17:236-245.

49. Malmsten M. Antimicrobial and antiviral hydrogels. *Soft Matter.* 2011;7(19):8725-8736.

50. Aydogdu MO, Oner ET, Ekren N, et al. Comparative characterization of the hydrogel added PLA/β-TCP scaffolds produced by 3D bioprinting. *Bioprinting.* 2019;13:e00046.

51. Yan J, Wang Y, Zhang X, et al. Snakegourd root/Astragalus polysaccharide hydrogel preparation and application in 3D printing. *International journal of biological macromolecules.* 2019;121:309-316.

52. Nguyen NT-P, Nguyen LV-H, Tran NM-P, Nguyen T-H, Huynh C-K, Van TV. Synthesis of cross-linking chitosan-hyaluronic acid based hydrogels for tissue engineering applications. Paper presented at: International Conference on the Development of Biomedical Engineering in Vietnam2017.

53. Qian C, Zhang T, Gravesande J, Baysah C, Song X, Xing J. Injectable and self-healing polysaccharide-based hydrogel for pH-responsive drug release. *International journal of biological macromolecules.* 2019;123:140-148.

54. Song L, Li L, He T, et al. Peritoneal adhesion prevention with a biodegradable and injectable N,O-carboxymethyl chitosan-aldehyde hyaluronic acid hydrogel in a rat repeated-injury model. *Sci Rep.* Nov 21 2016;6:37600.

55. Khorshidi S, Karkhaneh A. A self-crosslinking tri-component hydrogel based on functionalized polysaccharides and gelatin for tissue engineering applications. *Mater. Lett.* 2016;164:468-471.

56. Intini C, Elviri L, Cabral J, et al. 3D-printed chitosan-based scaffolds: An in vitro study of human skin cell growth and an in-vivo wound healing evaluation in experimental diabetes in rats. *Carbohydrate polymers.* 2018;199:593-602.

57. Ye K, Felimban R, Traianedes K, et al. Chondrogenesis of infrapatellar fat pad derived adipose stem cells in 3D printed chitosan scaffold. *PLoS One.* 2014;9(6).

58. Lee J-Y, Choi B, Wu B, Lee M. Customized biomimetic scaffolds created by indirect three-dimensional printing for tissue engineering. *Biofabrication.* 2013;5(4):045003.

59. Shen J, Shi D, Dong L, Zhang Z, Li X, Chen M. Fabrication of polydopamine nanoparticles knotted alginate scaffolds and their properties. *Journal*

of Biomedical Materials Research Part A. 2018;106(12):3255-3266.

60. Weng L, Chen X, Chen W. Rheological characterization of in situ crosslinkable hydrogels formulated from oxidized dextran and N-carboxyethyl chitosan. *Biomacromolecules.* 2007;8(4):1109-1115.

61. Nguyen NT-P, Nguyen LV-H, Tran NM-P, et al. The effect of oxidation degree and volume ratio of components on properties and applications of in situ cross-linking hydrogels based on chitosan and hyaluronic acid. *Materials Science and Engineering: C.* 2019;103:109670.

62. Li L, Wang N, Jin X, et al. Biodegradable and injectable in situ cross-linking chitosan-hyaluronic acid based hydrogels for postoperative adhesion prevention. *Biomaterials.* 2014;35(12):3903-3917.

63. Bootsma K, Fitzgerald MM, Free B, et al. 3D printing of an interpenetrating network hydrogel material with tunable viscoelastic properties. *Journal of the mechanical behavior of biomedical materials.* 2017;70:84-94.

64. Deng Y, Ren J, Chen G, et al. Injectable in situ cross-linking chitosan-hyaluronic acid based hydrogels for abdominal tissue regeneration. *Scientific Reports.* 2017;7(1):2699.

65. Jungst T, Smolan W, Schacht K, Scheibel T, Groll Jr. Strategies and molecular design criteria for 3D printable hydrogels. *Chemical reviews.* 2016;116(3):1496-1539.

66. Aguado BA, Mulyasasmita W, Su J, Lampe KJ, Heilshorn SC. Improving viability of stem cells during syringe needle flow through the design of hydrogel cell carriers. *Tissue Engineering Part A.* 2011;18(7-8):806-815.

67. Hölzl K, Lin S, Tytgat L, Van Vlierberghe S, Gu L, Ovsianikov A. Bioink properties before, during and after 3D bioprinting. *Biofabrication.* 2016;8(3):032002.

68. Nair K, Gandhi M, Khalil S, et al. Characterization of cell viability during bioprinting processes. *Biotechnology Journal: Healthcare Nutrition Technology.* 2009;4(8):1168-1177.

69. Huber D, Grzelak A, Baumann M, et al. Anti-inflammatory and anti-oxidant properties of laccase-synthesized phenolic-O-carboxymethyl chitosan hydrogels. *New biotechnology.* 2018;40:236-244.

70. Caliari SR, Burdick JA. A practical guide to hydrogels for cell culture. *Nature methods.* 2016;13(5):405.

71. Peng X, Peng Y, Han B, Liu W, Zhang F, Linhardt RJ. -stimulated crosslinking of catechol-conjugated hydroxyethyl chitosan as a tissue adhesive. *Journal of Biomedical Materials Research Part B: Applied Biomaterials.* 2018.

72. Barbucci R, Magnani A, Consumi M. Swelling behavior of carboxymethylcellulose hydrogels in relation to cross-linking, pH, and charge density. *Macromolecules.* 2000;33(20):7475-7480.

73. Xin Y, Yuan J. Schiff's base as a stimuli-responsive linker in polymer chemistry. *Polymer Chemistry.* 2012;3(11):3045-3055.

74. Zhang ZP, Rong MZ, Zhang MQ. Polymer engineering based on reversible covalent chemistry: A promising innovative pathway towards new materials and new functionalities. *Progress in Polymer Science.* 2018;80:39-93.

75. Hozumi T, Kageyama T, Ohta S, Fukuda J, Ito T. Injectable hydrogel with slow degradability composed of gelatin and hyaluronic acid cross-linked by Schiff's base formation. *Biomacromolecules.* 2018;19(2):288-297.

76. Mercê ALR, Carrera LCM, Romanholi LKS, Recio MaÁL. Aqueous and solid complexes of iron (III) with hyaluronic acid: potentiometric titrations and infrared spectroscopy studies. *Journal of inorganic biochemistry.* 2002;89(3-4):212-218.

77. Zeng R, Lin C, Lin Z, et al. Approaches to cutaneous wound healing: basics and future directions. *Cell and tissue research.* 2018;374(2):217-232.

78. Palao-Suay R, Aguilar MR, Parra-Ruiz FJ, et al. Anticancer and antiangiogenic activity of surfactant-free

nanoparticles based on self-assembled polymeric derivatives of vitamin E: Structure–activity relationship. *Biomacromolecules.* 2015;16(5):1566-1581.

79. Schweigert N, Zehnder AJ, Eggen RI. Chemical properties of catechols and their molecular modes of toxic action in cells, from microorganisms to mammals. *Environ. Microbiol.* 2001;3(2):81-91.

80. Nagababu E, Rifkind JM, Boindala S, Nakka L. Assessment of antioxidant activity of eugenol in vitro and in vivo. *Free Radicals and Antioxidant Protocols*: Springer; 2010:165-180.

81. Puertas-Bartolomé M, Fernández-Gutiérrez M, García-Fernández L, Vázquez-Lasa B, San Román J. Biocompatible and bioadhesive low molecular weight polymers containing long-arm catechol-functionalized methacrylate. *European Polymer Journal.* 2018;98:47-55.

82. Huber D, Grzelak A, Baumann M, et al. Anti-inflammatory and anti-oxidant properties of laccase-synthesized phenolic- O -carboxymethyl chitosan hydrogels. *New Biotechnology.* 2018;40:236-244.

83. Cai Y, Luo Q, Sun M, Corke H. Antioxidant activity and phenolic compounds of 112 traditional Chinese medicinal plants associated with anticancer. *Life Sci.* 2004;74(17):2157-2184.

84. He L, He T, Farrar S, Ji L, Liu T, Ma X. Antioxidants maintain cellular redox homeostasis by elimination of reactive oxygen species. *Cellular Physiology and Biochemistry.* 2017;44(2):532-553.

85. Gülçin İ. Antioxidant activity of caffeic acid (3, 4-dihydroxycinnamic acid). *Toxicology.* 2006;217(2-3):213-220.

86. Wiegand C, Hipler UC. Polymer-based Biomaterials as Dressings for Chronic Stagnating Wounds. Paper presented at: Macromolecular symposia2010.

87. Bjarnsholt T, Kirketerp-Møller K, Jensen PØ, et al. Why chronic wounds will not heal: a novel hypothesis. *Wound repair and regeneration.* 2008;16(1):2-10.

88. Novo E, Parola M. Redox mechanisms in hepatic chronic wound healing and fibrogenesis. *Fibrogenesis & tissue repair.* 2008;1(1):5.

89. Eming SA, Krieg T, Davidson JM. Inflammation in wound repair: molecular and cellular mechanisms. *Journal of Investigative Dermatology.* 2007;127(3):514-525.

90. Francesko A, da Costa DS, Lisboa P, Reis RL, Pashkuleva I, Tzanov T. GAGs-thiolated chitosan assemblies for chronic wounds treatment: control of enzyme activity and cell attachment. *J. Mater. Chem.* 2012;22(37):19438-19446.

91. Perelshtein I, Ruderman E, Francesko A, Fernandes MM, Tzanov T, Gedanken A. Tannic acid NPs–synthesis and immobilization onto a solid surface in a one-step process and their antibacterial and anti-inflammatory properties. *Ultrason. Sonochem.* 2014;21(6):1916-1920.

92. Rojkind M, Dominguez-Rosales J-A, Nieto N, Greenwel P. Role of hydrogen peroxide and oxidative stress in healing responses. *Cellular and Molecular Life Sciences CMLS.* 2002;59(11):1872-1891.

93. Cawston TE, Wilson AJ. Understanding the role of tissue degrading enzymes and their inhibitors in development and disease. *Best Practice & Research Clinical Rheumatology.* 2006;20(5):983-1002.

94. Xu LQ, Neoh K-G, Kang E-T. Natural Polyphenols as Versatile Platforms for Material Engineering and Surface Functionalization. *Progress in Polymer Science.* 2018.

95. Chen W, Shen X, Hu Y, et al. Surface functionalization of titanium implants with chitosan-catechol conjugate for suppression of ROS-induced cells damage and improvement of osteogenesis. *Biomaterials.* 2017;114:82-96.

96. Kojima M, Morisaki T, Izuhara K, et al. Lipopolysaccharide increases cyclo-oxygenase-2 expression in a colon carcinoma cell line through nuclear factor-κB activation. *Oncogene.* 2000;19(9):1225.

97. Dileep KV, Tintu I, Mandal PK, Karthe P, Haridas M, Sadasivan C. Binding to PLA2 May Contribute to the Anti-Inflammatory Activity of Catechol. *Chemical biology & drug design.* 2012;79(1):143-147.

98. Zheng LT, Ryu G-M, Kwon B-M, Lee W-H, Suk K. Anti-inflammatory effects of catechols in lipopolysaccharide-stimulated microglia cells: inhibition of microglial neurotoxicity. *Eur. J. Pharmacol.* 2008;588(1):106-113.

99. Larrosa M, Luceri C, Vivoli E, et al. Polyphenol metabolites from colonic microbiota exert anti-inflammatory activity on different inflammation models. *Mol. Nutr. Food Res.* 2009;53(8):1044-1054.

100. Huang J, de Paulis T, May JM. Antioxidant effects of dihydrocaffeic acid in human EA. hy926 endothelial cells. *The Journal of nutritional biochemistry.* 2004;15(12):722-729.

101. Mège R-M, Gavard J, Lambert MJCoicb. Regulation of cell–cell junctions by the cytoskeleton. 2006;18(5):541-548.

102. Shin J, Lee JS, Lee C, et al. Tissue adhesive catechol-modified hyaluronic acid hydrogel for effective, minimally invasive cell therapy. *Advanced Functional Materials.* 2015;25(25):3814-3824.

103. Neto AI, Cibrão AC, Correia CR, et al. Nanostructured Polymeric Coatings Based on Chitosan and Dopamine-Modified Hyaluronic Acid for Biomedical Applications. *Small.* 2014;10(12):2459-2469.

104. Akkineni AR, Ahlfeld T, Lode A, Gelinsky M. A versatile method for combining different biopolymers in a core/shell fashion by 3D plotting to achieve mechanically robust constructs. *Biofabrication.* 2016;8(4):045001.

105. Gu Q, Tomaskovic-Crook E, Lozano R, et al. Functional 3D neural mini-tissues from printed gel-based bioink and human neural stem cells. *Advanced healthcare materials.* 2016;5(12):1429-1438.

106. Noh I, Kim N, Tran HN, Lee J, Lee C. 3D printable hyaluronic acid-based hydrogel for its potential application as a bioink in tissue engineering. *Biomaterials research.* 2019;23(1):3.

107. Mohammad G, Pandey H, Tripathib K. Diabetic wound healing and its angiogenesis with special reference to nanoparticles. *Dig J Nanomater Bios.* 2008;3:203-208.

108. Mohandas A, Anisha B, Chennazhi K, Jayakumar R. Chitosan–hyaluronic acid/VEGF loaded fibrin nanoparticles composite sponges for enhancing angiogenesis in wounds. *Colloids and Surfaces B: Biointerfaces.* 2015;127:105-113.

109. Nillesen ST, Geutjes PJ, Wismans R, Schalkwijk J, Daamen WF, van Kuppevelt TH. Increased angiogenesis and blood vessel maturation in acellular collagen–heparin scaffolds containing both FGF2 and VEGF. *Biomaterials.* 2007;28(6):1123-1131.

110. Carmeliet P. Angiogenesis in life, disease and medicine. *Nature.* 2005;438(7070):932-936.

111. Mao Z, Shi H, Guo R, et al. Enhanced angiogenesis of porous collagen scaffolds by incorporation of TMC/DNA complexes encoding vascular endothelial growth factor. *Acta biomaterialia.* 2009;5(8):2983-2994.

112. Elviri L, Bianchera A, Bergonzi C, Bettini R. Controlled local drug delivery strategies from chitosan hydrogels for wound healing. *Expert opinion on drug delivery.* 2017;14(7):897-908.

113. Ferrara N, Gerber H-P, LeCouter J. The biology of VEGF and its receptors. *Nature medicine.* 2003;9(6):669-676.

114. Elçin YM, Dixit V, Gitnick G. Extensive in vivo angiogenesis following controlled release of human vascular endothelial cell growth factor: implications for tissue engineering and wound healing. *Artificial Organs.* 2001;25(7):558-565.

115. Park H-J, Jin Y, Shin J, et al. Catechol-functionalized hyaluronic acid hydrogels enhance angiogenesis and osteogenesis of human adipose-derived stem cells in critical tissue defects. *Biomacromolecules.* 2016;17(6):1939-1948.

116. Xu M, Khan A, Wang T, et al. Mussel-Inspired Hydrogel with Potent in Vivo Contact-Active Antimicrobial and Wound Healing Promoting Activities. *ACS Applied Bio Materials.* 2019;2(8):3329-3340.

CHAPTER

07

GENERAL CONCLUSIONS

General Conclusions

In this Thesis, novel mussel-inspired polymers have been developed and applied for the preparation of advanced materials with bioactive properties for regenerative medicine applications, such as skin tissue regeneration.

-The synthesis of two different families of long-arm catechol containing polymers have been successfully carried out using the hydrocaffeic acid as catechol containing molecule and following two different pathways: 1) functionalization of a monomer with catechol groups and its subsequent free-radical copolymerization with *N*-vinylcaprolactam to obtain catechol containing copolymers **(VCL_CEMA)**, and 2) direct conjugation of catechol molecules to *N*-vinylcaprolactam-co-2-hydroxyethyl methacrylate copolymers to obtain **catechol conjugated terpolymers.** The free radical copolymerization reaction of VCL and CEMA was clearly controlled by the catechol nature of the CEMA monomer giving statistical copolymers with CEMA contents between 0.9 and 13.5 mole %, low number average molecular weights and very low polydispersity index. On the other hand, the second pathway allowed obtaining catechol conjugated terpolymers with higher catechol contents (2, 22 and 29 mole %), high weight average molecular weights and enhanced availability of the catechol side groups.

-CEMA/VCL monomer composition had a great influence on the final polymer properties. Thus, copolymers with relatively low catechol contents (0.9–3.6 mole %) presented thermoresponsive behavior and excellent antioxidant and anti-inflammatory activities whereas VCL_CEMA copolymers with relatively high catechol content (13.5 mole %) allowed obtaining hydrogels with gelatin that demonstrated excellent bone bioadhesive properties. These findings suggest that VCL_CEMA polymers can be used as a tool for the preparation of biomedical systems with tunable properties with enormous potential for the development of **"smart" drug controlled delivery systems** and preparation of **gels** as scaffolds for regeneration processes to treat for example osteochondral diseases.

-Catechol conjugated terpolymers with different catechol compositions (2 and 22 mol %) allowed the fabrication of **2D films** with bioactive properties: the presence of long-arm catechol moieties demonstrated to provide films with strong bioadhesive properties to porcine skin in wet conditions; prevention for UV-induced skin damage; antioxidant properties for scavenging the ROS generated by hBMSCs; and attenuation of the inflammatory damage in macrophages cultures. Catechol composition of terpolymers strongly influenced the mentioned bioactive properties. On the other hand, all these bioactive properties are key features in the wound-healing process and,

therefore, these bioinspired materials are proposed as excellent candidates for their use in the preparation of bioadhesive and bioactive wound dressings.

-IPN hydrogel scaffolds containing chitosan, hyaluronic acid and a catechol conjugated terpolymer (22 mole % catechol) have been successfully fabricated. This IPN design provided a suitable microenvironment to support hBMSCs proliferation, excellent efficiency to protect cells against oxidative stress damage and suppression of the inflammatory response. IPN hydrogels presented high bioadhesion to porcine skin attributed to the catechol moieties and allowed the *in situ* controlled and sustained delivery of catechol species. Furthermore, *in vivo* histological studies revealed that the IPN membranes were biocompatible inducing normal inflammatory responses as well as faster vascularization compared to samples without catechol. Thus, the catechol bearing terpolymer endows the IPN hydrogel backbone with bioactive functionality; this together with the catechol controlled release pattern, make this system to have a great potential to assist in chronic wounds and enhance the tissue regeneration process.

-**3D bioprinted hydrogel scaffolds** of carboxymethylchitosan and oxidized hyaluronic acid have been effectively fabricated using a novel 3D extrusion printing approach which allows printing with living cells what means a step forward compared to supports fabricated using other conventional techniques in which cell seeding takes place after scaffold fabrication. The novel bioprinting methodology based on a dual-syringe system with a static mixing tool has demonstrated multiple advantages: gelation during the extrusion process provides enough viscosity for printing with high shape fidelity while using low viscosity precursor solutions, enabling high viability of the printed cells; and the crosslinking during extrusion avoids the need of an additional treatment to maintain the printed shape. The crosslinking kinetics of the reactive bioink optimized to match the printing process gave rise to biocompatible scaffolds with moderate swelling, good shape stability and cell viability around 90% after 14 days of culture. Since precursors' concentrations and printing conditions can be easily varied, this printing approach offers high versatility and we envision that it can be adaptable to a wide range of reactive systems with appropriate crosslinking kinetics to be employed in future for broad applications in regenerative medicine and tissue-engineering.

-**Self-assembling catechol containing NP** have been prepared using catechol conjugated polymers with two catechol compositions (2 and 29 mol %). Spherical and monodispersed nanoparticles obtained demonstrated high stability and ability to serve as nano-vehicles to carry hydrophobic drugs such as coumarin-6, providing sustained release profiles. *In vitro* biological studies demonstrated that catechol functionalized NP protect cells against oxidative stress damage induced by radical oxygen species (ROS), regulate of the inflammatory response, and promote

upregulation of the vascular endothelial growth factor (VEGF). Thus, we conclude that wound healing promoting activities of NP have a promising application in TE and DDS.

-Finally, **3D bioprinted hydrogel constructs of natural polymers containing the novel catechol functionalized nanoparticles** (NP29) have been developed following the 3D bioprinting approach previously developed. 2 Layers grid square scaffolds with the NP uniformly distributed have been successfully obtained with good resolution and shape fidelity. Further adjustment of the mixing printhead would allow to build up bigger constructs in follow up studies. *In vitro* cell culture studies demonstrated the ability of the bioink to support cell proliferation, and the wound healing promoting activities of the catechol functionalized nanoparticles: regulation of the radical oxygen species production, anti-inflammatory response and upregulation of vascular endothelial growth factor expression. Therefore, we envision that catechol functionalized NP loaded bioink developed in this work have promising applicability for wound healing therapies with several advantages: 1) the controlled release of the NP in the wound site provide localized bioactive function; 2) functionalized NP can act as nanocarriers for multiple hydrophobic drugs so the NP action could be extended with encapsulated drug; 3) printing approach used allows tailoring of geometry, materials and formulation doses based on patient requirements for wound specific treatments.

ANNEX I

CONTRIBUTION OF BIOACTIVE HYALURONIC ACID AND GELATIN TO REGENERATIVE MEDICINE. METHODOLOGIES OF GELS PREPARATION AND ADVANCED APPLICATIONS

Ana Mora-Boza[1,2*], María Puertas-Bartolomé [1,2*], Blanca Vázquez-Lasa[1,2], Julio San Román[1,2], Antonio Pérez-Caballer[3] and Marta Olmeda-Lozano[4]

[1] Institute of Polymer Science and Technology, ICTP-CSIC 28006 Madrid, Spain
[2] CIBER-BBN, Health Institute Carlos III. 28029 Madrid, Spain
[3]Faculty of Health Science, Francisco de Vitoria University, 28223, Madrid, Spain
[4]University Hospital Infanta Elena, 28342, Madrid, Spain

European Polymer Journal 95 (2017) 11-26

Research Article

Contribution of bioactive hyaluronic acid and gelatin to regenerative medicine. Methodologies of gels preparation and advanced applications

Ana Mora-Boza*, María Puertas-Bartolomé*, Blanca Vázquez-Lasa, Julio San Román, Antonio Pérez-Caballer and Marta Olmeda-Lozano

European Polymer Journal 95 (2017) 11–26

DOI: 10.1016/j.eurpolymj.2017.07.039

I

ANNEX II

IN SITU CROSSLINKABLE POLYMER SYSTEMS AND COMPOSITES FOR OSTEOCHONDRAL REGENERATION

María Puertas-Bartolomé[1,2*], Lorena Benito[3], Marta Olmeda-Lozano[4]

[1] Institute of Polymer Science and Technology, ICTP-CSIC 28006 Madrid, Spain
[2] CIBER-BBN, Health Institute Carlos III. 28029 Madrid, Spain
[3]Faculty of Medicine, University of Salamanca, 37007 Salamanca, Spain
[4]University Hospital Infanta Elena, Madrid, Spain

Advances in Experimental Medicine and Biology 1058 (2018) 327-355

Book Chapter

In situ crosslinkable polymer systems and composites for osteochondral regeneration

María Puertas-Bartolomé*, Lorena Benito and Marta Olmeda-Lozano

Advances in Experimental Medicine and Biology 1058 (2018) 327-355

DOI: 10.1007/978-3-319-76711-6_15

ABSTRACT

Injectable hydrogels have demonstrated being a promising strategy for cartilage and bone tissue engineering applications, owing to their minimal invasive injection procedure, easy incorporation of cells and bioactive molecules, improved contact with the surrounding tissues and ability to match defects with complex irregular shapes, characteristics of osteoarthritic pathology. These unique properties make them highly suitable bioscaffolds for treating defects which are otherwise not easily accessible without and invasive surgical procedure. In this book chapter it has been summarized the novel appropriate injectable hydrogels for cartilage and bone tissue engineering applications of the last few years, including the most commonly used materials for the preparation, both natural and synthetic, and their fabrication techniques. The design of a suitable injectable hydrogel with an adequate gelation time that gathers perfect bioactive, biocompatible, biodegradable and good mechanical properties for clinical repair of damaged cartilage and bone tissue is a challenge of significant medical interest that remain to be achieved.

Keywords: *Hydrogels · In situ cross-linking · Biopolymers · Composites · Osteochondral*

II

APPENDIX A

LIST OF ABBREVIATIONS

List of Abbreviations

AF	Annulus fibrosus
^{1}H-NMR	Proton nuclear magnetic resonance spectra
4SPEG	Poly(ethylene glycol) ether tetrasuccinimidyl glutarate
A_0	Absorbance of DPPH• in the absence of antioxidant
A_1	Absorbance of DPPH• in the presence of antioxidant
AB	Alamar Blue
AB dye	10 % AB solution in phenol red free DMEM medium
ACVA	4,4'-azobis(4-cyanovaleric acid)
AEMA	2-aminoethylmethacrylate hydrochloride
AFM	Atomic force microscopy
AIBN	Azobisisobutironitrilo
Alg-ox	Oxidized alginate
AM/UC	Amniotic membrane and umbilical cord
ANOVA	Analysis of variance
ASTM	American society for testing and materials
ATR-FTIR	Attenuated total internal reflectance/Fourier transform infrared
ATRP	Atom transfer radical polymerization
BCP	Biphasic calcium phosphate
BMS	Bone marrow stimulation
BSA	Bovine serum albumin
C6	Coumarin-6
C6NPn	NPn loaded with C6 where n corresponds to the catechol composition
CAD	Computer aided design
catechol	Ortho-dihydroxyphenol
CDC	Cardiosphere-derived cells
CDFH-DA	2',7'-dichlorofluorescin diacetate
CEMA	2-(3-(3,4-dihydroxyphenyl) propanamido) ethyl methacrylate monomer
CFL	Capillary force lithography
Ch	Chitosan
Ch-GA/Tyr	Chitosan–glycolic acid/tyrosine
Ch/HAox	Crosslinked membrane of Ch and HAox

Ch/HAox/T	Hydrogel membrane of Ch, HAox and T
Ch/HAox/T/Fe	Hydrogel membrane of Ch, HAox, T and Fe
CLSM	Confocal laser scanning microscopy
CMCh	Carboxymethylchitosan
CMChn/HAoxn-HAn	Bioink formulation composed of CMCh, HAox and HA, where n corresponds to the weight percentage of the precursor solution
CMChNP29/HAox-HA	Bioink formulation composed of CMCh, HAox, HA and NP29
CS	Chondroitin sulfate
CV	Cell viability
DAPI	4′,6-diamidino-2-phenylindole
DCF	2',7'-dichlorofluorescein
DDS	Drug delivery system
Dex	Dextran
Dex-ox	Oxidized dextran
D_h	Mean hydrodynamic diameter
DHF	Denatured human fibrinogen
DLS	Dynamic light scattering
DMA	Dopamine methacrylamide
DMEM	Dulbecco's modified Eagle's medium
DMF	*N,N*-dimethylformamide
DMS	Dexamethasone
DMSO	Dimethyl sulfoxide
DOPA	L-3,4-dihydroxyphenylalanine
DPPH·	2-diphenyl-2-picrylhydrazil radical
DPSCs	Dental pulp stem cells
DSC	Differential scanning calorimetry
DTGA	Differential thermogravimetric analysis
ECM	Extracellular matrix
EDA	Ethylendiamine
EDC	1-(3-dimethyl-aminopropyl)-3-ethyl carbodiimide
EDX	Energy-dispersive X-ray spectroscopy
EE	Encapsulation efficiency
EES	Erythematous effective spectrum
F	Feed mole fraction

f	Copolymer mole fraction
FBS	Fetal bovine serum
FDA	Fluorescein diacetate
FE-SEM	Field emission scanning electron microscopy
FTIR	Fourier transform infrared spectroscopy
G/Copol	Gel of VCL_CEMA13.5 copolymer and gelatin
G′	Storage modulus
G′′	Loss modulus
GA	Glycolic acid
GAG	Glycosaminoglycan
GBM	Malignant glioblastoma
Gel	Gelatin
Gel-S	Thiol modified gelatin
GelNB	Norbornene functionalized gelatin
GFP	Green fluorescent protein
GK	Dipeptide glycine-lysine
GP	Glycerophosphate
GPC	Gel permeation chromatography
Griess	1:1 mixture of 0.1 % *N-(*1-naphthyl) ethylenediamine in water and 1% sulphanilamide in 5 % phosphoric acid
GSSG	Oxidized glutathione
GTA	Glutaraldehyde
Gtn-HPA	Gelatin–hydroxyphenylpropionic acid
H	2-hydroxyethyl methacrylate
H-E	Haematoxylin and eosin
HA	Hyaluronic acid
HA-S	Thiol modified HA
HAox	Hyaluronic acid oxidized
HAVIC	Human aortic valvular interstitial cells
hBMSCs	Human bone marrow mesenchymal stem cells
HCA	Hydrocaffeic acid
HCCl	Chloride acid derivative of the hydrocaffeic acid
HDF	Human dermal fibroblasts
HEPES	4-(2-hydroxyethyl)-1-piperazineethanesulfonic acid

HPAM	Polyacrylamide
HPAM	Partially hydrolyzed polyacrylamide
HPPA	3-(4-hydroxyphenyl) propanamide
HR-MS	High resolution mass spectrometry
HRP	Horseradish peroxidase
HUVECs	Human umbilical cord vein endothelial cells
hVFF	Human vocal fold fibroblasts
ICP-OES	Inductively coupled plasma optical emission spectroscopy
IPN	Interpenetrated polymer network
IVD	Intervertebral disc
LAP	Lithium phenyl-2,4,6-trimethylbenzoylphosphinate
LCST	Lower critical solution temperature
LDE	Laser doppler electrophoresis
LMWHA	Low molecular weight hyaluronic acid
LPS	Lipopolysaccharides from *E. coli*
M-HGC	Methacrylated hexanoyl glycol chitosan
MA	Methacryloyl groups
Man	Azido-modified mannose
MAPs	Mussel adhesive proteins
MEW	Melt electrospinning writing
Mfps	Mussel foot proteins
MFX	Microfacture
MGSB	MegaGen synthetic bone
miRNA	Micro RNA
M_n	Number average molecular weight
MP	Microparticle
MPEG	Methoxy poly-ethylene glycol
MRI	Magnetic resonance imaging
MSCs	Human mesenchymal stem cells
MTGase	Transglutaminase
M_w	Weight average molecular weight
mW/cm^2	Milliwatt per square centimeter
M_w/M_n	Average molecular weights polydispersity

nano-HA	Nano-hydroxyapatite
NB	*o*-nitrobenzyl
NFC	Nanofibrillar cellulose
nHA-g-PLGA	*N*-hydroxyapatite-graft- poly(L-glutamic acid)
nHAp	Nanocrystalline hydroxyapatite
NHS	*N*-hydroxysuccinimide
NO	Nitric oxide
NP	Nanoparticles
NPn	Terpolymers where n corresponds to the catechol composition
NSCS	Neural stem cells
OA	Osteoarthritis
OD	Oxidation degree
PAMP	Peptide proadrenomedullin N-terminal 20 peptide
PBS	Phosphate buffered saline
PBST	0.1% Triton -X 100 and 5% w/v bovine serum albumin
PCEMA	PolyCEMA
PCL	Poly(e-caprolactone)
PDI	Particle dispersion index
PEG	Poly(ethylene glycol)
PEG-DA	Poly(ethylene glycol) diacrylate
PEGDA	Poly(ethylene glicol) diacrylate
PEGDVS	Poly(ethylene glicol) divinyl sulfone
PFA	Paraformaldehyde
PGA	Poly(glycolic acid)
PI	Photoinitiator
PI	Propidium iodide
PIC	Phototriggered-imine-crosslink
PLA	Poly(lactic acid)
PLGA	Poly(L-glutamic acid)
PLGA–ADH	Hydrazide-modified poly(L-glutamic acid)
PLGA–CHO	Aldehyde-modified poly(L-glutamic acid)
PLLA	Poly(L-lactic acid)
PNIPAM	Poly(*N*-isopropylacrylamide)

PPLG	Poly(γ-propargyl-Lglutamate)
PRP	Plattelet rich plasma
PVA	Poly(vinyl alcohol)
PVCL	Poly(*N*-vinylcaprolactam)
QTOF	Quadrupole-time of flight
RAFT	Reversible addition-fragmentation chain transfer
RAW 264.7	RAW 264.7 macrophages
RM	Regenerative medicine
RNS	Reactive nitrogen species
ROMP	Ring-opening metathesis polymerization
RSA	Radical scavenging activity
r.t.	Room temperature
RT_FTIR	Real time-FTIR
SD	Stndard deviation
Semi-IPN	Semi-interpenetrated polymer network
siRNA	Small interfering RNA
SPF	Sun protection factor
T	Terpolymer
TE	Tissue engineering
T_g	Glass transition temperature
TGA	Thermogravimetric analysis
THA	Thiolated hyaluronic acid
Tn	Terpolymer where n corresponds to the catechol composition
Tyr	Tyramine
UTM	Universal testing machine
UV	Ultraviolet
UV vis	Ultraviolet-visible
V	*N*-vinylcaprolactam
VCL	*N*-vinylcaprolactam
VCL_CEMA	N-vinylcaprolactam-co-[2-(3-(3,4-dihydroxyphenyl) propanamido) ethyl methacrylate] copolymers
VEGF	Vascular endothelial growth factor
VFLP	Human vocal fold lamina propia

VHCn	Catechol conjugated polymers where n corresponds to the catechol composition
VHn	*N*-vinylcaprolactam -co- 2-hydroxyethyl methacrylate copolymers where n corresponds to the H content
VIC	Valvular interstitial cells
Vis	Visible
W_0 or W_d	Initial weight of dried sample for swelling and degradation assays
W_t	Weight sample at time t for swelling and degradation assays
xerogels	Dried hydrogels
ΔW %	Percentage of weight remaining
ξ	Zeta potential

APPENDIX B

AUTHOR CONTRIBUTIONS

Publications

Results obtained during the realization of this Doctoral Thesis have led to the publications of different SCI and no SCI articles as it is exposed below.

SCI PUBLICATIONS

3D printed construct with catechol functionalized nanoparticles for wound healing applications.

Authors: Puertas-Bartolomé M, Wlodarczyk-Biegun M K, del Campo A, Vázquez-Lasa B*, San Román J
Under consideration for publcication

3D printing of a reactive hydrogel bioink using a static mixing tool.

Authors: Puertas-Bartolomé M, Wlodarczyk-Biegun M K, del Campo A, Vázquez-Lasa B*, San Román J
Under consideration for publcication

Bioadhesive functional hydrogels: Controlled release of catechol species with antioxidant and antiinflammatory behavior.

Authors: Puertas-Bartolomé M, Benito-Garzón L, Fung S., Kohn J, Vázquez-Lasa B*, San Román J
Published: Materials Science and Engineering: C 105 (2019) 110040
DOI: 10.1016/j.msec.2019.110040

Bioactive and Bioadhesive Catechol Conjugated Polymers for Tissue Regeneration.

Authors: Puertas-Bartolomé M, Vázquez-Lasa B*, San Román J
Published: Polymers 10 (2018) 768
DOI: 10.3390/polym10070768

In Situ Cross-Linkable Polymer Systems and Composites for Osteochondral Regeneration.

Authors: Puertas-Bartolomé M*, Benito-Garzón L., Olmeda-Lozano M
Published: Chapter XXV of the book "Osteochondral Tissue Engineering": Advances in Experimental Medicine and Biology 1058 (2018) 327-355
DOI: 10.1007/978-3-319-76711-6_15

Biocompatible and bioadhesive low molecular weight polymers containing long-arm catechol-functionalized methacrylate.

Authors: Puertas-Bartolomé M, Fernández-Gutiérrez M, García-Fernández L*, Vázquez-Lasa B*, San Román J
Published: European Polymer Journal 98 (2018) 47–55
DOI:10.1016/j.eurpolymj.2017.11.011

Contribution of bioactive hyaluronic acid and gelatin to regenerative medicine.

Authors: Mora-Boza A*, Puertas-Bartolomé M*, Vázquez-Lasa B, San Román J, Pérez-Caballer A, Olmeda-Lozano M
Published: European Polymer Journal 95 (2017) 11-26
DOI: 10.1016/j.eurpolymj.2017.07.039

NO SCI PUBLICATIONS

Clinical application and biofabrication of injectable polymeric systems for osteochondral lesson reparation

Authors: Mora-Boza A*, Puertas-Bartolomé M*, Vázquez-Lasa B
Published: Revista de Plásticos Modernos 115 (2018) 731

Conference Communications

Results obtained during the realization of this Doctoral Thesis have been presented in numerous conferences presented below.

European Polymer Congress 2019 (Crete, Greece). Oral presentation: "*Bioadhesive and bioactive interpenetrating polymer supports for Tissue Engineering"* San Román J, Puertas-Bartolomé M, Vázquez-Lasa B, Benito-Garzón L, Fung S., Kohn J.

13th International Symposium on Frontiers in Biomedical Polymers 2019 (Tenerife, Spain). Oral presentation: "*3D printing of a reactive hydrogel loaded with catechol containing nanoparticles"* Puertas-Bartolomé M, Wlodarczyk-Biegun M K, del Campo A, Vázquez-Lasa B, San Román J.

XLI Congreso de la Sociedad Ibérica de Biomecánica y Biomateriales SIBB 2018 (Madrid, Spain). Oral presentation: "*Bioactive hybrid hydrogels for tissue engineering*" Puertas-Bartolomé M, Benito-Garzón L, Fung S., Kohn J, Vázquez-Lasa B, San Román J.

Progress in Polymer Science and Engineering 2018 (Huelva, Spain). Oral presentation: *"In vivo biocompatible and bioadhesive interpenetrated scaffolds for wound closure and tissue regeneration processes"* Puertas-Bartolomé M, Benito-Garzón L, Fung S., Kohn J, Vázquez-Lasa B, San Román J.

29th Annual Meeting of the European Society for Biomaterials ESB 2018 (Maastricht, Netherlands). Poster presentation: "*Mussel-inspired interpenetrated scaffolds for wound healing regeneration"* Puertas-Bartolomé M, Benito-Garzón L, Fung S., Kohn J, Vázquez-Lasa B, San Román J. (Poster presentation award).

2018 TERMIS World Congress (Kyoto, Japan). Poster presentation: "*Biocompatible interpenetrated scaffolds for wound healing processes with bioadhesive properties*" Puertas-Bartolomé M, Benito-Garzón L, Fung S., Kohn J, Vázquez-Lasa B, San Román J.

Summer School on Tissue Engineering and Regenerative Medicine 2017 (Trento, Italy). Oral presentation: "*Catechol conjugated polymers for tissue regeneration"* Puertas-Bartolomé M, Vázquez-Lasa B, San Román J.

II Seminario de Jóvenes Investigadores en Polímeros 2017 (Madrid, Spain). Oral presentation: "*Preparation of bioactive and bioinspired tissue adhesive materials in physiological conditions"* Puertas-Bartolomé M, Fung S., Kohn J, Vázquez-Lasa B, San Román J.

28th annual conference of the European Society for Biomaterials ESB 2017 (Athens, Greece). Poster presentation: "*Novel Bioinspired Functional Polymers with Bioadhesive and Thermosensitive Properties*" Puertas-Bartolomé M, Fernández-Gutiérrez M, García-Fernández L, Vázquez-Lasa B, San Román J.

International Symposium on Bioinspired Macromolecular Systems 2017 (Aveiro, Portugal). Poster communication: "*Interpenetrated resorbable bioadhesive tissue engineering scaffolds*" Puertas-Bartolomé M, Fung S., Kohn J, Vázquez-Lasa B, San Román J.

I Seminario de Jóvenes Investigadores en Polímeros 2016 (Madrid, Spain). Oral communication: "*Development of Bioinspired polymers"* Puertas-Bartolomé M, Lillo A, Vázquez-Lasa B, San Román J.

XXXIX Congreso de la sociedad Ibérica de Biomecánica y Biomateriales SIBB 2016 (León, Spain). Oral communication: "*New bioactive polymers for Tissue Engineering*" Puertas-Bartolomé M, Lillo A, Vázquez-Lasa B, San Román J.

XIV Reunión del Grupo Especializado de Polímeros GEP 2016 (Burgos, Spain). Poster communication: "*Development of Functionalized Polymers. An Approach Mimicking Nature*" Puertas-Bartolomé M, Lillo A, Vázquez-Lasa B, San Román J.

Summer School in Tissue Engineering and Regenerative Medicine 2016 (Riva del Garda, Italy). Poster and Oral communication: "*Biodegradable functional polymers with bioadhesive properties*". Puertas-Bartolomé M, Lillo A, Vázquez-Lasa B, San Román J.

Short Research Stays

During the realization of this Doctoral Thesis, two research stays have been carried out as described below.

Dynamic Biomaterials Group, Leibniz-Institute for New Materials (INM), Saarbrücken, Germany.

Proyect: 3D printing of a reactive hydrogel bioink using a static mixing tool
Supervisor: Prof. Aránzazu del Campo Bécares.
Stay: 01/03/19-16/05/19
Foundation: M. Puertas-Bartolomé FPI scholarship BES-2015-075161

New Jersey Center for Biomaterials (NJCB), Rutgers University, Piscataway, NJ, EEUU.

Proyect: Preparation of bioactive and bioinspired tissue scaffolds with bioadhesive properties in physiological conditions
Supervisor: Prof. Joachim Kohn
Stay: 15/05/17-15/08/17
Foundation: ICF International Summer Exchange